

Cosmology with the line-of-sight shear of strong gravitational lenses

Pierre Fleury ¹, Daniel Johnson ¹, Théo Duboscq,¹
Natalie B. Hogg ^{2,3}, Julien Larena ¹

¹Laboratoire Univers et Particules de Montpellier, CNRS & Université de Montpellier,
Parvis Alexander Grothendieck, F-34095 Montpellier Cedex 05, France

²Institute of Astronomy, University of Cambridge,
Madingley Road, Cambridge, CB3 0HA, UK

³Kavli Institute for Cosmology, University of Cambridge, Cambridge, UK

E-mail: theo.duboscq@umontpellier.fr, pierre.fleury@lupm.in2p3.fr,
natalie.hogg@ast.cam.ac.uk, daniel.johnson@umontpellier.fr,
julien.larena@umontpellier.fr

Abstract. Stage-IV photometric galaxy surveys are designed to measure the position and shapes of billions of galaxies. Their aim is to characterise the large-scale distribution of matter in the Universe using galaxy clustering and weak gravitational lensing. As a byproduct, stage-IV surveys are expected to detect more than a hundred thousand strong gravitational lenses. In this article, we propose the use of weak-lensing perturbations to strong lenses, specifically their line-of-sight (LOS) shear, as a cosmological probe. This new observable allows us to define three new correlation functions: the LOS shear with itself, with galaxy positions, and with galaxy shapes, thereby promoting the standard 3×2 pt correlation method to a 6×2 pt scheme. We design estimators for these new correlation functions and determine their expectation values as a function of the matter power spectrum. We then derive the analytical expression for the full covariance matrix of the 6×2 pt correlation scheme. Considering various scenarios for the stage-IV strong-lensing samples, we demonstrate that the cosmological information carried by the LOS shear of strong lenses will be detectable with a very high signal-to-noise ratio, even in the most pessimistic of cases. Strong lenses are thus extremely promising cosmological probes, whose synergy with galaxy positions and shapes should also contribute to mitigating systematics in stage-IV surveys.

Keywords: Strong gravitational lensing, weak gravitational lensing, dark matter

Contents

1	Introduction	1
2	Line-of-sight shear in strong lensing	4
2.1	Tidal perturbations to a strong lens	4
2.2	Measuring the LOS shear with strong-lensing images	5
2.3	LOS shear from cosmological perturbations	6
3	Cosmology with the line-of-sight shear	7
3.1	A six times two-point correlation scheme	7
3.2	Estimators of the LOS correlation functions	9
3.2.1	Autocorrelation of the LOS shear (LL)	9
3.2.2	Cross-correlation of LOS shear and galaxy ellipticity (LE)	12
3.2.3	Cross-correlation of LOS shear and galaxy positions (LP)	12
3.3	Expectation values of the estimators in Λ CDM	13
3.3.1	Three distinct notions of average	13
3.3.2	The LL signal	14
3.3.3	The LE signal	15
3.3.4	The LP signal	16
3.4	Angular power spectra	16
3.4.1	Spherical-harmonic decomposition	17
3.4.2	Relation between correlation functions and power spectra	17
3.4.3	Expression of the LL, LE and LP power spectra	18
3.5	Standard 3×2 pt observables with our notation	21
4	Uncertainties and covariance matrix	22
4.1	Definition of the covariance matrix	22
4.2	Technical subtlety: coincident indices	22
4.3	Recipe to calculate the covariance matrix	23
4.3.1	The formula	24
4.3.2	Using the formula	24
4.4	Result and comments on the sources of uncertainty	26
4.5	Numerical implementation	27
5	Forecasted detectability	28
5.1	Optimistic scenario	28
5.2	Conservative scenario	31
5.3	Detectability assessment	33
6	Conclusion	35
A	Detailed calculation of $\text{Cov}[(\widehat{\mathbf{L}+\mathbf{P}}_B)_\alpha, (\widehat{\mathbf{L}+\mathbf{P}}_D)_\beta]$	36
A.1	Galaxy-sample average [...]	36
A.2	Lens sample average [...]	37
A.3	Cosmic average $\langle \dots \rangle$	37
A.4	Putting everything together	38

A.5	Polarisation angles	39
A.6	Final expression	40
B	Angular binning procedure	40
B.1	Binning algorithm given a target SNR	41
B.2	Determining the target SNR	41
C	Monte Carlo integration and error analysis	41

1 Introduction

Gravitational lensing is the phenomenon resulting from the deflection of light rays by the gravitational fields between the source and the observer. Most of the time, gravitational lensing only leads to small effects – a slight magnification, or demagnification, of light sources, accompanied by a slight distortion of their shapes. The latter manifestation of weak lensing, known as cosmic shear, produces alignment patterns of background galaxies – tangentially around foreground matter overdensities, and radially around underdensities [1]. The larger the density fluctuation, the more apparent the pattern, which is why cosmic shear has become a key probe of the large-scale distribution of matter in the Universe. It is particularly efficient at constraining the combination of cosmological parameters $S_8 = \sigma_8 \sqrt{\Omega_m}/0.3$ [2, 3], where Ω_m is the relative contribution of matter density to the dynamics of cosmic expansion, and σ_8 is the standard deviation of the matter density contrast smoothed on a scale of $8h^{-1}$ Mpc.

Stage-III photometric galaxy surveys, namely the Dark Energy Survey (DES) [4], the Subaru Hyper Suprime-Cam (HSC) survey [5, 6], and the Kilo-Degree Survey (KiDS) [7], have constrained $S_8 \approx 0.8$ with a precision ranging from 1.5% to 5%. These constraints do not come from cosmic shear alone, but from the so-called 3×2 pt correlation scheme, in which the two-point correlation function of the apparent ellipticity of galaxies (cosmic shear) is combined with the two-point correlation function of galaxy positions (galaxy clustering) and their cross-correlation (galaxy–galaxy lensing). Stage-IV surveys, such as *Euclid* [8] and the Legacy Survey of Space and Time (LSST) of the Vera C. Rubin Observatory [9], are expected to improve these constraints by about an order of magnitude [10], thanks to unprecedented catalogues of billions of galaxies with excellent imaging quality. In the era of stage-IV galaxy surveys, our ability to extract cosmological information will no longer be limited by statistics, but by systematic uncertainties, such as the intrinsic alignment of galaxies, their redshift distribution, and the modelling of small-scale baryonic processes. Controlling systematics, is, therefore, the main challenge of stage-IV surveys.

Due to their sensitivity, resolution, and their wide sky coverage, stage-IV surveys will also observe an abundance of the rarer strong manifestations of gravitational lensing, namely multiple images, arcs and Einstein rings, which typically occur when a foreground galaxy happens to lie directly on line of sight to another, more distant, galaxy. As a rule of thumb, there is one strong-lensing event every ten thousand observed galaxies, which implies that stage-IV catalogues shall comprise over a hundred thousand strong lenses [11], a number that is compatible with cosmological applications. This is the topic of the present article.

To first approximation, a strong gravitational lens may be modelled as some concentration of matter in an otherwise homogeneous and isotropic Universe. In this approach, light deflection only occurs in the vicinity of the main deflector, but on the scales relevant to strong lensing, the Universe is far from being homogeneous, and the propagation of light is perturbed

by the matter structures between the source, the main deflector, and the observer. If the most prominent matter concentrations happen to lie far from the line of sight (LOS), then they may be treated in the tidal regime [12–16], whereby their net effect is captured by a single complex parameter: the LOS shear [17]. Most importantly, elaborating on an earlier approach [18, 19], ref. [20] demonstrated on mocks that the LOS shear can be directly measured on individual strong-lensing images. Put simply, this means that *Einstein rings are standardisable shapes*,¹ whose distortions are a probe of cosmological perturbations. Albeit still in their infancy, actual measurements of the LOS shear have already been performed [21, 22] on a sample of 45 lenses from the Sloan Lens Advanced Camera for Surveys (SLACS) catalogue [23].

In this article, we present a complete framework for the use of the LOS shear of strong lenses as a cosmological probe. In a nutshell, we propose to add the LOS shear to the standard list of observables, namely galaxy positions and shapes, so as to promote the 3×2 pt correlation method to a 6×2 pt one. This strategy is mainly motivated by the fact that galaxies and strong lenses are subject to different systematics, which should be significantly mitigated by their combination. We then evaluate the detectability of a cosmological signal from the LOS shear in the context of stage-IV surveys.

The remainder of the article is organised as follows. In sec. 2, we summarise the main concepts associated with the LOS shear in strong lensing, and establish its expression in cosmological perturbation theory. In sec. 3, we present the 6×2 pt correlation method, we define estimators for the three new correlation functions involving the LOS shear and we derive their expectation values in standard cosmology. In sec. 4, we analytically calculate the full covariance matrix of the 6×2 pt correlations, with a view for its use in a Fisher forecast. Finally, we apply these results in sec. 5 to evaluate the uncertainties on our new observables, and thus assess their detectability with stage-IV galaxy surveys.

Conventions and notation \equiv indicates a definition. We use bold symbols for vectors and matrices. A hatted bold symbol ($\hat{\mathbf{u}}$) is a unit vector; other hatted quantities indicate either a noisy observable ($\hat{\gamma}_{\text{LOS}}$) or an estimator ($\widehat{(\text{O}_1\text{O}_2)}$). There are many indices in this work ($a, A, i, \alpha, \mu, \dots$) which are consistently associated with a specific meaning (see table 1). We work with units such that the speed of light is unity, $c = 1$.

Frequently asked questions

- *What is line-of-sight (LOS) shear?* It is a complex number, γ_{LOS} , which captures the effect of tidal perturbations along the LOS of a strong lens. The setup is depicted in fig. 1, where (o) observes a source (s) strongly lensed by a deflector (d), with LOS perturbations. This configuration actually involves three shears, $\gamma_{\text{od}}, \gamma_{\text{os}}, \gamma_{\text{ds}}$, where γ_{ab} would be the complex ellipticity, as seen from (a), of a small circular source at (b), due to weak lensing. The combination $\gamma_{\text{LOS}} = \gamma_{\text{od}} + \gamma_{\text{os}} - \gamma_{\text{ds}}$ affects the image in a way that is maximally independent of the source and main lens. Thus, the LOS shear may be seen as the net weak-lensing distortion of a strong-lensing image.
- *What is the difference between LOS shear and the usual weak-lensing shear?* The normal weak-lensing shear is only one of the three terms, namely γ_{os} , in the

¹This does not mean that Einstein rings are or need to be perfectly circular in the absence of LOS perturbations, but rather that one can distinguish, in an image, between the morphological features due to the main deflector and those due to LOS perturbations.

expression of γ_{LOS} . The contribution of some matter lump to γ_{os} peaks if it lies halfway between (o) and (s). For γ_{LOS} , that contribution is enhanced between (o) and (d) and suppressed between (d) and (s); see eqs. (2.10) to (2.12).

- *How can we measure the LOS shear from strong-lensing data?* An image $I(\boldsymbol{\theta})$ consists of surface brightness, I , in pixels, $\boldsymbol{\theta}$. If the image is produced by gravitational lensing of a source I_s , then $I(\boldsymbol{\theta}) = I_s[\boldsymbol{\theta} - \boldsymbol{\alpha}(\boldsymbol{\theta})]$, where $\boldsymbol{\alpha}$ is the lensing displacement field. When interpreting this image, one must model both the source profile $I_s(\boldsymbol{\theta})$ and the lensing displacement $\boldsymbol{\alpha}(\boldsymbol{\theta})$. In that context, the LOS shear γ_{LOS} is a parameter in $\boldsymbol{\alpha}(\boldsymbol{\theta})$ which can be inferred from the data. In `LENSTRONOMY`, this is implemented in the `LINEOF SIGHT` module.
- *How can we use the LOS shear in cosmology?* Equations (2.10) to (2.12) show that γ_{LOS} depends on the gravitational potential Φ , just like the density contrast (2.6) or the weak-lensing shear (2.14). Measuring correlation functions of these quantities then informs us about the matter power spectrum. Current galaxy surveys exploit three correlation functions built from galaxy positions (P) and ellipticities (E): EE (cosmic shear), PP (galaxy clustering) and EP (galaxy–galaxy lensing). Adding the LOS shear (L) allows us to define three new correlation functions (LL, LE, LP), thereby promoting the standard $3 \times 2\text{pt}$ method to $6 \times 2\text{pt}$ (see fig. 2).
- *Stage-IV surveys will observe $\mathcal{O}(10^9)$ galaxies and $\mathcal{O}(10^5)$ lenses. How can the latter compete with the former?* In cosmic shear, a very large number of galaxies are required for the cosmological signal to exceed their intrinsic shape noise. This is because, in the apparent ellipticity of a galaxy, $\varepsilon = \varepsilon_0 + \gamma$, the intrinsic contribution, ε_0 , is typically 30 times larger than the weak-lensing shear, γ . In other words, the signal-to-noise ratio (SNR) of weak lensing is about 3% for one galaxy. In contrast, we should measure the LOS shear on individual strong lenses with an SNR of about 100%, so that comparatively few lenses are needed to extract a cosmological signal. Furthermore, we expect the LOS shear to be immune to cosmic-shear systematics like intrinsic alignment, which makes these probes highly complementary.
- *Why compute the $6 \times 2\text{pt}$ covariance matrix analytically instead of using simulations?* Analytical calculations have the advantage of producing results that are easier to interpret. Since the project to use the LOS shear as a cosmological observable is at an early stage, interpretation is essential to design and optimise the future observational strategy (which lenses to keep? how to bin them by redshift and angular separation?). Furthermore, analytical results are more flexible: it is easier to add new ingredients to a formula than to run an entirely new suite of simulations. Not to mention that simulating a cosmological sample of perturbed strong lenses is significantly more challenging than simulating a galaxy sample.
- *Will strong lenses improve the measurements of cosmological parameters?* In this article, we demonstrate that the new correlation functions, LL, LE and LP, are detectable from stage-IV surveys with high SNR, across a range of angular scales. We are currently conducting Fisher forecasts to quantify the expected gain in precision and accuracy for cosmological parameters such as Ω_m and σ_8 ; the results will be presented in a subsequent paper.

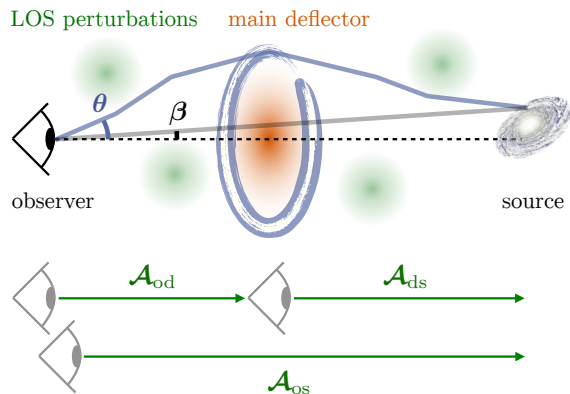


Figure 1. A strong-lensing system where a background galaxy (source), lies behind a foreground galaxy (main deflector), while inhomogeneities near the LOS are treated as tidal perturbations. In the absence of the main lens and LOS perturbations, a point in the source galaxy is observed at β ; θ is an image of that point by the entire system {main deflector + LOS perturbations}. The 2×2 distortion matrices \mathcal{A}_{ab} ($a, b \in \{o, d, s\}$) quantify the effect of the LOS perturbations when a source at (b) is observed from (a).

2 Line-of-sight shear in strong lensing

2.1 Tidal perturbations to a strong lens

Consider the scenario depicted in fig. 1, where a source galaxy is well aligned with a foreground galaxy acting as a strong gravitational lens. Let us denote with β the position at which some point within the source galaxy would be observed in the absence of the lens, through a homogeneous and isotropic Universe. We then denote with θ the position of an image of that point, i.e. the direction in which it is observed in the presence of deflectors.

If the main deflector were isolated, that is, far from any other cosmic inhomogeneity, then the relationship between β and θ – known as the lens equation – would read $\beta = \theta - \nabla\Psi(\theta)$, where $\Psi(\theta)$ is the lensing potential of the main deflector [24], and ∇ denotes the two-dimensional gradient with respect to θ . If, however, cosmological perturbations are present on the LOS, then the previous relation is modified to [12–17]

$$\beta = \mathcal{A}_{os}\theta - \mathcal{A}_{ds}(\nabla\Psi)(\mathcal{A}_{od}\theta), \quad (2.1)$$

where \mathcal{A}_{os} , \mathcal{A}_{ds} , \mathcal{A}_{od} are called distortion matrices. Each one of the \mathcal{A}_{ab} , with $a, b \in \{o, d, s\}$, is a 2×2 matrix that encodes the effect of weak LOS perturbations, with respect to a homogeneous–isotropic Universe, when a source at (b) is observed from (a). For instance, in the absence of the main deflector ($\nabla\Psi = \mathbf{0}$), the lens equation (2.1) reduces to $\beta = \mathcal{A}_{os}\theta$, thereby illustrating how LOS perturbations alone affect the appearance of images.

Such a description of LOS effects is valid only if the secondary deflectors can be treated in the *tidal regime*. This means that their gravitational field is well-approximated, at the scale of the strong-lensing image, by a second-order expansion of their gravitational potential around the LOS [15, 17]. Physically speaking, this corresponds either to smooth distributions of matter lying near the LOS, or to concentrations of matter lying far from it. See refs. [17, 25] for a description of LOS effects beyond the tidal regimes, accounting in particular for flexion [26].

If the LOS perturbations are weak, the distortion matrices \mathcal{A}_{ab} are approximately symmetric [27]. As such, they can be decomposed into a scalar component and symmetric trace-free component as

$$\mathcal{A}_{ab} = \mathbf{1} - \begin{bmatrix} \kappa_{ab} & 0 \\ 0 & \kappa_{ab} \end{bmatrix} - \begin{bmatrix} \text{Re}(\gamma_{ab}) & \text{Im}(\gamma_{ab}) \\ \text{Im}(\gamma_{ab}) & -\text{Re}(\gamma_{ab}) \end{bmatrix}, \quad (2.2)$$

where the convergence κ_{ab} is caused by the smooth matter on the LOS, while the complex shear γ_{ab} is due to concentrations of matter around the LOS, between (a) and (b).

2.2 Measuring the LOS shear with strong-lensing images

From a strong-lensing image such as an Einstein ring, it is generally impossible to identify the effect of individual LOS perturbations \mathcal{A}_{os} , \mathcal{A}_{od} , \mathcal{A}_{ds} , or distinguish them from the properties of the main deflector, Ψ . These degeneracies are partly due to our ignorance of the position and morphology of the source: in eq. (2.1), β is a parameter to be fitted just like Ψ and \mathcal{A}_{ab} .

This source-position degeneracy [28] can nonetheless be exploited so as to effectively reduce the number of parameters in the lens equation [17]. Multiplying eq. (2.1) on the left with $\mathcal{A}_{\text{od}}\mathcal{A}_{\text{ds}}^{-1}$, and defining the displaced source position $\beta' = \mathcal{A}_{\text{od}}\mathcal{A}_{\text{ds}}^{-1}\beta$, we have

$$\beta' = \mathcal{A}_{\text{LOS}}\theta - (\nabla\Psi_{\text{eff}})(\theta), \quad \text{with} \quad \begin{cases} \mathcal{A}_{\text{LOS}} \equiv \mathcal{A}_{\text{od}}\mathcal{A}_{\text{ds}}^{-1}\mathcal{A}_{\text{os}} \\ \Psi_{\text{eff}}(\theta) \equiv \Psi(\mathcal{A}_{\text{od}}\theta) \end{cases}. \quad (2.3)$$

Equation (2.3) is the *minimal LOS model* [17]. It is formally equivalent to the description of a single-plane lens system, which would consist of a main deflector with potential $\Psi_{\text{eff}}(\theta)$, together with an “external convergence” and an “external shear” encoded in the distortion matrix \mathcal{A}_{LOS} . On the one hand, the expression of the effective potential Ψ_{eff} shows that there is a strong degeneracy between the foreground perturbations \mathcal{A}_{od} and the properties of the main deflector [29]. On the other hand, the expression of \mathcal{A}_{LOS} shows that it would be ill-advised to try to measure \mathcal{A}_{od} , \mathcal{A}_{os} , \mathcal{A}_{ds} independently from one another. It is, however, possible to measure the shear component of \mathcal{A}_{LOS} , that is

$$\boxed{\gamma_{\text{LOS}} = \gamma_{\text{od}} + \gamma_{\text{os}} - \gamma_{\text{ds}}} \quad (2.4)$$

in the weak-lensing limit ($\kappa_{\text{ab}}, |\gamma_{\text{ab}}| \ll 1$). We shall refer to γ_{LOS} as the *LOS shear* throughout. From a theoretical point of view, one expects γ_{LOS} to be distinguishable from the properties of the main lens, such as its ellipticity. This is because the LOS shear represents a strictly homogeneous tidal field, while the main lens’s tidal field always displays some radial gradient. See ref. [30] for a comparison of the morphological features of shear and ellipticity.

The practical measurability of the LOS shear from realistic strong-lensing images was assessed in ref. [20]. This proof of concept relied on a sample of 64 mock Hubble Space Telescope (HST) images, produced by complex analytical lens models, in the presence of tidal LOS perturbations. It was shown that the LOS shear can be accurately measured, with a mean uncertainty on the order of 0.01, provided that the model for the main lens is elaborate enough. This corresponds to a signal-to-noise ratio of order unity for individual lenses. The first measurements of the LOS in real data were made [21, 22] in 45 strong lenses from the SLACS catalogue [23]; this work also investigated possible systematics, such as the role of boxiness/diskiness in lens mass profiles [31].

Caveats

Albeit encouraging, these results also emphasise that LOS shear measurements are still in their infancy. In particular, it is unclear what “elaborate enough” means in practice for a lens model. In the context of Bayesian forward modelling of an image, if the actual lens possesses morphological features that are not accounted for in the model, then the sampler will tend to use the free shear in order to compensate for the missing features, thereby leading to spurious biases in the best-fit value of γ_{LOS} . An eloquent example was found with the mock analysis of ref. [20]: if a lens consists of a baryonic core and a dark-matter halo whose centres are offset, and if one tries to fit the image produced by that lens assuming that both components share

the same centre, then the measured γ_{LOS} is clearly biased; the bias disappears if the model allows for the offset as a free parameter.

Whilst the necessary features of a good lens model – as far as the LOS shear is concerned – are still to be determined, we can already claim that the standard elliptical power-law (EPL) model does not fulfil them. In addition to the biases observed in mocks [20, 32], studies on real data lead to the same conclusion. Analysing HST data using EPL plus external shear, ref. [32] found suspicious correlations between the orientation of the external shear and the main lens’s ellipticity, which suggests that the external-shear parameter may account for details of the lens’s azimuthal structure that are not well-described by a mere ellipticity [33]. Reference [21], besides, finds that the best-fit values of γ_{LOS} for SLACS lenses modelled as EPL plus LOS shear are typically ten times larger than expectations from cosmology.

Another potential source of systematics in γ_{LOS} comes from neglecting higher-order LOS effects, such as the LOS flexion. Reference [25] derived a minimal LOS flexion model, which features four additional complex parameters. In most realistic situations, the LOS flexion is too small to be measured, but it does produce a systematic bias on γ_{LOS} if not accounted for.

In this article, we shall assume that the LOS shear is strictly due to cosmological perturbations, and that it can be measured on strong-lensing images without systematic biases, albeit with a signal-to-noise ratio that may be smaller than unity on individual images. Our goal is to investigate its statistical measurability through correlation functions.

2.3 LOS shear from cosmological perturbations

Let us assume that the space-time geometry experienced by light on its way from the source to the main deflector, and then to the observer, is well approximated by a spatially flat Friedmann–Lemaître–Robertson–Walker model with perturbations. The line element reads

$$ds^2 = -(1 + 2\Phi) a^2(\eta) d\eta^2 + (1 - 2\Phi) a^2(\eta) \left[d\chi^2 + \chi^2 (d\theta^2 + \sin^2 \theta d\varphi^2) \right], \quad (2.5)$$

where $a(\eta)$ is the background scale factor, η is conformal time, χ is the comoving distance to an arbitrary origin, θ and φ are polar coordinates on the two-sphere, and $\Phi(\eta, \chi, \theta, \varphi)$ is the gravitational potential produced by matter inhomogeneities. The latter is connected to the density perturbations via the Poisson equation,

$$\Delta\Phi = 4\pi G a^{-1} \bar{\rho}_0 \delta, \quad (2.6)$$

where $\bar{\rho}_0$ is today’s mean cosmic density and $\delta \equiv (\rho - \bar{\rho})/\bar{\rho}$ the dimensionless density contrast.

Solving the null geodesic deviation equation at leading order in Φ , we find that the shear produced on an image at (b) observed from (a) can be expressed in terms of a potential as

$$\gamma_{\text{ab}}(\hat{\mathbf{u}}) = \frac{1}{2} \bar{\partial}^2 \Psi_{\text{ab}}(\hat{\mathbf{u}}), \quad (2.7)$$

where $\bar{\partial}$ is the spin-raising operator (or eth² derivative); it acts on the angular variables (θ, φ) , which we gather into the unit vector $\hat{\mathbf{u}}$ representing the corresponding position on the two-sphere; see e.g. ref. [35] and references therein for details on the $\bar{\partial}$ operator. The potential Ψ_{ab} is a weighted projection of the gravitational potential along the lightcone between (a) and (b),

$$\Psi_{\text{ab}}(\hat{\mathbf{u}}) = 2 \int_0^\infty \frac{d\chi}{\chi} K(\chi; \chi_{\text{a}}, \chi_{\text{b}}) \Phi(\eta_0 - \chi, \chi, \hat{\mathbf{u}}), \quad (2.8)$$

² “Eth” is the name of the phonetic character $\bar{\partial}$, although it seems to be mostly referred to as “edth” in the mathematical literature since ref. [34].

where η_0 is conformal time today, and the integration kernel reads

$$K(\chi; \chi_a, \chi_b) = \begin{cases} \frac{(\chi_b - \chi)(\chi - \chi_a)}{\chi(\chi_b - \chi_a)} & \text{if } \chi_a \leq \chi \leq \chi_b, \\ 0 & \text{otherwise.} \end{cases} \quad (2.9)$$

The expression of the LOS shear then follows from eq. (2.4), implying that γ_{LOS} derives from the potential $\Psi_{\text{LOS}} = \Psi_{\text{od}} + \Psi_{\text{os}} - \Psi_{\text{ds}}$; in other words,

$$\gamma_{\text{LOS}} = \frac{1}{2} \bar{\partial}^2 \Psi_{\text{LOS}}, \quad (2.10)$$

$$\Psi_{\text{LOS}}(\hat{\mathbf{u}}, \chi_d, \chi_s) = 2 \int_0^\infty \frac{d\chi}{\chi} K_{\text{LOS}}(\chi; \chi_d, \chi_s) \Phi(\eta_0 - \chi, \chi, \hat{\mathbf{u}}), \quad (2.11)$$

$$K_{\text{LOS}}(\chi; \chi_d, \chi_s) = \begin{cases} \frac{\chi_s - \chi}{\chi_s} + \frac{\chi_d - \chi}{\chi_d} & \text{if } 0 \leq \chi \leq \chi_d, \\ \frac{\chi_s - \chi}{\chi_s} - \frac{(\chi - \chi_d)(\chi_s - \chi)}{\chi(\chi_s - \chi_d)} & \text{if } \chi_d \leq \chi \leq \chi_s, \\ 0 & \text{if } \chi_s \leq \chi. \end{cases} \quad (2.12)$$

In the above, χ_d and χ_s respectively denote the comoving distances from the observer to the deflector and to the source, in a strong-lensing system.

For comparison, the usual weak-lensing shear γ affecting the apparent shapes of galaxies corresponds to the (os) part of the above only. In other words, if a galaxy at comoving distance χ_* is observed in the direction $\hat{\mathbf{u}}$, then its apparent (complex) ellipticity reads

$$\varepsilon = \varepsilon_0 + \gamma(\hat{\mathbf{u}}, \chi_*), \quad (2.13)$$

where ε_0 denotes the intrinsic ellipticity that would be observed in the absence of lensing, and

$$\gamma(\hat{\mathbf{u}}, \chi_*) = \frac{1}{2} \bar{\partial}^2 \Psi(\hat{\mathbf{u}}, \chi_*), \quad \Psi(\hat{\mathbf{u}}, \chi_*) = 2 \int_0^\infty \frac{d\chi}{\chi} K(\chi; 0, \chi_*) \Phi(\eta_0 - \chi, \chi, \hat{\mathbf{u}}). \quad (2.14)$$

3 Cosmology with the line-of-sight shear

As seen in subsec. 2.3, in particular with eq. (2.11), the LOS shear directly depends on the gravitational field along the LOS of a strong-lens system. As such, it is a potential cosmological probe. In this section, we present a method to extract cosmological information from the LOS shear, inspired from the standard methods of current galaxy surveys.

3.1 A six times two-point correlation scheme

Stage-IV galaxy surveys, such as *Euclid* [8] or the Legacy Survey of Space and Time (LSST) of the Vera C. Rubin Observatory [9] will measure the position, redshift, and apparent ellipticity of $\mathcal{O}(10^9)$ galaxies. Cosmological information is usually extracted from the data with the 3×2 pt correlation method, which consists of: (1) the two-point correlation of galaxy positions, called *galaxy clustering*, $\text{PP} \sim \langle \delta_g \times \delta_g \rangle$, where δ_g denotes the density contrast of galaxy number counts; (2) the two-point correlation of galaxy ellipticities ε , called *cosmic shear*, $\text{EE} \sim \langle \varepsilon \times \varepsilon \rangle$; and (3) the cross-correlation of galaxy shapes and positions, called *galaxy-galaxy lensing*, $\text{EP} \sim \langle \varepsilon \times \delta_g \rangle$.

Thanks to their wide sky coverage and the quality of their imaging, these surveys are also expected to deliver an unprecedentedly large sample of $\mathcal{O}(10^5)$ strong lenses [11, 36, 37].

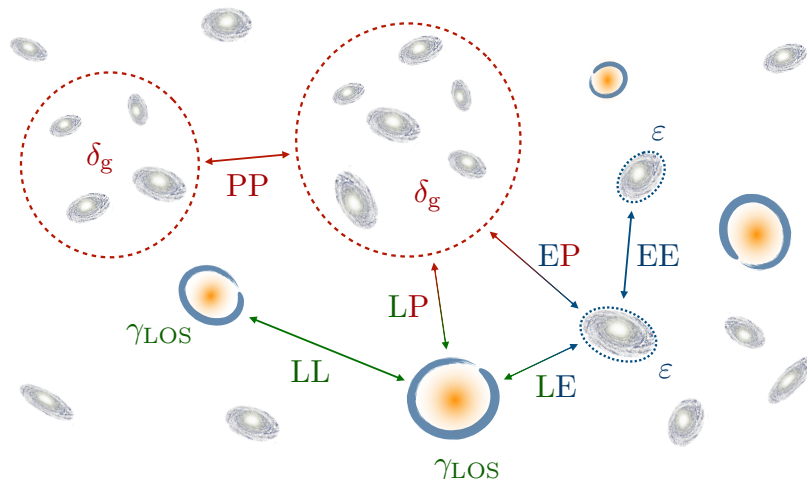


Figure 2. Stage-IV galaxy surveys will observe the position and apparent ellipticity ε of more than a billion galaxies, and more than a hundred thousand strong lenses, from which we should be able to measure the LOS shear γ_{LOS} . Measuring all the two-point correlation functions of the galaxy position (P), ellipticity (E) and the LOS shear of lenses (L) defines the $6 \times 2\text{pt}$ correlation scheme.

If the LOS shear is measured from a significant fraction of this sample, then it could be used as a cosmological probe. By analogy with cosmic shear, we may naturally consider the two-point correlation of the LOS shear, $\text{LL} \sim \langle \gamma_{\text{LOS}} \times \gamma_{\text{LOS}} \rangle$; then, since the LOS shear has the same physical origin as the shear applied to galaxies, we may add the cross-correlation between LOS shear and galaxy ellipticities, $\text{LE} \sim \langle \gamma_{\text{LOS}} \times \varepsilon \rangle$; and finally, by analogy with galaxy-galaxy lensing, signal should be present in the cross-correlation between LOS shear and galaxy positions, $\text{LP} \sim \langle \gamma_{\text{LOS}} \times \delta_g \rangle$, because galaxies trace the matter distribution whose gravitational effect is responsible for γ_{LOS} . As summarised in fig. 2, the inclusion of strong lenses would promote the $3 \times 2\text{pt}$ method to a $6 \times 2\text{pt}$ method: EE, EP, PP, LL, LE, LP.

Albeit ten thousand times less abundant than galaxies, strong lenses will result in much more precise measurements of the (LOS) shear. Indeed, following the results of [20], the typical uncertainty on individual measurements of γ_{LOS} is expected to be $\Delta\gamma_{\text{LOS}} \approx 0.01 \sim \gamma_{\text{LOS}}$, leading to a signal-to-noise ratio (SNR) of order unity for individual measurements. For comparison, the intrinsic ellipticity of galaxies, responsible for shape noise in cosmic shear, is $\Delta\gamma = \varepsilon_0 \approx 0.3 \sim 30 \times \gamma$, which means an SNR of about 3% for individual measurements [7].

In addition, the LOS shear of strong lenses is expected to be subject to very different systematics compared to the standard $3 \times 2\text{pt}$ observables. For instance, it should be immune to intrinsic alignments. For these reasons, the $6 \times 2\text{pt}$ correlation method has the potential to significantly enhance the cosmological power of stage-IV galaxy surveys by exploiting the synergy of weak-lensing and strong-lensing probes.

Let us mention for completeness that a first attempt to combine weak and strong lensing was performed by ref. [38] in the COSMOS field. The authors of that work considered a cross-correlation analogous to LE, but since they modelled only 3 out of the 67 lenses of the HST/COSMOS catalogue [39],³ no signal could be measured. Note also that the concepts of minimal LOS model and LOS shear were not yet established at the time, which could explain the mismatch between the weak-lensing and strong-lensing shears observed by ref. [38].

³The more recent COSMOS-Web Lens Survey catalogue [40–42] consists of over 100 strong lens candidates.

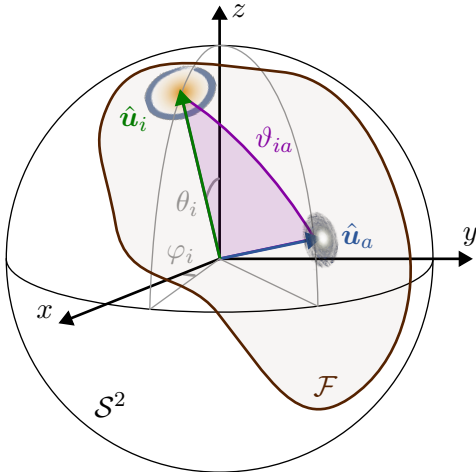


Figure 3. Schematic summary of the galaxy survey setup and some of our notation. The survey footprint $\mathcal{F} \subset \mathcal{S}^2$ contains G galaxies observed in directions $\hat{\mathbf{u}}_a$, and L strong lenses observed in directions $\hat{\mathbf{u}}_i$. A direction $\hat{\mathbf{u}}$ is parameterised by its polar coordinates (θ, φ) ; the angle formed by the directions $\hat{\mathbf{u}}_i, \hat{\mathbf{u}}_a$ is denoted with ϑ_{ia} .

3.2 Estimators of the LOS correlation functions

In this article, we shall focus on the three new correlation functions compared to the standard 3×2 pt method, namely LL, LE and LP. The first step is to define their estimators.

Setup Consider a galaxy survey with footprint $\mathcal{F} \subset \mathcal{S}^2$, where \mathcal{S}^2 is the celestial two-sphere; we denote with Ω the survey area, that is the total solid angle covered by \mathcal{F} . We assume that the survey contains a total number of G galaxies and L lenses, and we denote with $n_G \equiv G/\Omega, n_L \equiv L/\Omega$ the corresponding angular densities.⁴

Notation We denote with $\hat{\mathbf{u}} \in \mathcal{S}^2$ a direction in the celestial sphere, which may also be parameterised by its polar coordinates (θ, φ) with respect to an arbitrary system of axes. In order to optimise the readability of the subsequent equations, indices will depend on the objects that they refer to, as summarised in table 1. We denote with $\vartheta_{\mu\nu}$ the angle formed by any two directions $\hat{\mathbf{u}}_\mu, \hat{\mathbf{u}}_\nu \in \mathcal{S}^2$. See fig. 3 for an illustrated summary.

Tomographic bins If the galaxy sample is large enough, we may divide it into T tomographic (redshift) bins, in which case G_A will denote the number of galaxies in the A^{th} bin, and $n_A \equiv G_A/\Omega$. We shall order the set of galaxy indices per redshift bin as

$$\left\{ \underbrace{1, 2, \dots, G_1}_{\mathcal{G}_1}, \underbrace{G_1 + 1, G_1 + 2, \dots, G_1 + G_2}_{\mathcal{G}_2}, \dots, \underbrace{G - G_T + 1, G - G_T + 2, \dots, G}_{\mathcal{G}_T} \right\}, \quad (3.1)$$

so that \mathcal{G}_A denotes the set of galaxies in the A^{th} tomographic bin, with $|\mathcal{G}_A| = G_A$.

3.2.1 Autocorrelation of the LOS shear (LL)

The estimators of the LOS shear two-point correlation functions are defined similarly to the standard cosmic shear estimators [43].

Noise First of all, in order to account for the uncertainty of individual LOS shear measurements, we introduce an additive noise term η_{LOS} which will encode both instrumental errors and systematics. Specifically, we shall write the *measured* value of the LOS shear on lens i as

$$\hat{\gamma}_i^{\text{LOS}} = \gamma_i^{\text{LOS}} + \eta_i^{\text{LOS}}, \quad (3.2)$$

⁴For example, the *Euclid* survey is expected to observe $G = 2 \times 10^9$ photometric galaxies and $L = 1.7 \times 10^5$ galaxy-scale strong lenses over $\Omega = 15\,000 \text{ deg}^2$; this implies $n_G = 40 \text{ arcmin}^{-2}$ and $n_L = 11 \text{ deg}^{-2}$.

Alphabet	Position in alphabet	Letter case	Occurrences	Refers to
Latin	beginning	lowercase	a, b, c, d	galaxy
Latin	beginning	uppercase	A, B, C, D	tomographic bin
Latin	middle	lowercase	i, j, k, l	lens
Greek	beginning	lowercase	α, β	angular bin
Greek	middle	lowercase	μ, ν, ρ, σ	generic index

Table 1. Convention for indices throughout the article.

where γ_i^{LOS} is the *true* LOS shear field as defined in subsec. 2.3 and evaluated at lens i . Note the analogy between η_{LOS} and the intrinsic-ellipticity term ε_0 in cosmic shear; in that sense η_{LOS} may be considered as a kind of LOS shape noise. We shall assume throughout the article that LOS shear measurements are unbiased (η_{LOS} vanishes on average), and that the LOS noises of distinct lenses are independent.

Plus and cross polarisations Correlation functions aim to identify alignment patterns in pairs of LOS shear measurements. For a pair (ij) of lenses, the relative orientation of their LOS shear is conveniently expressed in terms of a basis adapted to the pair. The construction goes as follows (see fig. 4, left panel). Consider the great arc that connects $\hat{\mathbf{u}}_i$ to $\hat{\mathbf{u}}_j$, and denote with $\hat{\mathbf{t}}_{ij}$ the unit vector, tangent to that curve, oriented from i to j . A second unit vector tangent to \mathcal{S}^2 at $\hat{\mathbf{u}}_i$ may be defined as $\hat{\mathbf{n}}_{ij} \equiv \hat{\mathbf{u}}_i \times \hat{\mathbf{t}}_{ij}$. Together, these vectors form an orthonormal basis $(\hat{\mathbf{t}}_{ij}, \hat{\mathbf{n}}_{ij})$ of $T_i\mathcal{S}^2$ that is rotated by an angle ψ_{ij} with respect to the coordinate basis $(\hat{\mathbf{e}}_\theta, \hat{\mathbf{e}}_\varphi)$. We then define the *plus and cross polarisations* of the LOS shear of lens i as its real and imaginary parts when expressed in that basis; since γ_{LOS} is implicitly decomposed on the coordinate basis, we have

$$\hat{\gamma}_{+ij}^{\text{LOS}} + i\hat{\gamma}_{\times ij}^{\text{LOS}} = \hat{\gamma}_i^{\text{LOS}} e^{-2i\psi_{ij}} . \quad (3.3)$$

We stress that, in the notation $\gamma_{p ij}^{\text{LOS}}$, $p \in \{+, \times\}$, the indices i and j are not interchangeable, because the former indicates the lens whose LOS shear is being measured. The same construction may be performed for lens j , thereby leading to

$$\hat{\gamma}_{+ji}^{\text{LOS}} + i\hat{\gamma}_{\times ji}^{\text{LOS}} = \hat{\gamma}_j^{\text{LOS}} e^{-2i\psi_{ji}} . \quad (3.4)$$

The rotation angles ψ_{ij} and ψ_{ji} are different in general.⁵ However, when $\vartheta_{ij} \ll 1$ – a condition typically satisfied in practice – the tangent spaces $T_i\mathcal{S}^2, T_j\mathcal{S}^2$ coincide and we have $\psi_{ij} \approx \psi_{ji}$.

Simple estimator for the LOS shear autocorrelation Consider all pairs (ij) of lenses, and sort them according to their angular separation ϑ_{ij} . In practice, we introduce angular bins (\mathcal{P}_α) with limits (ϑ_α) ; \mathcal{P}_α is defined as the set of pairs of lenses (ij) such that $\vartheta_\alpha \leq \vartheta_{ij} < \vartheta_{\alpha+1}$. Since the LOS shear is a complex (or spin-two) quantity, two complementary correlation functions may be measured in the α^{th} angular bin, namely the plus and minus (\pm) correlations. Estimators for these may be defined as

$$(\widehat{\text{LL}})_\alpha^\pm \equiv \frac{1}{|\mathcal{P}_\alpha|} \sum_{(ij) \in \mathcal{P}_\alpha} \left(\hat{\gamma}_{+ij}^{\text{LOS}} \hat{\gamma}_{+ji}^{\text{LOS}} \pm \hat{\gamma}_{\times ij}^{\text{LOS}} \hat{\gamma}_{\times ji}^{\text{LOS}} \right), \quad (3.6)$$

⁵The explicit expression of the relevant phase, in terms of the polar coordinates of $\hat{\mathbf{u}}_i$ and $\hat{\mathbf{u}}_j$, reads

$$e^{-2i\psi_{ij}} = \frac{[\cos \theta_i \sin \theta_j \cos(\varphi_j - \varphi_i) - \sin \theta_i \cos \theta_j - i \sin \theta_j \sin(\varphi_j - \varphi_i)]^2}{[\cos \theta_i \sin \theta_j \cos(\varphi_j - \varphi_i) - \sin \theta_i \cos \theta_j]^2 + \sin^2 \theta_j \sin^2(\varphi_j - \varphi_i)}, \quad (3.5)$$

which is manifestly not symmetric under the exchange of i and j .

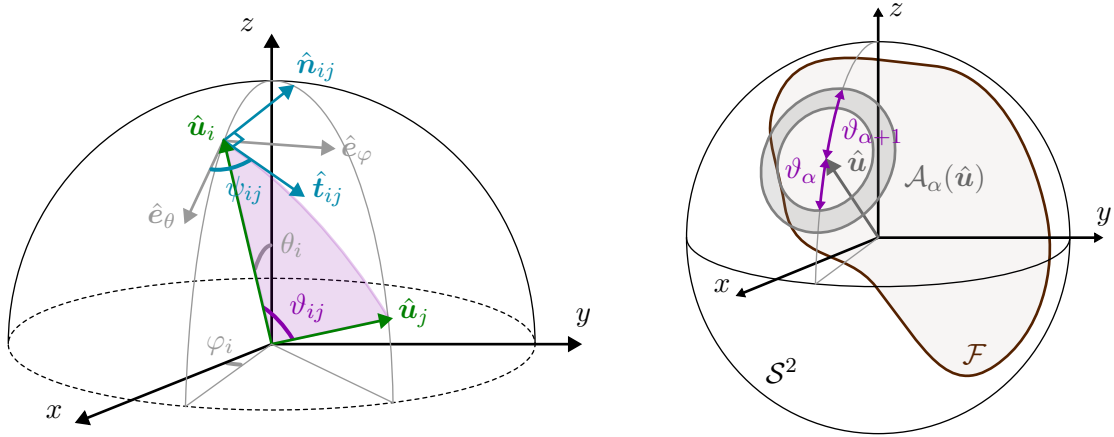


Figure 4. *Left panel:* Two directions $\hat{\mathbf{u}}_i$ and $\hat{\mathbf{u}}_j$ on the two-sphere form an angle ϑ_{ij} . The figure shows two orthogonal bases for the tangent space $T_i\mathcal{S}^2$ at $\hat{\mathbf{u}}_i$: the coordinate basis ($\hat{\mathbf{e}}_\theta, \hat{\mathbf{e}}_\varphi$) in grey; and the (ij) -basis ($\hat{\mathbf{t}}_{ij}, \hat{\mathbf{n}}_{ij}$) in turquoise. In the latter, $\hat{\mathbf{t}}_{ij}$ is tangent to the great circle connecting $\hat{\mathbf{u}}_i$ to $\hat{\mathbf{u}}_j$, and $\hat{\mathbf{n}}_{ij} \equiv \hat{\mathbf{u}}_i \times \hat{\mathbf{t}}_{ij}$. Both bases form an angle ψ_{ij} . The (ij) -basis is used to define the plus and cross polarisations of the shear for the couple of directions (ij) . *Right panel:* The annulus $\mathcal{A}_\alpha(\hat{\mathbf{u}})$ is defined by the points of \mathcal{S}^2 that form an angle $\vartheta \in [\vartheta_\alpha, \vartheta_{\alpha+1})$ with $\hat{\mathbf{u}}$. Its intersection with the survey footprint, $\mathcal{A}_\alpha(\hat{\mathbf{u}}) \cap \mathcal{F}$, represents the α^{th} angular bin about $\hat{\mathbf{u}}$.

where $|\mathcal{P}_\alpha|$ is the number of terms in the sum, that is the number of pairs (ij) in \mathcal{P}_α . A more general definition could involve different weights for the lenses in the sum.

Alternative expression For later convenience, we shall rewrite eq. (3.6) as follows, so as to make it formally closer to LE, LP estimators that we define in the next paragraphs,

$$\widehat{(\mathbb{L}\mathbb{L})}_\alpha^\pm = \widehat{(\mathbb{L}^+\mathbb{L}^+)}_\alpha \pm \widehat{(\mathbb{L}^\times\mathbb{L}^\times)}_\alpha \quad (3.7)$$

$$\widehat{(\mathbb{L}^p\mathbb{L}^p)}_\alpha = \frac{1}{L^2} \sum_{i=1}^L \sum_{j=1}^L W_{ij}^\alpha \hat{\gamma}_{p|ij}^{\text{LOS}} \hat{\gamma}_{p|ji}^{\text{LOS}} \quad \text{for } p \in \{+, \times\}. \quad (3.8)$$

In the above, we have explicitly split $\widehat{(\mathbb{L}\mathbb{L})}_\alpha^\pm$ into their two elementary polarisation terms. Furthermore, we have turned the sum over pairs $(ij) \in \mathcal{P}_\alpha$ into a sum over all lenses in the sample by introducing the weighted window function

$$W_{ij}^\alpha \equiv \frac{L^2}{|\mathcal{P}_\alpha|} \times \begin{cases} 1 & \text{if } \vartheta_\alpha \leq \vartheta_{ij} < \vartheta_{\alpha+1}, \\ 0 & \text{otherwise, or if } i = j. \end{cases} \quad (3.9)$$

The prefactor in the above expression may be simplified by estimating the number of pairs $|\mathcal{P}_\alpha|$ in the α^{th} bin. Let $\mathcal{A}_\alpha(\hat{\mathbf{u}})$ denote the annulus spanned by the points in \mathcal{S}^2 forming, with $\hat{\mathbf{u}}$, an angle between ϑ_α and $\vartheta_{\alpha+1}$ (see fig. 4, right panel). If a lens is observed at $\hat{\mathbf{u}}$, then $\mathcal{A}_\alpha(\hat{\mathbf{u}})$ is the region where other lenses can make, with the former one, a pair in \mathcal{P}_α . Let $\Omega_\alpha(\hat{\mathbf{u}})$ be the solid angle covered by $\mathcal{A}_\alpha(\hat{\mathbf{u}}) \cap \mathcal{F}$. For a full-sky survey ($\mathcal{F} = \mathcal{S}^2$), Ω_α does not depend on $\hat{\mathbf{u}}$, in which case $|\mathcal{P}_\alpha| = L \times n_L \Omega_\alpha = L^2 \Omega_\alpha / \Omega$. In a survey that does not cover the entire celestial sphere, the exact result for $|\mathcal{P}_\alpha|$ would depend on the survey geometry. Since most of the cosmological signal is carried by small angular separations ($\vartheta \ll 1$), we shall neglect such boundary effects in the remainder of this article – this is the *pseudo-full-sky*

approximation. When substituting the expression for $|\mathcal{P}_\alpha|$ in eq. (3.9), we obtain

$$W_{\mu\nu}^\alpha = \frac{\Omega}{\Omega_\alpha} \times \begin{cases} 1 & \text{if } \vartheta_\alpha \leq \vartheta_{\mu\nu} < \vartheta_{\alpha+1}, \\ 0 & \text{otherwise, or if } \mu = \nu. \end{cases} \quad (3.10)$$

In this new expression (3.10) of the weight function, the number of lenses L has disappeared, which makes it independent of the nature of the objects involved in the pairs; this is why we used generic indices μ, ν which may refer to either lenses or galaxies.

3.2.2 Cross-correlation of LOS shear and galaxy ellipticity (LE)

The estimator of the cross-correlation of the LOS shear with the apparent ellipticity of galaxies is almost identical to that of the LOS shear autocorrelation. The difference is that we should now consider pairs of lenses i and galaxies a rather than pairs of lenses. Averaging over a large number of pairs is expected to extract the relative alignment of the LOS shear and standard shear by removing the contribution of both noise and galaxy intrinsic ellipticities.

Just like γ_{LOS} , the apparent (complex) ellipticity ε_a of galaxy a may be decomposed into plus and cross polarisations when forming a pair with lens i ,

$$\varepsilon_{+ai} + i\varepsilon_{\times ai} = \varepsilon_a e^{-2i\psi_{ai}}, \quad (3.11)$$

where ψ_{ai} is defined as in fig. 4. Following the same construction as in subsubsection 3.2.1, we get the following estimators for the two LE correlation functions,

$$\widehat{(\text{LE}_A)_\alpha^\pm} = \widehat{(\text{L}^+\text{E}_A^+)_\alpha} \pm \widehat{(\text{L}^\times\text{E}_A^\times)_\alpha} \quad (3.12)$$

$$\widehat{(\text{L}^p\text{E}_A^p)_\alpha} = \frac{1}{LG_A} \sum_{i=1}^L \sum_{a \in \mathcal{G}_A} W_{ia}^\alpha \hat{\gamma}_{pia}^{\text{LOS}} \varepsilon_{pai}, \quad \text{for } p \in \{+, \times\}. \quad (3.13)$$

In the above, we have assumed that the galaxy sample is large enough to be divided into tomographic redshift bins; $\widehat{(\text{LE}_A)_\alpha^\pm}$ thus estimates the correlations between the strong lensing sample and the A^{th} tomographic sample, comprising G_A galaxies.

3.2.3 Cross-correlation of LOS shear and galaxy positions (LP)

The cross-correlation of LOS shear and galaxy positions is analogous to galaxy–galaxy lensing in the usual 3×2 pt analysis. It is based on the fact that galaxies, as matter overdensities, produce tangential shear around them. The LP estimator consists in extracting that information by summing the $+$ polarisation of the LOS shear (the \times polarisation vanishes on average) for all lens–galaxy pairs (ia) within a certain angular bin α ,

$$\widehat{(\text{L}^+\text{P}_A)_\alpha} = \frac{1}{LG_A} \sum_{i=1}^L \sum_{a \in \mathcal{G}_A} W_{ia}^\alpha \hat{\gamma}_{+ia}^{\text{LOS}}. \quad (3.14)$$

Just like in the LE case, we have assumed that the galaxy sample is large enough to be divided into tomographic redshift bins. Note that a tangential shear corresponds to $\gamma_+^{\text{LOS}} < 0$, so *the expectation value of LP will be negative.*

3.3 Expectation values of the estimators in Λ CDM

Let us now compute the expectation value of the estimators defined in subsec. 3.2, that is, the signal that we aim to detect. Before we perform the actual calculation, we must specify what *expectation value* really means in the present context.

3.3.1 Three distinct notions of average

In our current understanding of cosmology, randomness in the sky originates from the quantum fluctuations of the physical fields that eventually lead to cosmic structures via gravitational collapse. Technically speaking, this concept is implemented by treating the gravitational potential Φ – and all fields that derive from it, such as the density contrast δ and the peculiar velocity field – as Gaussian random fields.

In this context, an expectation value means an average over realisations of those fields, i.e. a theoretical average over realisations of the Universe. For the observables defined in subsec. 3.2, jumping from one realisation of the Universe to another has two consequences: on the one hand, the density and shear fields fluctuate; on the other hand, the positions and properties of their tracers (galaxies and lenses) change too. In practice, it is convenient to explicitly distinguish these two effects as *cosmic averaging* and *sample averaging*.

Cosmic averaging $\langle \dots \rangle$ will refer to averages over realisations \mathcal{U} of the *macroscopic* properties of the Universe, i.e. the underlying fields. It is the usual notion of average involved in, e.g., the definition of the matter power spectrum.

Galaxy-sample averaging $[\dots]$ will be the average over the properties of all the galaxies in the sample, given a realisation \mathcal{U} of the macroscopic properties of the Universe (in particular the density field). We shall parameterise a galaxy with (i) its redshift z ; (ii) its angular position $\hat{\mathbf{u}}$; and (iii) its intrinsic complex ellipticity ε_0 , which we gather into the quintuplet $\mathbf{\Gamma} = (z, \hat{\mathbf{u}}, \varepsilon_0)$. For an observable X that depends on the sample of G galaxies, the galaxy-sample average then reads

$$[X](\mathcal{U}) \equiv \left[\prod_{A=1}^T \prod_{a \in \mathcal{G}_A} \int d^5 \mathbf{\Gamma}_a p_A(\mathbf{\Gamma}_a | \mathcal{U}) \right] X(\mathbf{\Gamma}_1, \dots, \mathbf{\Gamma}_G), \quad (3.15)$$

where $p_A(\mathbf{\Gamma} | \mathcal{U})$ is the probability density function (PDF) of $\mathbf{\Gamma}$ in the A^{th} tomographic bin, given the cosmic realisation \mathcal{U} .

Let us be more explicit and decompose $p_A(\mathbf{\Gamma} | \mathcal{U})$ into elementary components:

$$p_A(\mathbf{\Gamma} | \mathcal{U}) d^5 \mathbf{\Gamma} = f_A(z) dz \times [1 + b(z) \delta(z, \hat{\mathbf{u}}; \mathcal{U})] \frac{d^2 \hat{\mathbf{u}}}{\Omega} \times p(\varepsilon_0; z) d^2 \varepsilon_0. \quad (3.16)$$

In eq. (3.16), $f_A(z)$ denotes the normalised redshift selection function of the survey in the A^{th} bin, which we assume to coincide with the *observed* redshift distribution in that bin. For a given line of sight $\hat{\mathbf{u}}$, this is modulated by the actual overdensity in galaxy number counts, which we assume to be linearly biased by $b(z)$ with respect to the total matter density contrast δ . Finally, $p(\varepsilon_0; z)$ denotes the PDF of the intrinsic ellipticity of galaxies at z , which we assume to be independent of $\hat{\mathbf{u}}$; we shall also neglect intrinsic alignments in this work.

Lens-sample averaging [...] will be the average over the relevant properties of strong lenses in the sample given a macroscopic realisation \mathcal{U} . We shall parameterise a lens with (i) a pair of redshifts $\mathbf{Z} = (z_d, z_s)$, which denote respectively the redshift of the main deflector and source of the system; (ii) its position $\hat{\mathbf{u}}$ in the sky; and (iii) the error η_{LOS} on the measurement of the LOS shear in that system, as introduced in eq. (3.2). We gather the aforementioned lens parameters into a sextuplet $\mathbf{\Lambda} = (\mathbf{Z}, \hat{\mathbf{u}}, \eta_{\text{LOS}})$. For an observable X that depends on a sample of L lenses, the lens-sample average then reads

$$[X](\mathcal{U}) \equiv \left[\prod_{i=1}^L \int d^6 \mathbf{\Lambda}_i p(\mathbf{\Lambda}_i | \mathcal{U}) \right] X(\mathbf{\Lambda}_1, \dots, \mathbf{\Lambda}_L), \quad (3.17)$$

where $p(\mathbf{\Lambda} | \mathcal{U})$ is the PDF of $\mathbf{\Lambda}$ in the cosmic realisation \mathcal{U} . In the following, we shall neglect lens clustering in the expression of $p(\mathbf{\Lambda} | \mathcal{U})$, which implies that the angular positions of lenses are simply Poisson-distributed. We assume, besides, that the noise η_{LOS} on LOS shear measurements is independent of the lens's position in the sky. Therefore,

$$p(\mathbf{\Lambda}) d^6 \mathbf{\Lambda} = p(\mathbf{Z}) d^2 \mathbf{Z} \times \frac{d^2 \hat{\mathbf{u}}}{\Omega} \times p(\eta_{\text{LOS}}; \mathbf{Z}) d^2 \eta_{\text{LOS}}, \quad (3.18)$$

where the dependence on the cosmic macroscopic realisation \mathcal{U} has dropped. As a consequence, lens-sample averaging and cosmic averaging commute in this framework.

This approximation is justified because none of the observables that we are interested in rely on lens clustering. In contrast, the LP cross-correlation directly depends on the fact that galaxies are not homogeneously distributed in the sky. Here, neglecting lens clustering is analogous to neglecting source clustering in cosmic shear, which leads to a small, higher-order, bias whose investigation is left for future work.⁶

3.3.2 The LL signal

Following the above, the expectation value of the estimator (3.7) of the autocorrelation function of LOS shear reads

$$(\text{LL})_{\alpha}^{\pm} \equiv \left\langle \left[(\widehat{\text{LL}})_{\alpha}^{\pm} \right] \right\rangle. \quad (3.19)$$

The averaging operator [...] does not appear because the galaxy sample is not involved in $(\widehat{\text{LL}})_{\alpha}^{\pm}$. Since the latter is a combination of the (++) and (××) correlation functions, we may work with those and start by evaluating their lens-sample average:

$$\left[(\widehat{\text{LP}^{\text{LP}}})_{\alpha} \right](\mathcal{U}) = \left[\prod_{i'=1}^L \int d^6 \mathbf{\Lambda}_{i'} p(\mathbf{\Lambda}_{i'}) \right] \frac{1}{L^2} \sum_{i=1}^L \sum_{j=1}^L W_{ij}^{\alpha} \hat{\gamma}_{\text{p}ij}^{\text{LOS}} \hat{\gamma}_{\text{p}ji}^{\text{LOS}} \quad (3.20)$$

$$= \int d^6 \mathbf{\Lambda}_1 p(\mathbf{\Lambda}_1) \int d^6 \mathbf{\Lambda}_2 p(\mathbf{\Lambda}_2) W_{12}^{\alpha} \hat{\gamma}_{\text{p}12}^{\text{LOS}} \hat{\gamma}_{\text{p}21}^{\text{LOS}} \quad (3.21)$$

$$= \int d^2 \mathbf{Z}_1 p(\mathbf{Z}_1) \int d^2 \mathbf{Z}_2 p(\mathbf{Z}_2) \int_{\mathcal{F}} \frac{d^2 \hat{\mathbf{u}}_1}{\Omega} \int_{\mathcal{F}} \frac{d^2 \hat{\mathbf{u}}_2}{\Omega} W_{12}^{\alpha} \hat{\gamma}_{\text{p}12}^{\text{LOS}} \hat{\gamma}_{\text{p}21}^{\text{LOS}}. \quad (3.22)$$

To obtain eq. (3.21), we have noticed that all L^2 terms in the double sum over i and j were identical due to the integration over $\mathbf{\Lambda}_i, \mathbf{\Lambda}_j$, which can be freely renamed $\mathbf{\Lambda}_1, \mathbf{\Lambda}_2$. This is possible because W_{ij}^{α} forbids the case $i = j$, which would lead to different expressions. In

⁶PF thanks Calum Murray for bringing this up during the *Rencontres de Moriond* in 2024.

eq. (3.22), we integrated over the noise term η_{LOS} , which does not contribute if we assume that the noise of different lenses is uncorrelated and averages to zero:

$$\int d^2\eta_{\text{LOS}} p(\eta_{\text{LOS}}; \mathbf{Z}) \eta_{\text{LOS}} = 0. \quad (3.23)$$

We then apply the cosmic-averaging operator $\langle \dots \rangle$. Since the only \mathcal{U} -dependence in the above lies in the LOS shear field γ_{LOS} , we may focus on

$$\langle \gamma_{\text{p12}}^{\text{LOS}} \gamma_{\text{p21}}^{\text{LOS}} \rangle = \begin{cases} \langle \text{Re} [\gamma_{\text{LOS}}(\hat{\mathbf{u}}_1) e^{-2i\psi_{12}}] \text{Re} [\gamma_{\text{LOS}}(\hat{\mathbf{u}}_2) e^{-2i\psi_{21}}] \rangle & \text{if } p = +, \\ \langle \text{Im} [\gamma_{\text{LOS}}(\hat{\mathbf{u}}_1) e^{-2i\psi_{12}}] \text{Im} [\gamma_{\text{LOS}}(\hat{\mathbf{u}}_2) e^{-2i\psi_{21}}] \rangle & \text{if } p = \times. \end{cases} \quad (3.24)$$

Now, because of the principles of statistical homogeneity and isotropy of our Universe, these expectation values only depend on the angle ϑ_{12} formed by $\hat{\mathbf{u}}_1, \hat{\mathbf{u}}_2$. Besides, we shall work in the pseudo-full-sky approximation and neglect the boundary effects due to $\mathcal{F} \neq \mathcal{S}^2$. As a result, all values of $\hat{\mathbf{u}}_1$ in eq. (3.24) are equivalent and we may choose to place it at the North pole $\hat{\mathbf{u}}_1 = \hat{\mathbf{z}}$. This allows us to remove the integral over $\hat{\mathbf{u}}_1$ in eq. (3.22), while implying $\psi_{12} = \psi_{21} = 0$ (see fig. 4). Putting everything together, we finally get

$$\boxed{(\text{LL})_{\alpha}^{\pm} = \frac{2\pi}{\Omega_{\alpha}} \int_{\vartheta_{\alpha}}^{\vartheta_{\alpha+1}} d\vartheta \sin \vartheta \int d^2\mathbf{Z}_1 p(\mathbf{Z}_1) \int d^2\mathbf{Z}_2 p(\mathbf{Z}_2) (\text{LL})^{\pm}(\vartheta; \mathbf{Z}_1, \mathbf{Z}_2),} \quad (3.25)$$

with

$$\boxed{(\text{LL})^{+}(\vartheta; \mathbf{Z}_1, \mathbf{Z}_2) \equiv \langle \gamma_{\text{LOS}}(\hat{\mathbf{z}}; \mathbf{Z}_1) \gamma_{\text{LOS}}^*(\hat{\mathbf{u}}_{\vartheta}; \mathbf{Z}_2) \rangle,} \quad (3.26)$$

$$\boxed{(\text{LL})^{-}(\vartheta; \mathbf{Z}_1, \mathbf{Z}_2) \equiv \langle \gamma_{\text{LOS}}(\hat{\mathbf{z}}; \mathbf{Z}_1) \gamma_{\text{LOS}}(\hat{\mathbf{u}}_{\vartheta}; \mathbf{Z}_2) \rangle,} \quad (3.27)$$

where $\hat{\mathbf{u}}_{\vartheta} = (\vartheta, 0)$ is the unit vector in the (xz) -plane forming an angle ϑ with the North pole. In the expression of $\text{LL}^{\pm}(\vartheta; \mathbf{Z}_1, \mathbf{Z}_2)$, we used the statistical invariance under parity, which implies that $\langle \gamma_{+}^{\text{LOS}} \gamma_{\times}^{\text{LOS}} \rangle = 0$, in order to get rid of the real- and imaginary-part operators.

3.3.3 The LE signal

In the case of the cross-correlation between the LOS shear and the apparent shapes of galaxies, since both the lens and galaxy samples are involved, the expectation value is obtained by applying all three averaging operators defined in subsubsec. 3.3.1,

$$(\text{LE}_A)_{\alpha}^{\pm} \equiv \left\langle \left[\left[(\widehat{\text{LE}}_A)_{\alpha}^{\pm} \right] \right] \right\rangle. \quad (3.28)$$

The rest of the calculation is quite similar to the LL case. Taking the lens-sample and galaxy-sample averages in a cosmic realisation \mathcal{U} , we find

$$\begin{aligned} & \left[\left[(\widehat{\text{LPE}}_A^{\text{p}})_{\alpha} \right] \right] (\mathcal{U}) \\ &= \left[\prod_{i'=1}^L \int d^6\mathbf{\Lambda}_{i'} p(\mathbf{\Lambda}_{i'}) \right] \left[\prod_{A'=1}^T \prod_{a' \in \mathcal{G}_{A'}} \int d^5\mathbf{\Gamma}_{a'} p_{A'}(\mathbf{\Gamma}_{a'}) \right] \frac{1}{LG_A} \sum_{i=1}^L \sum_{a \in \mathcal{G}_A} W_{ia}^{\alpha} \hat{\gamma}_{pia}^{\text{LOS}} \varepsilon_{pai} \quad (3.29) \end{aligned}$$

$$= \int d^6\mathbf{\Lambda}_1 p(\mathbf{\Lambda}_1) \int d^5\mathbf{\Gamma}_2 p_A(\mathbf{\Gamma}_2) W_{12}^{\alpha} \hat{\gamma}_{p12}^{\text{LOS}} \varepsilon_{p21} \quad (3.30)$$

$$= \int d^2\mathbf{Z}_1 p(\mathbf{Z}_1) \int dz_2 f_A(z_2) \int_{\mathcal{F}} \frac{d^2\hat{\mathbf{u}}_1}{\Omega} \int_{\mathcal{F}} \frac{d^2\hat{\mathbf{u}}_2}{\Omega} W_{12}^{\alpha} \underbrace{[1 + b(z_2)\delta(z_2, \hat{\mathbf{u}}_2)]}_{\approx 1} \gamma_{p12}^{\text{LOS}} \gamma_{p21}. \quad (3.31)$$

When going from eq. (3.30) to eq. (3.31), we substituted the expressions (3.2) and (2.13) of ε and $\hat{\gamma}_{\text{LOS}}$, and we used the assumption that ε_0 and η_{LOS} average to zero and are uncorrelated. Furthermore, the galaxy overdensity $b_A \delta$ can be neglected here because γ and γ_{LOS} are already first-order terms in cosmological perturbations.

Averaging eq. (3.31) over cosmic realisations, exploiting statistical homogeneity and isotropy just like the LL case, finally yields

$$\boxed{(\text{LE}_A)_\alpha^\pm = \frac{2\pi}{\Omega_\alpha} \int_{\vartheta_\alpha}^{\vartheta_{\alpha+1}} d\vartheta \sin \vartheta \int d^2 \mathbf{Z}_1 p(\mathbf{Z}_1) \int dz_2 f_A(z_2) (\text{LE})^\pm(\vartheta; \mathbf{Z}_1, z_2) ,} \quad (3.32)$$

with

$$\boxed{(\text{LE})^+(\vartheta; \mathbf{Z}_1, z_2) = \langle \gamma_{\text{LOS}}(\hat{\mathbf{z}}; \mathbf{Z}_1) \gamma^*(\hat{\mathbf{u}}_\vartheta; z_2) \rangle ,} \quad (3.33)$$

$$\boxed{(\text{LE})^-(\vartheta; \mathbf{Z}_1, z_2) \equiv \langle \gamma_{\text{LOS}}(\hat{\mathbf{z}}; \mathbf{Z}_1) \gamma(\hat{\mathbf{u}}_\vartheta; z_2) \rangle .} \quad (3.34)$$

3.3.4 The LP signal

The expectation value of the cross-correlation between LOS shear and galaxy positions reads

$$(\text{L}^+\text{P}_A)_\alpha \equiv \left\langle \left[\widehat{(\text{L}^+\text{P}_A)_\alpha} \right] \right\rangle . \quad (3.35)$$

Applying the sample-averaging operators yields

$$\begin{aligned} & \left[\widehat{(\text{L}^+\text{P}_A)_\alpha} \right] (\mathcal{U}) \\ &= \left[\prod_{i'=1}^L \int d^6 \Lambda_{i'} p(\Lambda_{i'}) \right] \left[\prod_{A'=1}^T \prod_{a'=1}^{G_{A'}} \int d^5 \Gamma_{a'} p_{A'}(\Gamma_{a'}) \right] \frac{1}{LG_A} \sum_{i=1}^L \sum_{a=1}^{G_A} W_{ia}^\alpha \hat{\gamma}_{+ia}^{\text{LOS}} \end{aligned} \quad (3.36)$$

$$= \int d^6 \Lambda_1 p(\Lambda_1) \int d^5 \Gamma_2 p_A(\Gamma_2) W_{12}^\alpha \hat{\gamma}_{+12}^{\text{LOS}} \quad (3.37)$$

$$= \int d^2 \mathbf{Z}_1 p(\mathbf{Z}_1) \int dz_2 f_A(z_2) \int_{\mathcal{F}} \frac{d^2 \hat{\mathbf{u}}_1}{\Omega} \int_{\mathcal{F}} \frac{d^2 \hat{\mathbf{u}}_2}{\Omega} W_{12}^\alpha [1 + b(z_2) \delta(z_2, \hat{\mathbf{u}}_2)] \gamma_{+12}^{\text{LOS}} , \quad (3.38)$$

where, contrary to the LE case, we must keep the $b\delta$ term. Indeed, when applying the cosmic-average operator, the first term $\langle [1 + \dots] \gamma_{+12}^{\text{LOS}} \rangle$ in the integral vanishes due to statistical isotropy, and we are left with

$$(\text{L}^+\text{P}_A)_\alpha = \int d^2 \mathbf{Z}_1 p(\mathbf{Z}_1) \int dz_2 f_A(z_2) b(z_2) \int_{\mathcal{F}} \frac{d^2 \hat{\mathbf{u}}_1}{\Omega} \int_{\mathcal{F}} \frac{d^2 \hat{\mathbf{u}}_2}{\Omega} W_{12}^\alpha \langle \gamma_{+12}^{\text{LOS}} \delta(z_2, \hat{\mathbf{u}}_2) \rangle . \quad (3.39)$$

Exploiting again statistical homogeneity and isotropy, we obtain the final result

$$\boxed{(\text{L}^+\text{P}_A)_\alpha = \frac{2\pi}{\Omega_\alpha} \int_{\vartheta_\alpha}^{\vartheta_{\alpha+1}} d\vartheta \sin \vartheta \int d^2 \mathbf{Z}_1 p(\mathbf{Z}_1) \int dz_2 f_A(z_2) \text{L}^+\text{P}(\vartheta; \mathbf{Z}_1, z_2) ,} \quad (3.40)$$

with

$$\boxed{\text{L}^+\text{P}(\vartheta; \mathbf{Z}_1, z_2) \equiv \langle \gamma_{\text{LOS}}(\hat{\mathbf{z}}; \mathbf{Z}_1) b(z_2) \delta(\hat{\mathbf{u}}_\vartheta, z_2) \rangle .} \quad (3.41)$$

3.4 Angular power spectra

In modern cosmology, the properties of the matter distribution are commonly expressed in Fourier space, with the matter power spectrum, rather than in real space with the two-point correlation function. In that context, it is useful to express the angular power spectra associated with the correlation functions $(\text{LL})^\pm(\vartheta; \dots)$, $(\text{LE})^\pm(\vartheta; \dots)$ and $\text{L}^+\text{P}(\vartheta; \dots)$ in order to make cosmological predictions.

3.4.1 Spherical-harmonic decomposition

The expectation values of the three correlation functions LL, LE, and LP considered here involve three distinct fields on the two-sphere: $\delta(\hat{\mathbf{u}}, z)$, which is a scalar (or spin-zero) field; and $\gamma(\hat{\mathbf{u}}; z)$, $\gamma_{\text{LOS}}(\hat{\mathbf{u}}; \mathbf{Z})$ which are spin-two fields. The former may be decomposed over the standard spherical-harmonic basis $Y_{\ell m}(\hat{\mathbf{u}})$ according to

$$\delta(\hat{\mathbf{u}}, z) = \sum_{\ell=0}^{\infty} \sum_{m=-\ell}^{\ell} \delta_{\ell m}(z) Y_{\ell m}(\hat{\mathbf{u}}) , \quad \delta_{\ell m}(z) = \int_{S^2} d^2\hat{\mathbf{u}} Y_{\ell m}^*(\hat{\mathbf{u}}) \delta(\hat{\mathbf{u}}, z) , \quad (3.42)$$

and similarly for any other scalar field, such as the lensing potentials Ψ and Ψ_{LOS} . As for the shear fields, we must use spin-weighted spherical harmonics⁷

$$\gamma(\hat{\mathbf{u}}; z) = \sum_{\ell=0}^{\infty} \sum_{m=-\ell}^{\ell} \gamma_{\ell m}(z) {}_2Y_{\ell m}(\hat{\mathbf{u}}) , \quad \gamma_{\ell m}(z) = \int_{S^2} d^2\hat{\mathbf{u}} {}_2Y_{\ell m}^*(\hat{\mathbf{u}}) \gamma(\hat{\mathbf{u}}; z) ; \quad (3.44)$$

and similarly for $\gamma_{\text{LOS}}(\hat{\mathbf{u}}; \mathbf{Z})$, thereby defining harmonic coefficients $\gamma_{\ell m}^{\text{LOS}}(\mathbf{Z})$.

Because γ derives from the scalar lensing potential Ψ via eq. (2.14), their harmonic coefficients are related as

$$\gamma_{\ell m}(z) = \frac{1}{2} \sqrt{\frac{(\ell+2)!}{(\ell-2)!}} \Psi_{\ell m}(z) , \quad (3.45)$$

and similarly for the LOS shear and LOS potential.

We can then define the angular power spectrum for any two fields g, f (which may be identical) in our problem, regardless of their spin, as

$$\langle f_{\ell m} g_{\ell' m'}^* \rangle = \Delta_{\ell\ell'} \Delta_{mm'} C_{\ell}^{fg} . \quad (3.46)$$

The Kröneckers symbols⁸ $\Delta_{\ell\ell'}, \Delta_{mm'}$ in the above are due to statistical isotropy, i.e. the fact that, in real space, the two-point correlation of f, g only depends on the angle formed by the directions in which the fields are evaluated.

3.4.2 Relation between correlation functions and power spectra

Exact relations Substituting the harmonic decomposition of δ, γ and γ_{LOS} in eqs. (3.26), (3.27), (3.33), (3.34) and (3.41) for the LL, LE and LP correlation functions, and exploiting the properties of the spin-weighted spherical harmonics, we find

$$(\text{LL})^{\pm}(\vartheta; \mathbf{Z}_1, \mathbf{Z}_2) = \frac{1}{4\pi} \sum_{\ell=2}^{\infty} (2\ell+1) d_{\pm 22}^{\ell}(\vartheta) C_{\ell}^{\text{LL}}(\mathbf{Z}_1, \mathbf{Z}_2) , \quad (3.47)$$

$$(\text{LE})^{\pm}(\vartheta; \mathbf{Z}_1, z_2) = \frac{1}{4\pi} \sum_{\ell=2}^{\infty} (2\ell+1) d_{\pm 22}^{\ell}(\vartheta) C_{\ell}^{\text{LE}}(\mathbf{Z}_1, z_2) , \quad (3.48)$$

$$\text{L}^+\text{P}(\vartheta; \mathbf{Z}_1, z_2) = \frac{1}{4\pi} \sum_{\ell=2}^{\infty} (2\ell+1) d_{20}^{\ell}(\vartheta) C_{\ell}^{\text{LP}}(\mathbf{Z}_1, z_2) , \quad (3.49)$$

⁷Spin-weighted spherical harmonics are obtained by successive eth differentiation of the usual spherical harmonics according to

$${}_s Y_{\ell m}(\hat{\mathbf{u}}) = \sqrt{\frac{(\ell-s)!}{(\ell+s)!}} \partial^s Y_{\ell m}(\hat{\mathbf{u}}) . \quad (3.43)$$

⁸We use a capital Δ to avoid confusion with the density contrast δ .

where $d_{ss'}^\ell(\vartheta)$ denote elements of the Wigner- d matrices [44], and with the power spectra

$$C_\ell^{\text{LL}}(\mathbf{Z}_1, \mathbf{Z}_2) \equiv \left\langle \gamma_{\ell m}^{\text{LOS}}(\mathbf{Z}_1) \left[\gamma_{\ell m}^{\text{LOS}}(\mathbf{Z}_2) \right]^* \right\rangle, \quad (3.50)$$

$$C_\ell^{\text{LE}}(\mathbf{Z}_1, z_2) \equiv \left\langle \gamma_{\ell m}^{\text{LOS}}(\mathbf{Z}_1) \gamma_{\ell m}^*(z_2) \right\rangle, \quad (3.51)$$

$$C_\ell^{\text{LP}}(\mathbf{Z}_1, z_2) \equiv \left\langle \gamma_{\ell m}^{\text{LOS}}(\mathbf{Z}_1) b(z_2) \delta_{\ell m}^*(z_2) \right\rangle. \quad (3.52)$$

Small-angle approximation For $\vartheta \ll 1$, eqs. (3.47) to (3.49) are dominated by the terms with $\ell \gg 1$. In such conditions, the Wigner- d matrix elements may be approximated by Bessel functions J_n as [45]

$$d_{ss'}^\ell(\vartheta) \approx (-1)^{s-s'} J_{s-s'}(\ell\vartheta) \quad \text{for } \vartheta \ll 1 \quad s, s' \ll \ell; \quad (3.53)$$

in addition, the sums over ℓ may be turned into integrals to finally express the LL, LE, LP correlation functions as Hankel transformations of their power spectra:

$$\boxed{(LL)^\pm(\vartheta; \mathbf{Z}_1, \mathbf{Z}_2) \approx \int_0^\infty \frac{\ell d\ell}{2\pi} J_{0/4}(\ell\vartheta) C_\ell^{\text{LL}}(\mathbf{Z}_1, \mathbf{Z}_2),} \quad (3.54)$$

$$\boxed{(LE)^\pm(\vartheta; \mathbf{Z}_1, z_2) \approx \int_0^\infty \frac{\ell d\ell}{2\pi} J_{0/4}(\ell\vartheta) C_\ell^{\text{LE}}(\mathbf{Z}_1, z_2),} \quad (3.55)$$

$$\boxed{(L^+P)(\vartheta; \mathbf{Z}_1, z_2) \approx \int_0^\infty \frac{\ell d\ell}{2\pi} J_2(\ell\vartheta) C_\ell^{\text{LP}}(\mathbf{Z}_1, z_2).} \quad (3.56)$$

3.4.3 Expression of the LL, LE and LP power spectra

The observables $\delta, \gamma, \gamma_{\text{LOS}}$ considered in the LL, LE and LP correlations are all linearly related to the gravitational potential Φ . Their angular power spectra can thus be expressed in terms of the power spectrum of Φ , and hence of the matter power spectrum. In order to derive such expressions, the calculations are similar to the 3×2 pt literature – see, e.g., ref. [46] for the case of cosmic shear.

Harmonic coefficients The first step consists in expressing $\delta_{\ell m}, \gamma_{\ell m}, \gamma_{\ell m}^{\text{LOS}}$ in terms of the three-dimensional Fourier transform⁹ of the gravitational potential $\tilde{\Phi}(\eta, \mathbf{k})$, or of the density contrast $\tilde{\delta}(\eta, \mathbf{k})$. For that purpose, it is convenient to use eq. (3.45) so as to work with spin-zero quantities only. In the definition of $\delta_{\ell m}, \Psi_{\ell m}, \Psi_{\ell m}^{\text{LOS}}$, we introduce the Fourier transforms of δ, Φ , and substitute the Fourier–Bessel identity

$$e^{i\mathbf{k}\cdot\mathbf{x}} = 4\pi \sum_{\ell=0}^{\infty} \sum_{m=-\ell}^{\ell} i^\ell j_\ell(kx) Y_{\ell m}(\hat{\mathbf{x}}) Y_{\ell m}^*(\hat{\mathbf{k}}), \quad (3.58)$$

⁹We use the following convention for three-dimensional Fourier transforms,

$$\tilde{f}(\mathbf{k}) = \int d^3\mathbf{x} e^{-i\mathbf{k}\cdot\mathbf{x}} f(\mathbf{x}), \quad f(\mathbf{x}) = \int \frac{d^3\mathbf{x}}{(2\pi)^3} e^{i\mathbf{k}\cdot\mathbf{x}} \tilde{f}(\mathbf{k}). \quad (3.57)$$

where $j_\ell(x) \equiv \sqrt{\pi/(2x)} J_{\ell+1/2}(x)$ denotes the ℓ^{th} spherical Bessel function. Using the orthogonality and normalisation of spherical harmonics,¹⁰ we then obtain

$$\delta_{\ell m}(z) = 4\pi i^\ell \int \frac{d^3\mathbf{k}}{(2\pi)^3} j_\ell(k\chi) Y_{\ell m}^*(\hat{\mathbf{k}}) \tilde{\delta}(z, \mathbf{k}) , \quad (3.60)$$

$$\Psi_{\ell m}(z) = 8\pi i^\ell \int_0^\infty \frac{d\chi}{\chi} K(\chi; z) \int \frac{d^3\mathbf{k}}{(2\pi)^3} j_\ell(k\chi) Y_{\ell m}^*(\hat{\mathbf{k}}) \tilde{\Phi}(\eta_0 - \chi, \mathbf{k}) , \quad (3.61)$$

$$\Psi_{\ell m}^{\text{LOS}}(\mathbf{Z}) = 8\pi i^\ell \int_0^\infty \frac{d\chi}{\chi} K_{\text{LOS}}(\chi; \mathbf{Z}) \int \frac{d^3\mathbf{k}}{(2\pi)^3} j_\ell(k\chi) Y_{\ell m}^*(\hat{\mathbf{k}}) \tilde{\Phi}(\eta_0 - \chi, \mathbf{k}) , \quad (3.62)$$

with the lensing kernels K, K_{LOS} introduced in eqs. (2.9) and (2.12) and shorthand notation $K(\chi; z) \equiv K[\chi; 0, \chi(z)]$ and $K_{\text{LOS}}(\chi; \mathbf{Z}) \equiv K_{\text{LOS}}[\chi; \chi(z_a), \chi(z_s)]$. The Fourier transforms of $\tilde{\Phi}$ and δ are related by the Poisson equation (2.6) in Fourier space,

$$-k^2 \tilde{\Phi}(\eta, \mathbf{k}) = 4\pi G \bar{\rho}_0 [1 + z(\eta)] \tilde{\delta}(\eta, \mathbf{k}) = \frac{3}{2} H_0^2 \Omega_m [1 + z(\eta)] \tilde{\delta}(\eta, \mathbf{k}) . \quad (3.63)$$

Exact expressions of the power spectra Having expressed the harmonic coefficients $\delta_{\ell m}(z), \Psi_{\ell m}(z), \Psi_{\ell m}^{\text{LOS}}(\mathbf{Z})$, it is straightforward to obtain the following angular power spectra

$$\begin{aligned} \langle \Psi_{\ell m}^{\text{LOS}}(\mathbf{Z}_1) [\Psi_{\ell m}^{\text{LOS}}(\mathbf{Z}_2)]^* \rangle &= \frac{8}{\pi} \int_0^\infty \frac{d\chi}{\chi} K_{\text{LOS}}(\chi; \mathbf{Z}_1) \int_0^\infty \frac{d\chi'}{\chi'} K_{\text{LOS}}(\chi'; \mathbf{Z}_2) \\ &\quad \times \int_0^\infty dk k^2 j_\ell(k\chi) j_\ell(k\chi') P_\Phi(\eta_0 - \chi, \eta_0 - \chi', k) , \end{aligned} \quad (3.64)$$

$$\begin{aligned} \langle \Psi_{\ell m}^{\text{LOS}}(\mathbf{Z}_1) \Psi_{\ell m}^*(z_2) \rangle &= \frac{8}{\pi} \int_0^\infty \frac{d\chi}{\chi} K_{\text{LOS}}(\chi; \mathbf{Z}_1) \int_0^\infty \frac{d\chi'}{\chi'} K(\chi'; z_2) \\ &\quad \times \int_0^\infty dk k^2 j_\ell(k\chi) j_\ell(k\chi') P_\Phi(\eta_0 - \chi, \eta_0 - \chi', k) , \end{aligned} \quad (3.65)$$

$$\begin{aligned} \langle \Psi_{\ell m}^{\text{LOS}}(\mathbf{Z}_1) \delta_{\ell m}^*(z_2) \rangle &= \frac{4}{\pi} \int_0^\infty \frac{d\chi}{\chi} K_{\text{LOS}}(\chi; \mathbf{Z}_1) \\ &\quad \times \int dk k^2 j_\ell(k\chi) j_\ell(k\chi_2) \frac{k^2 P_\Phi(\eta_0 - \chi, \eta_0 - \chi_2, k)}{-4\pi G \bar{\rho}_0 (1 + z_2)} , \end{aligned} \quad (3.66)$$

with $\chi_2 \equiv \chi(z_2)$. In the above, $P_\Phi(\eta, \eta', k)$ denotes the power spectrum of the gravitational potential, defined as

$$\langle \tilde{\Phi}(\eta, \mathbf{k}) \tilde{\Phi}^*(\eta', \mathbf{k}') \rangle = (2\pi)^3 \delta_{\text{D}}(\mathbf{k} - \mathbf{k}') P_\Phi(\eta, \eta', k) , \quad (3.67)$$

where the Dirac delta is due to statistical homogeneity, and P_Φ only depends on the magnitude $k = |\mathbf{k}|$ of k due to statistical isotropy. The global factor of two between eq. (3.64), (3.65), and eq. (3.66) comes from the fact that Ψ is *twice* the line-of-sight projected potential.

The actual LL, LE, and LP power spectra defined in eqs. (3.50) to (3.52) are then obtained by multiplying eqs. (3.64) and (3.65) by the relevant prefactors following eq. (3.45), and averaging over redshifts. For small angular scales ($\ell \gg 1$), we may further simplify these expressions using Limber's approximation.

¹⁰We adopt the following convention for spherical harmonics,

$$\int d^2\hat{\mathbf{u}} Y_{\ell m}^*(\hat{\mathbf{u}}) Y_{\ell' m'}(\hat{\mathbf{u}}) = \delta_{\ell\ell'} \delta_{mm'} . \quad (3.59)$$

Power spectra in Limber's approximation For $\ell \gg 1$, Bessel functions $J_n(x)$ are very small for $x < n$, they are at maximum at $x = n$, and then experience slowly decaying but rapid oscillations for $x > n$. When integrated with a slowly varying function, it implies that J_n can be approximated as

$$J_n(x) \approx \delta_D(x - n) . \quad (3.68)$$

In all the subsequent results, we shall assume the validity of Limber's approximation.

When substituted in eqs. (3.64) and (3.65), Limber's approximation reduces the number of integrals by two, with $\chi = \chi'$ and $k\chi = \ell + 1/2$. The final angular power spectrum of any couple of observables $O_1, O_2 \in \{L, E, P\}$ then takes the following compact form,

$$C_\ell^{O_1 O_2} = \int_0^\infty d\chi Q_{O_1}(\chi) Q_{O_2}(\chi) P_m \left[\eta_0 - \chi, \frac{\ell + 1/2}{\chi} \right], \quad (3.69)$$

where $P_m(\eta, k) = [(3/2)\Omega_m H_0^2 (1+z)]^2 P_\Phi(\eta, \eta, k)$ is the matter power spectrum, and the integration kernels Q_O read

$$Q_L(\chi; \mathbf{Z}) \equiv -\frac{3}{2} \Omega_m H_0^2 [1 + z(\chi)] K_{\text{LOS}}(\chi; \mathbf{Z}) , \quad (3.70)$$

$$Q_E(\chi; z_*) \equiv -\frac{3}{2} \Omega_m H_0^2 [1 + z(\chi)] K(\chi; z_*) , \quad (3.71)$$

$$Q_P(\chi; z_*) \equiv \frac{b(z_*)}{\chi_*} \delta_D(\chi - \chi_*) , \quad (3.72)$$

where χ_* is the comoving distance of a source at z_* . Note that the above equally applies to the usual correlation functions and power spectra of the 3×2 pt scheme, i.e. PP, PE and EE.

The integration kernels defined in eqs. (3.70) to (3.72) all have the units of an inverse length squared. In the full expressions (3.25), (3.32) and (3.40) of the expectation values of the LL, LE and LP correlation functions, the redshift integrals may be absorbed in the power spectra, thereby defining redshift-averaged spectra $\bar{C}_\ell^{O_1 O_2}$ for $O_1, O_2 \in \{L, E_A, P_A\}$; these have the same formal expression as in eq. (3.69) but with redshift-averaged kernels

$$\bar{Q}_L(\chi) \equiv \int d^2 \mathbf{Z} p(\mathbf{Z}) Q_L(\chi; \mathbf{Z}) , \quad (3.73)$$

$$\bar{Q}_{E_A}(\chi) \equiv \int dz_* f_A(z_*) Q_E(\chi; z_*) , \quad (3.74)$$

$$\bar{Q}_{P_A}(\chi) \equiv \int dz_* f_A(z_*) Q_P(\chi; z_*) . \quad (3.75)$$

These three kernels are plotted in fig. 5 as a function of redshift for illustration. Since the integration kernels have the units of an inverse length squared, we plot the dimensionless combination $\chi(z)\bar{Q}(z)/H(z)$.¹¹ We used strong-lens and galaxy redshift distributions as expected from the *Euclid* survey (see subsec. 5.1 for details).

¹¹This specific combination is the integration kernel for the effective fields involved in our observables, expressed as a redshift-integral of the density contrast. For instance, $\bar{C}_\ell^{\text{LL}} = \langle \bar{\gamma}_{\ell m}^{\text{LOS}} (\bar{\gamma}_{\ell m}^{\text{LOS}})^* \rangle$ may be seen as the angular power spectrum of the redshift-integrated LOS shear $\bar{\gamma}_{\text{LOS}}(\hat{\mathbf{u}})$, whose expression is

$$\bar{\gamma}_{\text{LOS}}(\hat{\mathbf{u}}) \equiv \int d^2 \mathbf{Z} \gamma_{\text{LOS}}(\hat{\mathbf{u}}; \mathbf{Z}) = \int_0^\infty dz \underbrace{\left\{ \frac{\chi(z)\bar{Q}_L[\chi(z)]}{H(z)} \right\}}_{\text{plotted in fig. 5}} \underbrace{\left[\frac{\chi^{-2}(z)\delta^2 \Phi(\hat{\mathbf{u}}, z)}{4\pi G(1+z)\bar{\rho}_0} \right]}_{\sim \text{density contrast } \delta} . \quad (3.76)$$

The same goes for the effective fields associated with E, P.

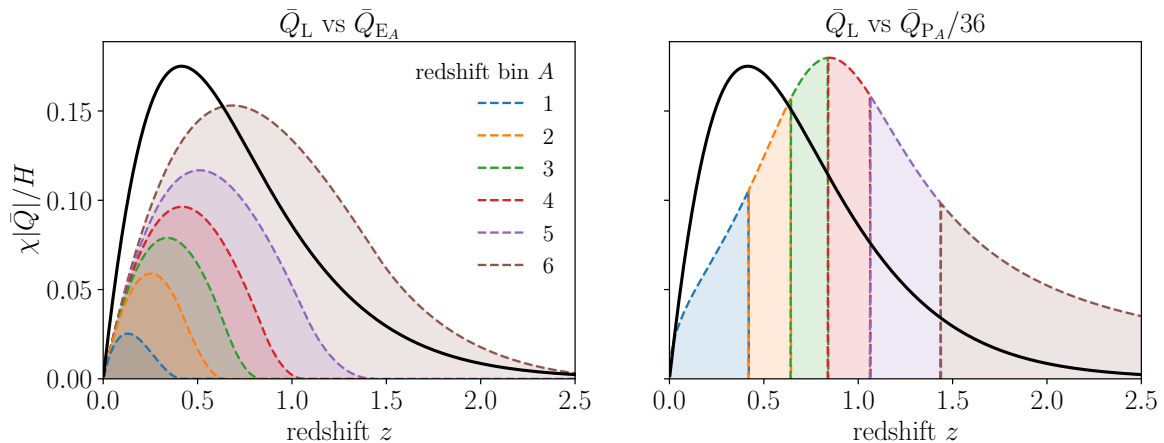


Figure 5. Integration kernels $\bar{Q}_O[\chi(z)]$, with $O = L, E, P$, for the angular power spectra of the 6×2 pt correlation scheme, as a function of redshift z . The kernels, defined in eqs. (3.73) to (3.75), are multiplied with $\chi(z)/H(z)$ to make them dimensionless. *Left:* Comparison of the LOS-shear kernel \bar{Q}_L (black solid line) with the cosmic-shear kernels \bar{Q}_{E_A} , for six equally-populated redshift bins A (dashed, coloured and shaded). *Right:* Comparison of \bar{Q}_L with the galaxy-position kernel \bar{Q}_{P_A} for the same six redshift bins; \bar{Q}_{P_A} is scaled by an arbitrary factor of $1/36$ for ease of comparison.

In fig. 5, we can see that the shape of $\bar{Q}_L(z)$ is similar to the shape of the standard cosmic-shear kernels $\bar{Q}_{E_A}(z)$; it peaks for cosmological perturbations around $z = 0.5$. On the left panel, the amplitude of \bar{Q}_{E_A} is seen to grow with the galaxy redshift bin A , which reflects that the more distant a galaxy is, the more its image is sheared. Since the overlap of \bar{Q}_{E_A} and \bar{Q}_L grows with A , we expect their cross correlation LE_A to do the same. The opposite is true for LP_A , as the overlap of \bar{Q}_{P_A} and \bar{Q}_L decreases with A ; this is due to the fact that foreground galaxies have a stronger impact on the LOS shear of strong lenses than background galaxies.

3.5 Standard 3×2 pt observables with our notation

Let us mention, for completeness, that the formalism and notation used in this section equally applies to the usual 3×2 pt correlation scheme. The two-point correlations of cosmic shear (EE), galaxy–galaxy lensing (EP) and galaxy clustering (PP) read, respectively

$$(\text{EE})^\pm(\vartheta; z_1, z_2) = \frac{1}{4\pi} \sum_{\ell=2}^{\infty} (2\ell + 1) d_{\pm 22}^\ell(\vartheta) C_\ell^{\text{EE}}(z_1, z_2) \approx \int_0^\infty \frac{\ell d\ell}{2\pi} J_{0/4}(\ell\vartheta) C_\ell^{\text{EE}}(z_1, z_2), \quad (3.77)$$

$$\text{E}^+\text{P}(\vartheta; z_1, z_2) = \frac{1}{4\pi} \sum_{\ell=2}^{\infty} (2\ell + 1) d_{20}^\ell(\vartheta) C_\ell^{\text{EP}}(z_1, z_2) \approx \int_0^\infty \frac{\ell d\ell}{2\pi} J_2(\ell\vartheta) C_\ell^{\text{EP}}(z_1, z_2), \quad (3.78)$$

$$\text{PP}(\vartheta; z_1, z_2) = \frac{1}{4\pi} \sum_{\ell=2}^{\infty} (2\ell + 1) d_{00}^\ell(\vartheta) C_\ell^{\text{PP}}(z_1, z_2) \approx \int_0^\infty \frac{\ell d\ell}{2\pi} J_0(\ell\vartheta) C_\ell^{\text{PP}}(z_1, z_2), \quad (3.79)$$

and the angular power spectra $C_\ell^{\text{EE}}, C_\ell^{\text{EP}}, C_\ell^{\text{PP}}$ are given by eq. (3.69) in Limber’s approximation, with the kernels provided in eqs. (3.71) and (3.72).

4 Uncertainties and covariance matrix

In order to assess the detectability of the LL, LE and LP correlations, we must evaluate the expected uncertainty on their measurements, i.e. the variance of the estimators defined in eqs. (3.7), (3.12) and (3.14). Since the ultimate goal will be to perform Fisher forecasts, we shall go one step further and calculate the full covariance matrix of our new observables, whose diagonal elements are precisely the desired uncertainties.

In this work, we have chosen to conduct an analytical, rather than numerical, evaluation of the covariance matrix. Albeit technically challenging, this approach has the advantage of producing results that are more easily adapted to changes in the cosmological and observational setup. In addition, analytical results are more directly interpretable, which is particularly advantageous for optimising the data-analysis strategy.

4.1 Definition of the covariance matrix

We are interested here in estimators of the two-point correlation functions of three classes of observables: LOS shear, apparent ellipticity and positions of galaxies. These estimators all take the form $(\widehat{O_1 O_2})_\alpha$, where $O_1, O_2 \in \{L^P, E_A^P, P_A\}$ and α denotes an angular bin. The covariance of any two such measurements is defined as

$$\text{Cov} \left[(\widehat{O_1 O_2})_\alpha, (\widehat{O_3 O_4})_\beta \right] \equiv \left\langle \left[\left[(\widehat{O_1 O_2})_\alpha (\widehat{O_3 O_4})_\beta \right] \right] \right\rangle - (O_1 O_2)_\alpha (O_3 O_4)_\beta, \quad (4.1)$$

with $(O_1 O_2)_\alpha$ the expectation value of the estimator $(\widehat{O_1 O_2})_\alpha$. The covariance *matrix* is the symmetric matrix formed by the covariance of every pair of estimators. The diagonal elements of the covariance matrix then correspond to the variance of the estimators,

$$\text{Var} \left[(\widehat{O_1 O_2})_\alpha \right] = \text{Cov} \left[(\widehat{O_1 O_2})_\alpha, (\widehat{O_1 O_2})_\alpha \right]. \quad (4.2)$$

We shall consider this variance as the (squared) uncertainty on measurements of the correlation function $O_1 O_2$ in the α^{th} angular bin.

The remainder of this subsection is dedicated to the actual calculation of the covariance matrix of the $6 \times 2\text{pt}$ correlation scheme.

4.2 Technical subtlety: coincident indices

There is an important technical subtlety that explains why the calculation of covariances is more complicated than that of the expectation value of the correlation functions. Readers who are only interested in a ready-to-use recipe may directly skip to subsec. 4.3.

We have already calculated, in subsecs. 3.3 and 3.4, the expectation values of our estimators. The remaining quantity to be evaluated in eq. (4.1) is, therefore, the first term on the right-hand side, which generally takes the form

$$\left\langle \left[\left[(\widehat{O_1 O_2})_\alpha (\widehat{O_3 O_4})_\beta \right] \right] \right\rangle = \frac{1}{N_1 N_2 N_3 N_4} \sum_{\mu=1}^{N_1} \sum_{\nu=1}^{N_2} \sum_{\rho=1}^{N_3} \sum_{\sigma=1}^{N_4} W_{\mu\nu}^\alpha W_{\rho\sigma}^\beta \left\langle \left[\left[m_{\mu\nu}^1 m_{\nu\mu}^2 m_{\rho\sigma}^3 m_{\sigma\rho}^4 \right] \right] \right\rangle, \quad (4.3)$$

where N_I is the number of objects (galaxies or lenses) relevant to observable $O_I \in \{L, E_A, P_A\}$, while $m_{\mu\nu}^I \in \{\hat{\gamma}_{\mu\nu}^{\text{LOS}}, \varepsilon_{\mu\nu}, 1\}$ is the measurement associated with O_I , made in the direction $\hat{\mathbf{u}}_\mu$ and paired with a second direction $\hat{\mathbf{u}}_\nu$ to form the local basis. When $O_I = P$, galaxy-sample averaging [...] eventually replaces $m_{\mu\nu}^I = 1$ with $m_{\mu\nu}^I = b\delta_{\mu\nu}$.

The core of the calculation then consists in evaluating $\langle [m_{\mu\nu}^1 m_{\nu\mu}^2 m_{\rho\sigma}^3 m_{\sigma\rho}^4] \rangle$. At first glance, this is a similar problem to the calculation of the LL, LE and LP expectation values performed in subsections 3.3.2 to 3.3.4. The first step is to apply the sample-averaging operators so as to get

$$\begin{aligned} & \langle [m_{\mu\nu}^1 m_{\nu\mu}^2 m_{\rho\sigma}^3 m_{\sigma\rho}^4] \rangle \\ &= \left[\prod_{i=1}^L \int d^6 \Lambda_i p(\Lambda_i) \right] \left[\prod_{A=1}^T \prod_{a \in \mathcal{G}_A} \int d^5 \Gamma_a p_A(\Gamma_a) \right] \langle m_{\mu\nu}^1 m_{\nu\mu}^2 m_{\rho\sigma}^3 m_{\sigma\rho}^4 \rangle. \end{aligned} \quad (4.4)$$

Now, in contrast with subsections 3.3.2 to 3.3.4, not all the terms of the form (4.4), involved in the quadruple sum of eq. (4.3), are equivalent. This is because the window functions $W_{\mu\nu}^\alpha, W_{\rho\sigma}^\beta$ ensure that $\mu \neq \nu$ and $\rho \neq \sigma$, but they do not prevent the cases $\mu = \rho, \mu = \sigma$, etc. As a result, several indices in eq. (4.4) may coincide, which affects the marginalisation scheme.

For example, when addressing $\text{Var}[(\widehat{L^+ E_A^+})_\alpha]$ the calculation will feature the term $\langle [[\hat{\gamma}_{+ia}^{\text{LOS}} \varepsilon_{+ai} \hat{\gamma}_{+jb}^{\text{LOS}} \varepsilon_{+bj}]] \rangle$. When all indices are distinct, sample averaging leads to

$$\begin{aligned} & \langle [[\hat{\gamma}_{+ia}^{\text{LOS}} \varepsilon_{+ai} \hat{\gamma}_{+jb}^{\text{LOS}} \varepsilon_{+bj}]] \rangle \\ &= \int d^6 \Lambda_i p(\Lambda_i) \int d^6 \Lambda_j p(\Lambda_j) \int d^5 \Gamma_a p_A(\Gamma_a) \int d^5 \Gamma_b p_A(\Gamma_b) \langle \hat{\gamma}_{+ia}^{\text{LOS}} \varepsilon_{+ai} \hat{\gamma}_{+jb}^{\text{LOS}} \varepsilon_{+bj} \rangle. \end{aligned} \quad (4.5)$$

But if, say, $i = j$, then we end up with only three integrals, because the corresponding term only features three indices (i, a, b) ,

$$\begin{aligned} & \langle [[\hat{\gamma}_{+ia}^{\text{LOS}} \varepsilon_{+ai} \hat{\gamma}_{+ib}^{\text{LOS}} \varepsilon_{+bi}]] \rangle \\ &= \int d^6 \Lambda_i p(\Lambda_i) \int d^5 \Gamma_a p_A(\Gamma_a) \int d^5 \Gamma_b p_A(\Gamma_b) \langle \hat{\gamma}_{+ia}^{\text{LOS}} \varepsilon_{+ai} \hat{\gamma}_{+ib}^{\text{LOS}} \varepsilon_{+bi} \rangle. \end{aligned} \quad (4.6)$$

A key difference between eq. (4.5) and eq. (4.6) is that the latter has a non-zero contribution from the LOS noise η_i^{LOS} , because the LOS shear is measured on the same lens i .

In summary, the evaluation of covariances is made more complicated by the presence of coincident indices in eq. (4.3). The calculation requires one to count the number of terms in the quadruple sum that have identical indices, and to treat those separately. Eventually, the terms whose indices are all different lead to *cosmic covariance*, while those with coinciding indices will lead to the contribution of *noise* and *sparsity covariance* [47], which may be seen as a generalisation of shot noise.

4.3 Recipe to calculate the covariance matrix

The above discussion emphasises that the analytical calculation of covariances is generally tedious, not to mention the fact that it must be repeated for all the combinations of $O_1 O_2$ and $O_3 O_4$, with $O_I \in \{\text{LP}, \text{E}_A^{\text{P}}, \text{P}_A\}$.

Fortunately, various shortcuts and patterns can be identified in the calculations, which eventually lead to a general recipe that is quite straightforward to use. We only present the recipe here; as a justification of its relevance, we present the explicit calculation of $\text{Cov}[(\widehat{L^+ P_A})_\alpha, (\widehat{L^+ P_B})_\beta]$ in appendix A.

4.3.1 The formula

The covariance of any pair of correlation functions reads

$$\boxed{\text{Cov} \left[\widehat{(\text{O}_1 \text{O}_2)}_\alpha, \widehat{(\text{O}_3 \text{O}_4)}_\beta \right] = \int_{\mathcal{F}} \frac{d^2 \hat{\mathbf{u}}_\mu}{\Omega} \int_{\mathcal{F}} \frac{d^2 \hat{\mathbf{u}}_\nu}{\Omega} W_{\mu\nu}^\alpha \int_{\mathcal{F}} \frac{d^2 \hat{\mathbf{u}}_\rho}{\Omega} \int_{\mathcal{F}} \frac{d^2 \hat{\mathbf{u}}_\sigma}{\Omega} W_{\rho\sigma}^\beta} \\ \times \left[\widetilde{(\text{O}_1 \text{O}_3)}_{\mu\nu, \rho\sigma} \widetilde{(\text{O}_2 \text{O}_4)}_{\nu\mu, \sigma\rho} + \widetilde{(\text{O}_1 \text{O}_4)}_{\mu\nu, \sigma\rho} \widetilde{(\text{O}_2 \text{O}_3)}_{\nu\mu, \rho\sigma} \right],} \quad (4.7)$$

where the tilded correlation functions such as $\widetilde{(\text{O}_1 \text{O}_3)}_{\mu\nu, \rho\sigma} \sim \langle m_{\mu\nu}^1 m_{\rho\sigma}^3 \rangle$ correspond to those computed in subsec. 3.3, with an *additional noise term* if $\text{O}_1 = \text{O}_3$. The weight function $W_{\mu\nu}^\alpha$ is defined in eq. (3.10).

Domain of validity Equation (4.7) is valid under the following assumptions:

- *Gaussianity.* We assume that the metric perturbation Φ can be treated as a Gaussian random field. All the observables considered here inherit that property, because they are linearly related to Φ . We may then apply Isserlis' theorem [48] to express four-point correlation functions in terms of two-point functions; this is why eq. (4.7) takes the general form

$$\text{Cov}[(\text{O}_1 \text{O}_2), (\text{O}_3 \text{O}_4)] \sim \langle m_1 m_2 m_3 m_4 \rangle - \langle m_1 m_2 \rangle \langle m_3 m_4 \rangle \quad (4.8)$$

$$\sim (\text{O}_1 \text{O}_3)(\text{O}_2 \text{O}_4) + (\text{O}_1 \text{O}_4)(\text{O}_2 \text{O}_3). \quad (4.9)$$

- *Pseudo full sky.* In the calculation of the covariance matrix, some terms involve integrals over directions $\hat{\mathbf{u}}_\mu, \hat{\mathbf{u}}_\nu, \dots$ that vanish in full sky due to the presence of trigonometric functions of their relative azimuthal angles. For $\mathcal{F} \neq \mathcal{S}^2$, such terms are not exactly zero near the boundaries of \mathcal{F} . We choose to neglect such boundary terms.
- *Large samples.* The full calculation of the covariance matrix features terms that are integrals of, e.g., $(\text{O}_1 \text{O}_3)(\text{O}_2 \text{O}_4)$ – without noise – divided by the lens or galaxy sample size, $L, G \gg 1$. It is safe to neglect such terms.

4.3.2 Using the formula

Let us now explain how to use eq. (4.7) in three steps.

Step 1: Set indices up Pick the required observables $\text{O}_1, \dots, \text{O}_4$ among $\{\text{P}_A, \text{E}_A^p, \text{L}^p\}$, where $p \in \{+, \times\}$ denotes polarisation. Replace the generic indices μ, ν, ρ, σ in eq. (4.7) with a, b, c, d or i, j, k, l depending on the nature (galaxy or lens) of the object that it refers to. Pairs of indices separated by a comma, like in $\widetilde{(\text{O}_1 \text{O}_3)}_{\mu\nu, \rho\sigma}$, are associated with the observables following their order: $(\mu\nu)$ is associated with O_1 and $(\rho\sigma)$ with O_3 . These pairs of indices appear due to the construction of local bases for spin-two observables. When $\text{O} = \text{P}$, keep only the first index of the pair. For example,

$$\text{Cov} \left[\widehat{(\text{L}^\times \text{E}_B^\times)}_\alpha, \widehat{(\text{L}^+ \text{P}_D)}_\beta \right] = \int_{\mathcal{F}} \frac{d^2 \hat{\mathbf{u}}_i}{\Omega} \int_{\mathcal{F}} \frac{d^2 \hat{\mathbf{u}}_b}{\Omega} W_{ib}^\alpha \int_{\mathcal{F}} \frac{d^2 \hat{\mathbf{u}}_k}{\Omega} \int_{\mathcal{F}} \frac{d^2 \hat{\mathbf{u}}_d}{\Omega} W_{kd}^\beta} \\ \times \left[\widetilde{(\text{L}^+ \text{L}^+)}_{ib, kd} \widetilde{(\text{E}_B^\times \text{P}_D)}_{bi, d} + \widetilde{(\text{L}^+ \text{P}_D)}_{ib, d} \widetilde{(\text{E}_B^\times \text{L}^+)}_{bi, kd} \right]. \quad (4.10)$$

Step 2: Unfold pairs of indices The correlation functions with pairs of indices are then expressed in terms of the regular correlation functions according to the following dictionary (we drop the tildes to alleviate notation here).

1. *Two spin-two observables:*

$$(\mathcal{O}_1^+ \mathcal{O}_3^+)_{\mu\nu,\rho\sigma} = \mathcal{O}_1^+ \mathcal{O}_3^+(\hat{\mathbf{u}}_\mu, \hat{\mathbf{u}}_\rho) \cos 2(\psi_{\mu\rho} - \psi_{\mu\nu}) \cos 2(\psi_{\rho\mu} - \psi_{\rho\sigma}) \\ + \mathcal{O}_1^\times \mathcal{O}_3^\times(\hat{\mathbf{u}}_\mu, \hat{\mathbf{u}}_\rho) \sin 2(\psi_{\mu\rho} - \psi_{\mu\nu}) \sin 2(\psi_{\rho\mu} - \psi_{\rho\sigma}) , \quad (4.11)$$

$$(\mathcal{O}_1^+ \mathcal{O}_3^\times)_{\mu\nu,\rho\sigma} = \mathcal{O}_1^+ \mathcal{O}_3^+(\hat{\mathbf{u}}_\mu, \hat{\mathbf{u}}_\rho) \cos 2(\psi_{\mu\rho} - \psi_{\mu\nu}) \sin 2(\psi_{\rho\mu} - \psi_{\rho\sigma}) \\ - \mathcal{O}_1^\times \mathcal{O}_3^\times(\hat{\mathbf{u}}_\mu, \hat{\mathbf{u}}_\rho) \sin 2(\psi_{\mu\rho} - \psi_{\mu\nu}) \cos 2(\psi_{\rho\mu} - \psi_{\rho\sigma}) , \quad (4.12)$$

$$(\mathcal{O}_1^\times \mathcal{O}_3^\times)_{\mu\nu,\rho\sigma} = \mathcal{O}_1^+ \mathcal{O}_3^+(\hat{\mathbf{u}}_\mu, \hat{\mathbf{u}}_\rho) \sin 2(\psi_{\mu\rho} - \psi_{\mu\nu}) \sin 2(\psi_{\rho\mu} - \psi_{\rho\sigma}) \\ + \mathcal{O}_1^\times \mathcal{O}_3^\times(\hat{\mathbf{u}}_\mu, \hat{\mathbf{u}}_\rho) \cos 2(\psi_{\mu\rho} - \psi_{\mu\nu}) \cos 2(\psi_{\rho\mu} - \psi_{\rho\sigma}) . \quad (4.13)$$

2. *One spin-two observable with one spin-zero observable:*

$$(\mathcal{O}_1^+ \mathcal{O}_3)_{\mu\nu,\rho} = \mathcal{O}_1^+ \mathcal{O}_3(\hat{\mathbf{u}}_\mu, \hat{\mathbf{u}}_\rho) \cos 2(\psi_{\mu\rho} - \psi_{\mu\nu}) , \quad (4.14)$$

$$(\mathcal{O}_1^\times \mathcal{O}_3)_{\mu\nu,\rho} = \mathcal{O}_1^+ \mathcal{O}_3(\hat{\mathbf{u}}_\mu, \hat{\mathbf{u}}_\rho) \sin 2(\psi_{\mu\rho} - \psi_{\mu\nu}) . \quad (4.15)$$

3. *Two spin-zero observables:* $(\mathcal{O}_1 \mathcal{O}_3)_{\mu,\rho} = \mathcal{O}_1 \mathcal{O}_3(\hat{\mathbf{u}}_\mu, \hat{\mathbf{u}}_\rho)$.

Step 3: Substitute the elementary building blocks After step 2, the covariance is fully expressed in terms of trigonometric functions and the following building blocks, which are redshift-integrated correlation functions, possibly with an additional noise term. The final result is obtained by substituting in their explicit expressions:

$$\widetilde{\text{L}^{\text{P}}\text{L}^{\text{P}}}(\hat{\mathbf{u}}_i, \hat{\mathbf{u}}_j) \equiv \int d^2 \mathbf{Z}_i p(\mathbf{Z}_i) \int d^2 \mathbf{Z}_j p(\mathbf{Z}_j) \text{L}^{\text{P}}\text{L}^{\text{P}}(\vartheta_{ij}; \mathbf{Z}_i, \mathbf{Z}_j) + \frac{\sigma_{\text{LOS}}^2}{2n_{\text{L}}} \delta_{\text{D}}(\hat{\mathbf{u}}_i - \hat{\mathbf{u}}_j) , \quad (4.16)$$

$$\widetilde{\text{L}^{\text{P}}\text{E}_B^{\text{P}}}(\hat{\mathbf{u}}_i, \hat{\mathbf{u}}_b) \equiv \int d^2 \mathbf{Z}_i p(\mathbf{Z}_i) \int dz_b p_B(z_b) \text{L}^{\text{P}}\text{E}^{\text{P}}(\vartheta_{ib}; \mathbf{Z}_i, z_b) , \quad (4.17)$$

$$\widetilde{\text{L}^+ \text{P}_B}(\hat{\mathbf{u}}_i, \hat{\mathbf{u}}_b) \equiv \int d^2 \mathbf{Z}_i p(\mathbf{Z}_i) \int dz_b p_B(z_b) \text{L}^{\text{P}}(\vartheta_{ib}; \mathbf{Z}_i, z_b) , \quad (4.18)$$

$$\widetilde{\text{E}_A^{\text{P}}\text{E}_B^{\text{P}}}(\hat{\mathbf{u}}_a, \hat{\mathbf{u}}_b) \equiv \int dz_a p_A(z_a) \int dz_b p_B(z_b) \text{E}^{\text{P}}\text{E}^{\text{P}}(\vartheta_{ab}; z_a, z_b) + \frac{\delta_{AB}\sigma_A^2}{2n_A} \delta_{\text{D}}(\hat{\mathbf{u}}_a - \hat{\mathbf{u}}_b) , \quad (4.19)$$

$$\widetilde{\text{E}_A^+ \text{P}_B}(\hat{\mathbf{u}}_a, \hat{\mathbf{u}}_b) \equiv \int dz_a p_A(z_a) \int dz_b p_B(z_b) \text{E}^+ \text{P}(\vartheta_{ab}; z_a, z_b) , \quad (4.20)$$

$$\widetilde{\text{P}_A^{\text{P}}\text{P}_B}(\hat{\mathbf{u}}_a, \hat{\mathbf{u}}_b) \equiv \int dz_a p_A(z_a) \int dz_b p_B(z_b) \text{P}^{\text{P}}(\vartheta_{ab}; z_a, z_b) + \frac{\delta_{AB}}{n_A} \delta_{\text{D}}(\hat{\mathbf{u}}_a - \hat{\mathbf{u}}_b) . \quad (4.21)$$

Each of the three tilded autocorrelation functions ($\widetilde{\text{L}\text{L}}$, $\widetilde{\text{E}\text{E}}$, $\widetilde{\text{P}\text{P}}$) exhibits a Dirac-delta term. Those *noise terms* effectively account for the cases of coincident indices in the sum of eq. (4.3), which were discussed in subsec. 4.2.

In $\widetilde{\text{P}_A^{\text{P}}\text{P}_A}$, this is the usual shot noise, or Poisson noise, which is inversely proportional to the surface density n_A of galaxies in the A^{th} tomographic bin. In $\widetilde{\text{E}_A^{\text{P}}\text{E}_A^{\text{P}}}$, the noise term is

proportional to σ_A^2 , which is the variance of the apparent ellipticity of galaxies in that bin,

$$\sigma_A^2 \equiv \int d^5 \mathbf{\Gamma} p_A(\mathbf{\Gamma}) \langle |\varepsilon|^2 \rangle \quad (4.22)$$

$$= \int d^5 \mathbf{\Gamma} p_A(\mathbf{\Gamma}) \left[|\varepsilon_0|^2 + \langle |\gamma|^2 \rangle \right] \quad (4.23)$$

$$= \underbrace{\int dz f_A(z) \int d^2 \varepsilon_0 p(\varepsilon_0; z) |\varepsilon_0|^2}_{\text{shape noise } \sigma_{\varepsilon_0, A}^2} + \underbrace{\int dz f_A(z) (\text{EE})^+(0; z, z)}_{\text{shear variance}}. \quad (4.24)$$

We see that σ_A^2 receives a contribution from intrinsic ellipticities, usually referred to as shape noise, as well as a contribution from the variance of the weak-lensing shear. The latter contribution, which is absent from the standard weak-lensing literature, has been recently introduced in ref. [47] as *sparsity variance*. It comes from the fact that cosmic-shear measurements are performed on a finite sample of galaxies that are randomly distributed in the sky; this leads to an uncertainty on estimates of the EE correlation function that would persist even if we could perfectly measure the shear on individual galaxies.

In cosmic shear, sparsity variance leads to a sub-percent contribution to the covariance matrix, because $|\gamma| \ll |\varepsilon_0|$. The situation is quantitatively different for the LOS shear. The noise term in $\overline{\text{LL}}$ is proportional to the variance of the *measured* LOS shear,

$$\sigma_{\text{LOS}}^2 \equiv \int d^6 \mathbf{\Lambda} p(\mathbf{\Lambda}) \langle |\hat{\gamma}_{\text{LOS}}|^2 \rangle \quad (4.25)$$

$$= \int d^6 \mathbf{\Lambda} p(\mathbf{\Lambda}) \left[|\eta_{\text{LOS}}|^2 + \langle |\gamma_{\text{LOS}}|^2 \rangle \right] \quad (4.26)$$

$$= \underbrace{\int d^2 \mathbf{Z} p(\mathbf{Z}) \int d^2 \eta_{\text{LOS}} p(\eta_{\text{LOS}}; \mathbf{Z}) |\eta_{\text{LOS}}|^2}_{\text{LOS shear measurement noise } \sigma_{\eta_{\text{LOS}}}^2} + \underbrace{\int d^2 \mathbf{Z} p(\mathbf{Z}) (\text{LL})^+(0; \mathbf{Z}, \mathbf{Z})}_{\text{LOS shear variance } \sigma_{\gamma_{\text{LOS}}}^2}, \quad (4.27)$$

which combines the variance of the noise on individual LOS shear measurements, $\sigma_{\eta_{\text{LOS}}}$, with the variance of the LOS signal, $\sigma_{\gamma_{\text{LOS}}}$. Since we expect $\sigma_{\eta_{\text{LOS}}} \sim \sigma_{\gamma_{\text{LOS}}}$, sparsity variance must absolutely be taken into account in the covariance matrix of the $6 \times 2\text{pt}$ correlation scheme.

When dealing with forecasts, σ_A^2 and σ_{LOS}^2 must be estimated by assuming the noise properties and a cosmological model. Eventually, these quantities will be measured directly from the data.

4.4 Result and comments on the sources of uncertainty

We calculated the full covariance matrix of the $6 \times 2\text{pt}$ scheme using the recipe presented in subsec. 4.3. Due to the lengthiness of the resulting expressions, we do not report them here. Instead, they are presented in the *Encyclopædia Covariandis*, a separate document stored in a dedicated [public Github repository](#).

The covariance of two correlation-function estimators is generally composed of three types of contributions: $\text{Cov} = \text{CCov} + \text{NCov} + \text{SCov}$.

- *Cosmic covariance*, CCov , is caused by the intrinsically correlated nature of the physical fields at play. It is the limit of Cov if we could observe an infinite number of galaxies and lenses ($L, G \rightarrow \infty$), i.e. eq. (4.7) without tildes on the right-hand side. The associated variance, $\text{CCov}(\widehat{\text{O}}_1 \text{O}_2, \widehat{\text{O}}_1 \text{O}_2)$, is an irreducible uncertainty on $\text{O}_1 \text{O}_2$, due to the fact that we observe a single realisation of the cosmic fields on a finite sky.

- *Noise covariance*, **NCov**, is due to (i) the uncertainty η_{LOS} on individual measurements of the LOS shear; and (ii) the intrinsic ellipticity ε_0 of galaxies (shape noise).
- *Sparsity covariance*, **SCov**, comes from the fact that we observe a finite number of galaxies and strong lenses with random positions. It may be seen as a generalisation of shot noise [47]. This contribution would persist even if galaxies were intrinsically spherical and if we could measure γ_{LOS} with an arbitrarily large precision.

In practice, **NCov** and **SCov** always come together, via σ_A^2 and σ_{LOS}^2 defined in eqs. (4.22) and (4.25).¹² The relative importance of **SCov** and **NCov** is driven by the signal-to-noise ratio of individual observations. For standard cosmic shear, **SCov** \ll **NCov** because the intrinsic ellipticity of a galaxy is typically larger than the weak-lensing shear; in other words, the second term on the right-hand side of eq. (4.24) may be neglected. But for the LOS shear, **SCov** \sim **NCov** because the uncertainty on γ_{LOS} for a single strong lens is comparable to the expected signal. Sparsity covariance is therefore a crucial concept in this work.

4.5 Numerical implementation

The correlation functions and their covariance are computed using the Python code **LOSCOV**, which we made publicly available. The code assumes, as input parameters, a background cosmology and the survey specifications. These include sky coverage, Ω ; the limits of the tomographic redshift bins, z_A ; the properties of the galaxy sample – G , $f_A(z)$, $\sigma_{\varepsilon_0,A}$ – and those of the strong-lens sample – L , $p(\mathbf{Z})$, $\sigma_{\eta_{\text{LOS}}}$. The limits of the angular bins, ϑ_α , can be either set by hand or computed automatically according to a chosen mathematical prescription. **LOSCOV** then returns the binned correlation functions and associated covariance for those specifications, examples of which are presented in sec. 5.

The matter power spectrum, $P_m(z, k)$,¹³ is computed using **CAMB** [49, 50] for $z \in [0, 7]$, up to $k = 500 \text{ Mpc}^{-1}$, and then further extrapolated as a power law to $k = 10^{10} \text{ Mpc}^{-1}$. The angular power spectra, $C_\ell^{\text{O}_1\text{O}_2}$, of eq. (3.69) are computed by discrete integration over χ , and the corresponding correlation functions are obtained by performing Hankel transforms (3.54) with the **HANKEL** package [51]. We make extensive use of the **NUMPY** [52] and **SCIPY** [53] functions throughout. Figures are plotted with **MATPLOTLIB** [54].

As for the covariance matrix, which involves a number of four- and five-dimensional integrals (see *Encyclopædia Covariancis*), numerical integrators such as `numpy.nquad` do not converge on reasonable timescales if we use a realistic numbers of angular and redshift bins. We therefore rely on Monte Carlo integration, record the numerical uncertainties associated with each calculation, and ensure that the relative error is sufficiently small – see appendix C for details. With 10^7 Monte-Carlo samples, one “redshift block”, e.g. $\text{Cov}[(\widehat{\text{LE}}_1)_\alpha^+, (\widehat{\text{L}^+\text{P}}_2)_\beta]$ for all α, β , takes about one day to compute; parallelising to process all blocks simultaneously allows us to evaluate the full covariance matrix on the same timescale.

¹²Some variances, such as $\text{Var}(\widehat{\text{L}^+\text{L}^+})_\alpha$ – see eq. (11) in the *Encyclopædia Covariancis* – contain terms proportional to $\sigma_{\text{LOS}}^4 = (\sigma_{\eta_{\text{LOS}}}^2 + \sigma_{\gamma_{\text{LOS}}}^2)^2$. We choose to count the cross term, $2\sigma_{\eta_{\text{LOS}}}^2\sigma_{\gamma_{\text{LOS}}}^2$, as a part of **NCov**, so that **SCov** represents the contribution that survives in the absence of noise ($\sigma_{\eta_{\text{LOS}}} = 0$). The same is true for terms proportional to $\sigma_{\text{LOS}}^2\sigma_A^2$ or σ_A^4 . This convention will tend to boost the contribution of noise with respect to that of sparsity.

¹³In practice, we use the Weyl power spectrum as computed from **CAMB**,

$$P_W^{\text{CAMB}}(z, k) \equiv k^4 P_\Phi(z, k) = \left(\frac{3}{2} H_0^2 \Omega_m\right)^2 (1+z)^2 P_m(z, k). \quad (4.28)$$

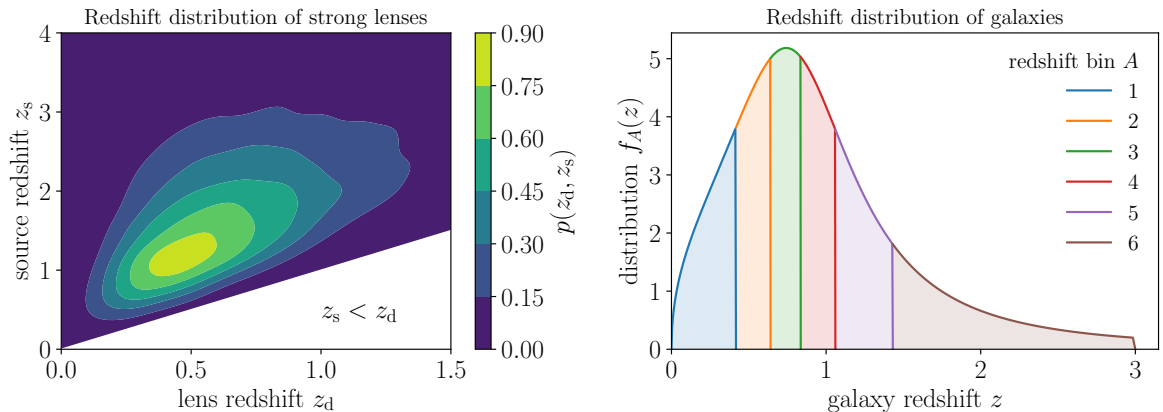


Figure 6. Redshift distributions used in our forecasts. *Left:* Expected distribution $p(\mathbf{Z})$ of the *Euclid* strong lenses from [LENSPOP](#). *Right:* Expected distribution $f_A(z)$ of *Euclid* galaxies in six bins.

5 Forecasted detectability

Let us now apply our analytical results to forecast the detectability of the LL, LE, and LP correlations in a stage-IV galaxy survey. Specifically, we consider in this section an *optimistic scenario* (subsec. 5.1) and a *conservative scenario* (subsec. 5.2), which differ by: (i) the number L of strong-lensing systems with a measurement of the LOS shear; and (ii) the mean uncertainty $\sigma_{\eta_{\text{LOS}}}$ on these measurements. The galaxy sample is the same in both scenarios, and the survey footprint is assumed to cover $\Omega = 15\,000 \text{ deg}^2$.

5.1 Optimistic scenario

Strong-lensing sample We assume

$$L = 10^5, \quad \sigma_{\eta_{\text{LOS}}} = 0.05 \quad (\text{optimistic scenario}). \quad (5.1)$$

For reference, the complete *Euclid* survey is expected to detect 1.7×10^5 strong lenses [11]; thus, our optimistic scenario supposes that we shall get reliable measurements of the LOS shear on about 60% of that sample. As for its uncertainty, the proof of concept carried out by Hogg et al. [20] found¹⁴ $\sigma_{\eta_{\text{LOS}}} = 0.014$ using mock lenses built with analytical profiles. We choose to inflate that uncertainty in order to allow for the many possible systematics associated with lens-mass modelling, source modelling, and lens-light subtraction. The redshift distribution $p(\mathbf{Z}) = p(z_d, z_s)$ of the strong-lensing systems is adapted from the output of [LENSPOP](#) [11] for the *Euclid* survey, and is depicted in the left panel of fig. 6.

Galaxy sample We assume a total number of observed galaxies $G = 2 \times 10^9$, divided into six equally populated redshift bins, so that $G_A = G/6$. The total redshift distribution is adapted from eq. (10) of ref. [55], which we artificially divide into six; the resulting distributions $f_A(z)$ in each bin are depicted on the right panel of fig. 6. Following ref. [56], we model the galaxy bias as $b(z) = 0.9 + 1.1 z^{2.4}/(1+z)$. The amplitude of shape noise is assumed to be identical

¹⁴In that reference, the quoted uncertainty of $\bar{\sigma} = 0.01$ corresponds to the standard deviation of one component (real or imaginary) of η_{LOS} . Since $\sigma_{\eta_{\text{LOS}}}^2 = [|\eta_{\text{LOS}}|^2] = 2 \times [\text{Re}(\eta_{\text{LOS}})^2]$, that quoted uncertainty must take on a factor $\sqrt{2}$ to match the definitions considered here.

in all tomographic bins, $\sigma_{\varepsilon_0,A}/\sqrt{2} = 0.3$. This is slightly larger than the value reported by KiDS–Legacy, where the same quantity ranges between 0.26 and 0.3 depending on the tomographic bin, with a mean value of 0.28 (see table 1 of ref. [7]).

Iso-SNR angular binning The expectation value of the correlation functions, $(\text{LL})_{\alpha}^{\pm}$, $(\text{LE}_A)_{\alpha}^{\pm}$, $(\text{L}^+\text{P})_{\alpha}$, and the covariance matrix all depend on the angular binning of the pairs of lenses and galaxies. Let us denote with $[\vartheta_{\alpha}, \vartheta_{\alpha+1})$ the limits of the N angular bins. In this work, we choose the ϑ_{α} so that all angular bins roughly have the same signal-to-noise ratio (SNR) for a given correlation function $(\text{O}_1\text{O}_2)_{\alpha}$,

$$\text{SNR}(\text{O}_1\text{O}_2; \vartheta_{\alpha}, \vartheta_{\alpha+1}) \equiv \frac{(\text{O}_1\text{O}_2)_{\alpha}}{\sqrt{\text{Var}(\text{O}_1\text{O}_2)_{\alpha}}} \approx R, \quad (5.2)$$

where R is the target SNR, which we fix to be at least $R_{\min} = 6$ (8), for LL (LE and LP) in the optimistic scenario. In addition, we fix the maximum number of bins to $N_{\max} \approx 20$, so that the actual target SNR may exceed R_{\min} .¹⁵ See appendix B for details. In this framework, *the binning scheme generally differs from one correlation function to another.*

All correlations are detectable Figure 7 shows the expected signal and 68% uncertainties for all the correlation functions $(\text{O}_1\text{O}_2)_{\alpha}$ defined in this article, as a function of angular separation.¹⁶ These results demonstrate that all correlation functions will be detectable across a range of angular scales and redshifts in the optimistic scenario, which is compatible with stage-IV surveys like *Euclid*. We note that, as expected from fig. 5, detection prospects for LP_A (LE_A) increase for lower (higher) redshift bins A . The expected SNR exceeds 100 for LP_1 and 40 for LE_6 on angular scales of a few arcminutes.

Full covariance matrix and uncertainty budget It is instructive to examine how the total uncertainty on, e.g., LL, breaks down into its cosmic, noise and sparsity contributions. In fig. 8, we can see that the uncertainty budget is dominated by noise and sparsity, while cosmic variance remains subdominant. Here, we actually have $\sigma_{\eta_{\text{LOS}}} \approx \sigma_{\gamma_{\text{LOS}}}$ by coincidence; the contribution of noise appears larger than that of sparsity due to our conventional choice to count the cross-term $\propto 2\sigma_{\eta_{\text{LOS}}}\sigma_{\gamma_{\text{LOS}}}$ as a noise term. More generally, fig. 8 also emphasises that there is not so much to gain by increasing the precision on γ_{LOS} measurements, since one would quickly hit the sparsity floor. In other words, as far as LL is concerned, *many lenses with mediocre precision are better than few lenses with good precision.*

The fact that cosmic *variance* is generally subdominant compared to its noise and sparsity counterparts does not imply that cosmic *covariance* is always negligible. This appears clearly in fig. 9, which depicts the full covariance matrix for LL, LE and LP, normalised by the corresponding signal, that is $\text{Cov}[(\widehat{\text{O}_1\text{O}_2})_{\alpha}, (\widehat{\text{O}_3\text{O}_4})_{\beta}] / [(\text{O}_1\text{O}_2)_{\alpha}(\text{O}_3\text{O}_4)_{\beta}]$. The diagonal of that matrix thus corresponds to the squared SNR. We use a red-green-blue (RGB) colour coding in order to identify the relative contributions of cosmic, noise, and sparsity, respectively.

¹⁵Imposing both R_{\min} and N_{\max} aims to make a compromise between precise measurements of the correlation function on the one hand (large SNR), and resolving their evolution with angular separation ϑ on the other hand (large number of bins). At this stage, the values $R_{\min} = 8$ and $N_{\max} = 20$ are fixed arbitrarily and do not rely on any proper optimisation procedure, which is left for future work.

¹⁶We use the mean angular separation in the α^{th} bin, which is defined as

$$\bar{\vartheta}_{\alpha} = \frac{1}{\Omega_{\alpha}} \int_{\vartheta_{\alpha}}^{\vartheta_{\alpha+1}} 2\pi\vartheta d\vartheta = \frac{2}{3} \frac{\vartheta_{\alpha+1}^3 - \vartheta_{\alpha}^3}{\vartheta_{\alpha+1}^2 - \vartheta_{\alpha}^2}.$$

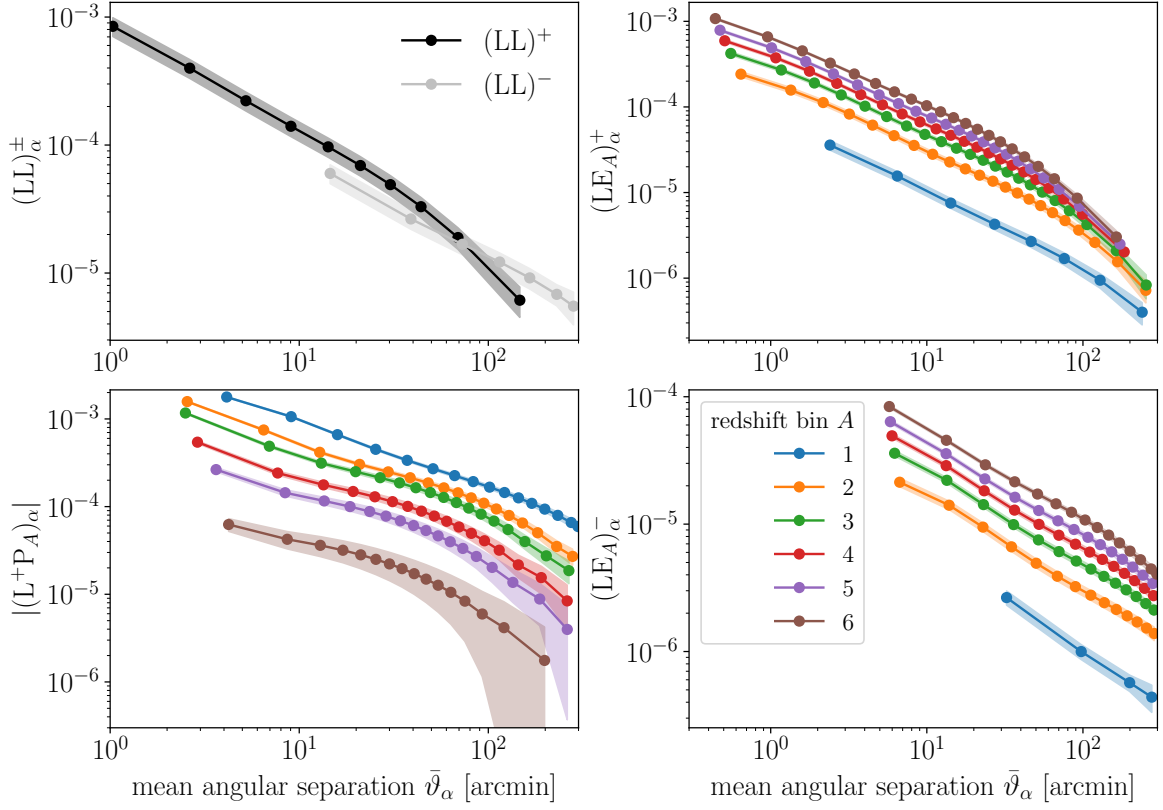


Figure 7. Detection prospects for the LL, LE and LP correlations in the *optimistic scenario* (5.1). In each panel, the points indicate the expected value of $(O_1 O_2)_{\alpha}$ as a function of the mean angular separation $\bar{\vartheta}_{\alpha}$ in the α^{th} bin. Shaded regions delimit the 1σ (68 %) uncertainty about each value, i.e. $(O_1 O_2)_{\alpha} \pm [\text{Var}(O_1 O_2)_{\alpha}]^{1/2}$.

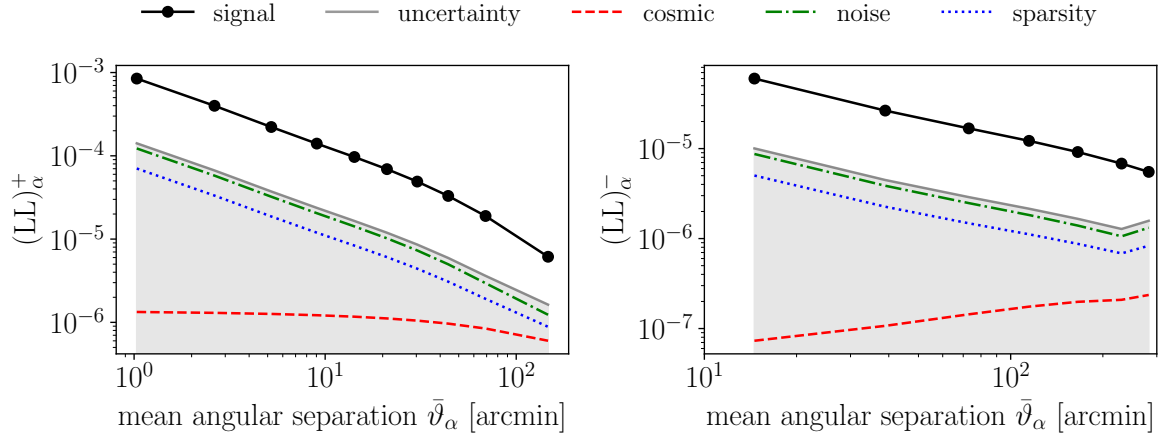


Figure 8. The expected signal and uncertainty on the autocorrelation of the LOS shear, LL^{\pm} , in the *optimistic scenario*. The contributions of cosmic, noise and sparsity variance are plotted in dashed red, dot-dashed green and blue dotted lines, respectively.

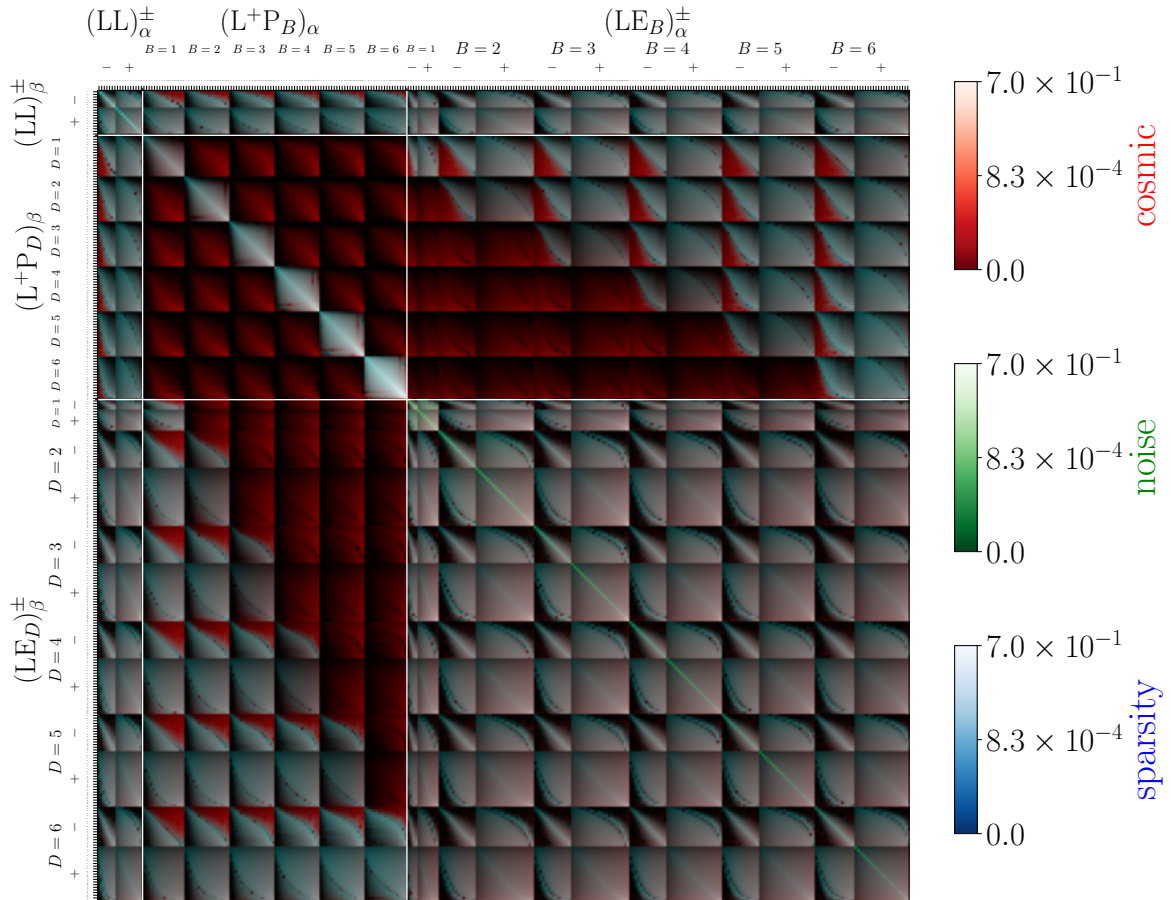


Figure 9. Full covariance matrix of the LL, LP and LE correlation functions in the *optimistic scenario*, normalised by the corresponding signals: $\text{Cov}[(\widehat{O_1 O_2})_\alpha, (\widehat{O_3 O_4})_\beta] / [(\widehat{O_1 O_2})_\alpha (\widehat{O_3 O_4})_\beta]$. Each matrix element is an RGB combination of the absolute value of the cosmic, noise and sparsity contributions to the total covariance. Brighter colours indicate a stronger covariance relative to signal.

The diagonal of fig. 9 shows that the uncertainty on LL and LP is a fair mix of noise and sparsity, while LE is (shape)-noise limited. As for cosmic covariance, it is only non-negligible in off-diagonal elements of the covariance matrix. While negligible in detectability considerations, this contribution will therefore play an important role in Fisher-matrix forecasts.

5.2 Conservative scenario

In the conservative scenario, we are more pessimistic about the strong-lensing sample: we divide by ten the number of lenses and multiply by two the uncertainty on LOS shear measurements, relative to the optimistic scenario,

$$\boxed{L = 10^4, \quad \sigma_{\eta_{\text{LOS}}} = 0.1 \quad (\text{conservative scenario}).} \quad (5.3)$$

The strong-lensing redshift distribution $p(\mathbf{Z})$ is unchanged (fig. 6). Our assumptions on the galaxy sample are the same as in the optimistic scenario, except that we do not divide it into tomographic redshift bins, so as to boost the SNR for LE and LP.

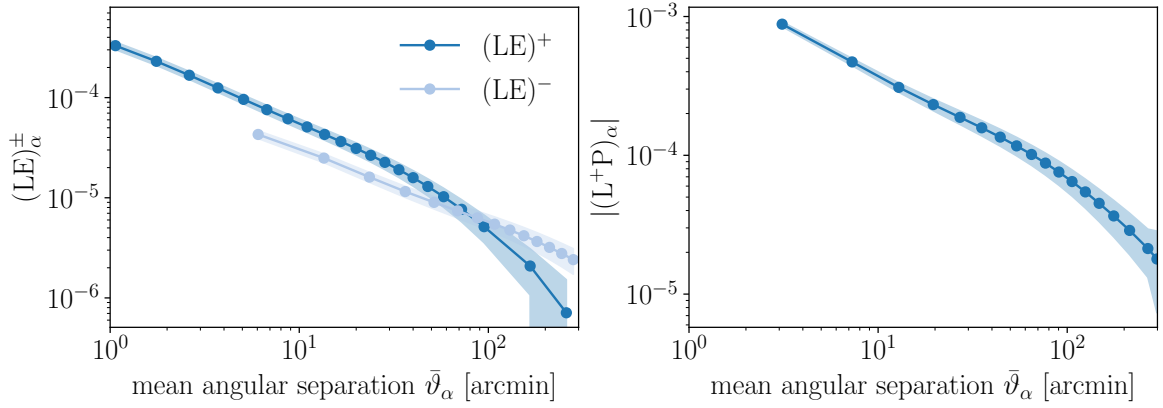


Figure 10. Detection prospects for the LE and LP correlations in the *conservative scenario* (5.3), where there is no redshift binning of the galaxy sample. In each panel, the points indicate the expected value of $(O_1O_2)_\alpha$ as a function of the mean angular separation $\bar{\vartheta}_\alpha$ in the α^{th} bin. Shaded regions delimit the 1σ (68 %) uncertainty about each value.

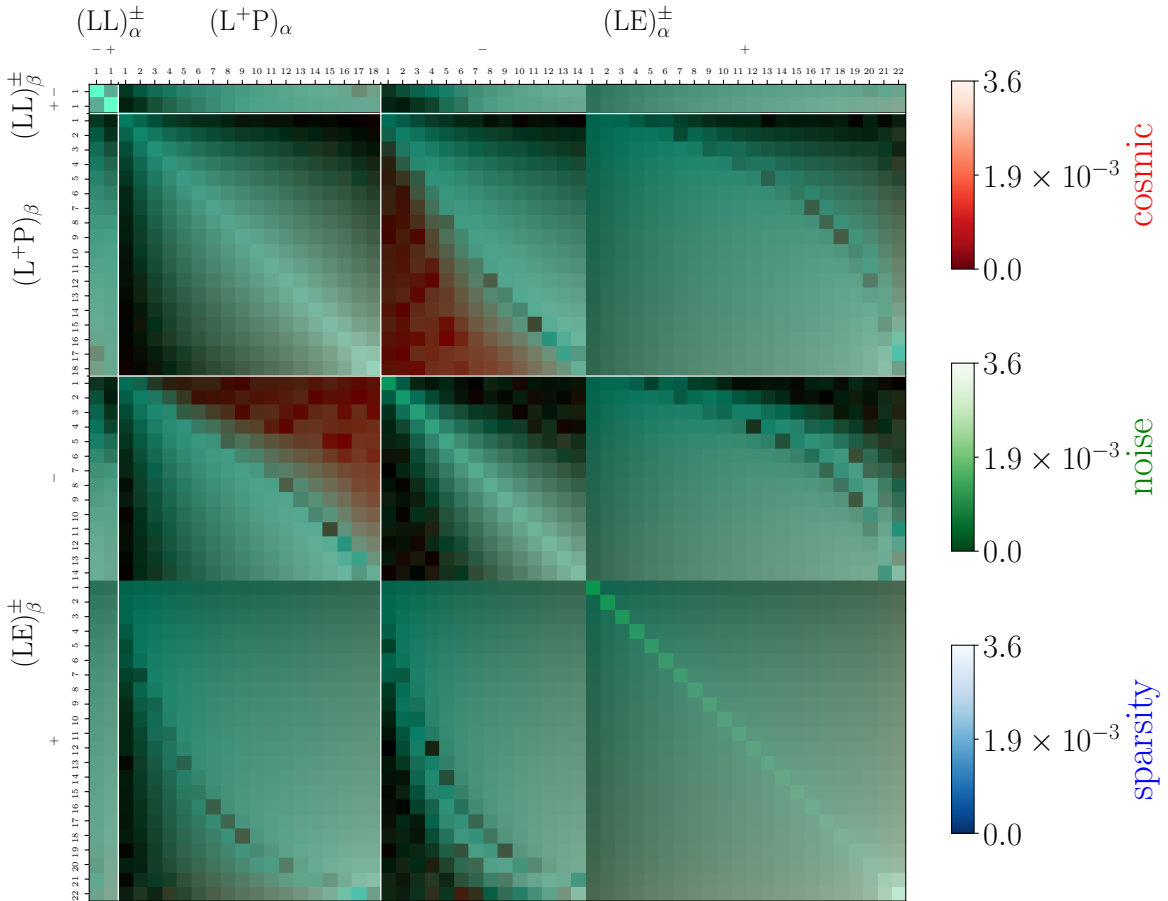


Figure 11. Same as fig. 9 but in the *conservative scenario*.

In this scenario, the autocorrelation of the LOS shear, LL, is not detectable (total SNR of about 0.5). On the other hand, thanks to the impressive size of the galaxy sample, the cross-correlations with galaxy ellipticities and positions, LE, LP, remain detectable with very high SNR, as seen in fig. 10. The full covariance matrix of LL, LE, LP is depicted in fig. 11. Compared to that of the optimistic scenario (fig. 9), we notice the brighter colours, which mean a higher covariance relative to signal, as well as a prominence of the green and blue colours, compatible with higher noise and sparsity.

5.3 Detectability assessment

Let us conclude this section by assessing the detectability of LL, LE and LP as a function of the parameters L and $\sigma_{\eta_{\text{LOS}}}$. To this end, we define a *single quantity* summarising the SNR for each correlation function. We fix the redshift distribution of the strong-lens sample and the properties of the galaxy sample, which we keep in a single redshift bin as in the conservative scenario. We then define the SNR of O_1O_2 as the maximum of the SNR function of eq. (5.2) that can be reached in a single angular bin $[0, \vartheta)$,

$$\text{SNR}(\text{O}_1\text{O}_2) \equiv \max_{\vartheta \in [2', 300']} \text{SNR}(\text{O}_1\text{O}_2; 0, \vartheta). \quad (5.4)$$

Unlike the binning procedure applied in subsecs. 5.1 and 5.2, we use here the full expression of the variance of O_1O_2 without relying on the approximations in eqs. (B.2) to (B.4).

Figure 12 shows the behaviour of $\text{SNR}(\text{O}_1\text{O}_2)$ for each $\text{O}_1\text{O}_2 \in \{(\text{LL})^\pm, (\text{LE})^\pm, \text{LP}\}$, as a function of L and $\sigma_{\eta_{\text{LOS}}}$. Level lines labelled with “ $N\sigma$ ” correspond to $\text{SNR}(\text{O}_1\text{O}_2) = N$. We used the same RGB colour coding as in figs. 9 and 11 so as to highlight which component (CCov, NCov, SCov) dominates the uncertainty budget. The positions of the optimistic and conservative scenarios of subsecs. 5.1 and 5.2 are indicated with crosses for reference.

The detection threshold For LL, a 5σ detection for the autocorrelation signal lies between the optimistic and conservative scenarios; no matter the precision in LOS shear measurements, no autocorrelation signal can be conclusively detected without at least $\approx 2 \times 10^4$ lenses. The cross-correlation signal is, however, much more accessible: with $\sigma_{\eta_{\text{LOS}}} = 0.05$, LP could be detected to 5σ with fewer than 200 lenses, and LE with ≈ 300 lenses. Alternatively, even with $\sigma_{\eta_{\text{LOS}}} = 1$ – an uncertainty two orders of magnitude larger than the typical value of γ_{LOS} and its uncertainty estimated with mock lenses – a *Euclid*-like sample of 10^5 lenses is still sufficient for a 5σ detection of the cross-correlation signals.

The limiting factor For a realistic number of lenses, $L < 10^6$, detectability is limited by noise or sparsity. In every case, we observe the same pattern: when precision in γ_{LOS} measurements is poor, NCov tends to dominate the uncertainty budget, and the SNR can be improved upon both by improving this precision or increasing the number of lenses. However, once $\sigma_{\eta_{\text{LOS}}}$ is sufficiently low ($\lesssim 5 \times 10^{-2}$ in the case of LL and LP), SCov begins to dominate, and meaningful gains to the SNR can only be made by observing more lenses. In the case of LE, the noise always remains significant because of the galaxy shape noise σ_{ε_0} , which is independent of $\sigma_{\eta_{\text{LOS}}}$ – this is why $(\text{LE})^-$ is nowhere cosmic-variance limited. In the other cases, the region of parameter space where CCov dominates corresponds to extreme values of the SNR;¹⁷ this is only achieved for $L > 10^7$, which is beyond the reach of stage-IV surveys.

¹⁷In fig. 12, the SNR of $(\text{LL})^+$ and $(\text{LE})^+$ saturates above 100σ , in the top-left corner of the plots, whereas it seems to grow indefinitely for the other correlation functions. This behaviour is due to the fact that we

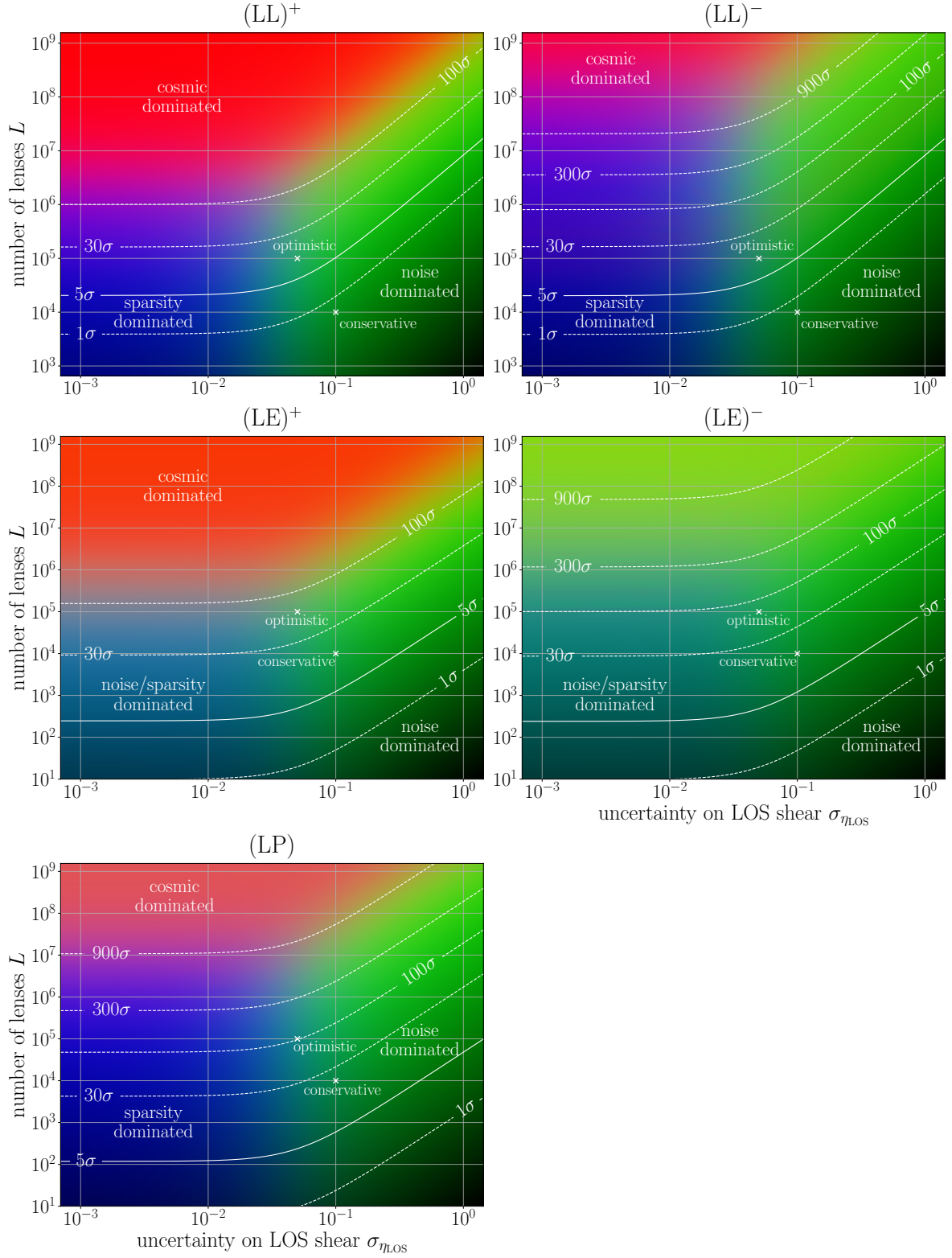


Figure 12. Detectability of the LL, LE, and LP correlations depending on the number of observed strong lenses, L , and the uncertainty on individual LOS shear measurements, $\sigma_{\eta_{\text{LOS}}}$, assuming a *Euclid*-like galaxy sample. The optimistic and conservative scenarios considered in subsections 5.1 and 5.2 are indicated with crosses for reference. Lines labelled with “ $N\sigma$ ” correspond to level lines of the total SNR function, $\text{SNR}(\text{O}_1\text{O}_2) = N$, if all pairs of lenses and galaxies are placed in a single, optimised angular bin (5.4), and if the galaxy sample consists of a single redshift bin. Red, green and blue colours represent the respective contributions of cosmic variance (CCov), noise (NCov) and sparsity variance (SCov) to the total variance of a correlation function O_1O_2 ; hence, they indicate the main limitation to precise measurements of O_1O_2 .

6 Conclusion

The line-of-sight (LOS) shear is a physical quantity which summarises the perturbations to a strong-lens system caused by cosmological inhomogeneities between the source, the main lens, and the observer. This quantity is expected to be directly measurable in strong-lensing images, independently of the properties of the main lens. As stage-IV galaxy surveys, such as *Euclid* and LSST, are expected to detect $\mathcal{O}(10^5)$ strong lenses in the near future, the LOS shear becomes a viable cosmological probe, alongside galaxy shapes and positions.

In this article, we extended the standard 3×2 pt correlation method, built from galaxy ellipticities (E) and positions (P), into a 6×2 pt correlation scheme comprising the LOS shear of strong lenses (L): LL, LE, LP, EE, EP, PP. Besides the added information, L will be subject to different systematics than E and P, thereby mitigating known cosmic-shear limitations (e.g. intrinsic alignments).

We defined estimators for the three new correlation functions involving the LOS shear, LL, LE, LP, and computed their expectation value (i.e. the expected signal) in a Λ CDM cosmology. We then established and applied a general method to analytically calculate the full covariance matrix of the 6×2 pt correlation scheme. The results are explicitly presented in the *Encyclopædia Covariancis*, and are implemented numerically in a publicly available Python code, `LOSCOV`. Analytical results have the double advantage of being flexible and easy to interpret. In particular, they allow us to understand the relative contribution of cosmic, sparsity and noise covariances in the final result.

For concreteness, we considered two observational scenarios. In the optimistic (but realistic) scenario, the LOS shear would be measured on $L = 10^5$ lenses, i.e. 60% of the expected *Euclid* strong-lensing sample, with a mean uncertainty of $\sigma_{\eta_{\text{LOS}}} = 0.05$, which is about 3.5 times larger than in the proof of concept [20]. In this scenario, all three new correlation functions, LL, LE and LP, are detectable with very high SNR. In the conservative scenario, with ten times fewer lenses ($L = 10^4$) and an uncertainty twice as large ($\sigma_{\eta_{\text{LOS}}} = 0.1$), only LE and LP are detectable, still with high SNR. More generally, a definitive detection of the LP and LE cross-correlation functions could be achieved with only a few hundred lenses if $\sigma_{\eta_{\text{LOS}}} = 0.05$. Even if $\sigma_{\eta_{\text{LOS}}} \approx 1$, i.e. two orders of magnitude larger than the expected uncertainty, the cross-correlations will still be detectable with the expected *Euclid* lens sample.

The work presented here was focused on theory and methodology. It is the first step towards a cosmological forecast which will be the topic of a subsequent article. In particular, we shall quantify the constraining power of the 6×2 pt method on cosmological parameters Ω_m and σ_8 , and assess the gain from adding the LOS shear to the usual 3×2 pt scheme. Particular attention will be paid to the mitigation of systematics such as galaxy intrinsic alignments.

Acknowledgements

We thank the informatics team at LUPM, in particular Stéphane Nou, for their support for and facilitation of our use of the lab’s computing cluster for the numerical aspects of this work. We also thank Giacomo Queirolo for discussions and comments on the draft. PF acknowledges support from the French *Agence Nationale de la Recherche* through the ELROND project (ANR-23-CE31-0002). DJ acknowledges support by the First Rand Foundation, South Africa,

imposed $\vartheta > 2'$ in the definition (5.4) of the SNR, which ensures that our numerical results are well behaved. In principle, however, since both $(\text{LL})^+(\vartheta)$ and $(\text{LE})^+(\vartheta)$ go to infinity as $\vartheta \rightarrow 0$, higher values of their SNR could be reached if we allowed for smaller values of the lower bound of ϑ .

and the Centre National de la Recherche Scientifique of France. NBH is supported by the research environment and infrastructure of the Handley Lab at the University of Cambridge.

CRedit authorship contribution statement

Pierre Fleury: Conceptualisation, Methodology, Formal analysis, Writing – Original Draft, Visualisation, Supervision, Project administration, Funding acquisition. **Daniel Johnson:** Software, Formal analysis, Writing – Original Draft, Visualisation. **Théo Duboscq:** Methodology, Formal analysis, Writing – Review & Editing. **Natalie B. Hogg:** Validation, Writing – Review & Editing. **Julien Larena:** Conceptualisation, Methodology, Supervision, Writing – Review & Editing.

A Detailed calculation of $\text{Cov}[(\widehat{\mathbf{L}+\mathbf{P}_B})_\alpha, (\widehat{\mathbf{L}+\mathbf{P}_D})_\beta]$

In this appendix, we present a complete and detailed calculation of

$$\begin{aligned} & \text{Cov} \left[(\widehat{\mathbf{L}+\mathbf{P}_B})_\alpha, (\widehat{\mathbf{L}+\mathbf{P}_D})_\beta \right] \\ &= \frac{1}{L^2 G_B G_D} \sum_{i=1}^L \sum_{b \in \mathcal{G}_B} \sum_{k=1}^L \sum_{d \in \mathcal{G}_D} \left\langle \left[\left[W_{ib}^\alpha W_{kd}^\beta \hat{\gamma}_{+ib}^{\text{LOS}} \hat{\gamma}_{+kd}^{\text{LOS}} \right] \right] \right\rangle - (\mathbf{L}+\mathbf{P}_B)_\alpha (\mathbf{L}+\mathbf{P}_D)_\beta . \end{aligned} \quad (\text{A.1})$$

Besides serving as an example of how such a derivation is performed, it should also demonstrate why the recipe presented in subsec. 4.3 works. The core of the calculation consists in evaluating the expectation value $\langle \left[\left[S_{ibkd}^{\alpha\beta} \right] \right] \rangle$ of the summand $S_{ibkd}^{\alpha\beta} \equiv W_{ib}^\alpha W_{kd}^\beta \hat{\gamma}_{+ib}^{\text{LOS}} \hat{\gamma}_{+kd}^{\text{LOS}}$.

A.1 Galaxy-sample average [...]

We first apply the galaxy-sample averaging operator,

$$\left[S_{ibkd}^{\alpha\beta} \right] = \left[\prod_{A=1}^T \prod_{a \in \mathcal{G}_A} d^5 \Gamma_a p_A(\Gamma_a) \right] S_{ibkd}^{\alpha\beta} . \quad (\text{A.2})$$

Here, contrary to subsec. 3.3, the galaxy indices b and d can be equal. If they are, only one integral over $\Gamma_b = \Gamma_d$ remains; this is only possible if the bins are identical, $B = D$. If the indices differ, then we must keep two separate integrals over Γ_b and Γ_d . In other words:

$$\left[S_{ibkd}^{\alpha\beta} \right] = (1 - \Delta_{bd}) \int d^5 \Gamma_2 p_B(\Gamma_2) \int d^5 \Gamma_4 p_D(\Gamma_4) S_{i2k4}^{\alpha\beta} + \Delta_{bd} \int d^5 \Gamma_2 p_B(\Gamma_2) S_{i2k2}^{\alpha\beta} , \quad (\text{A.3})$$

where Δ_{bd} is the Krönecker symbol.

When summing over the galaxies in the bins, this yields

$$\begin{aligned} \sum_{b \in \mathcal{G}_B} \sum_{d \in \mathcal{G}_D} \left[S_{ibkd}^{\alpha\beta} \right] &= (G_B G_D - \delta_{BD} G_D) \int d^5 \Gamma_2 p_B(\Gamma_2) \int d^5 \Gamma_4 p_D(\Gamma_4) S_{i2k4}^{\alpha\beta} \\ &\quad + \delta_{BD} G_B \int d^5 \Gamma_2 p_B(\Gamma_2) S_{i2k2}^{\alpha\beta} \end{aligned} \quad (\text{A.4})$$

$$= G_B G_D \int d^5 \Gamma_2 \int d^5 \Gamma_4 \tilde{p}_{BD}(\Gamma_2, \Gamma_4) S_{i2k4}^{\alpha\beta} . \quad (\text{A.5})$$

where we have introduced the effective PDF

$$\tilde{p}_{BD}(\mathbf{\Gamma}_2, \mathbf{\Gamma}_4) = \left(1 - \frac{\delta_{BD}}{G_B}\right) p_B(\mathbf{\Gamma}_2) p_D(\mathbf{\Gamma}_4) + \frac{\delta_{BD}}{G_B} p_B(\mathbf{\Gamma}_2) \delta_D(\mathbf{\Gamma}_2 - \mathbf{\Gamma}_4), \quad (\text{A.6})$$

which is indeed normalised to unity. The $\delta_{BD}/G_B \ll 1$ term in the first prefactor may be neglected in practice.

A.2 Lens sample average [...]

Similarly, taking the lens-sample average of $[S_{ibkd}^{\alpha\beta}]$ yields

$$\left[[S_{ibkd}^{\alpha\beta}]\right] = \left[\prod_{i'=1}^L \int d^6 \mathbf{\Lambda}_{i'} p(\mathbf{\Lambda}_{i'})\right] [S_{ibkd}^{\alpha\beta}] \quad (\text{A.7})$$

$$= (1 - \Delta_{ik}) \int d^6 \mathbf{\Lambda}_1 p(\mathbf{\Lambda}_1) \int d^6 \mathbf{\Lambda}_3 p(\mathbf{\Lambda}_3) [S_{1b3d}^{\alpha\beta}] + \Delta_{ik} \int d^6 \mathbf{\Lambda}_1 p(\mathbf{\Lambda}_1) [S_{1b1d}^{\alpha\beta}], \quad (\text{A.8})$$

where Δ_{ik} accounts for the possibility of equal indices. When summing over all lenses in the sample, we thus get

$$\sum_{i=1}^L \sum_{k=1}^L \left[[S_{ibkd}^{\alpha\beta}]\right] = L^2 \int d^6 \mathbf{\Lambda}_1 \int d^6 \mathbf{\Lambda}_3 \tilde{p}(\mathbf{\Lambda}_1, \mathbf{\Lambda}_3) \left[[S_{1b3d}^{\alpha\beta}]\right], \quad (\text{A.9})$$

$$\text{with } \tilde{p}(\mathbf{\Lambda}_1, \mathbf{\Lambda}_3) \equiv \left(1 - \frac{1}{L}\right) p(\mathbf{\Lambda}_1) p(\mathbf{\Lambda}_3) + \frac{1}{L} p(\mathbf{\Lambda}_1) \delta_D(\mathbf{\Lambda}_1 - \mathbf{\Lambda}_3). \quad (\text{A.10})$$

We may take $1 - 1/L \approx 1$ in the first prefactor.

A.3 Cosmic average \langle...\rangle

Putting together the results of the previous two subsections, and applying the cosmic-averaging operator, we end up with the following expression

$$\begin{aligned} & \frac{1}{L^2 G_B G_D} \sum_{i=1}^L \sum_{b \in \mathcal{G}_B} \sum_{k=1}^L \sum_{d \in \mathcal{G}_D} \langle \left[[S_{ibkd}^{\alpha\beta}]\right] \rangle \\ &= \int d^6 \mathbf{\Lambda}_1 \int d^5 \mathbf{\Gamma}_2 \int d^6 \mathbf{\Lambda}_3 \int d^5 \mathbf{\Gamma}_4 \tilde{p}(\mathbf{\Lambda}_1, \mathbf{\Lambda}_3) \langle \tilde{p}_{BD}(\mathbf{\Gamma}_2, \mathbf{\Gamma}_4) S_{1234}^{\alpha\beta} \rangle. \end{aligned} \quad (\text{A.11})$$

Extracting the density contrast Note that, in eq. (A.11), we have kept $\tilde{p}_{BD}(\mathbf{\Gamma}_2, \mathbf{\Gamma}_4)$ inside the cosmic-averaging operator because we cannot neglect the density contrast that appears in the definition (3.16) of $p_A(\mathbf{\Gamma})$. To be more explicit,

$$\begin{aligned} & \langle \tilde{p}_{BD}(\mathbf{\Gamma}_2, \mathbf{\Gamma}_4) S_{1234}^{\alpha\beta} \rangle \\ &= \frac{1}{\Omega^2} f_B(z_2) f_D(z_4) p(\varepsilon_{0,2}; z_2) p(\varepsilon_{0,4}; z_4) W_{12}^\alpha W_{34}^\beta \langle (1 + \delta_2^g)(1 + \delta_4^g) \hat{\gamma}_{+12}^{\text{LOS}} \hat{\gamma}_{+34}^{\text{LOS}} \rangle \\ &+ \frac{\delta_{BD}}{G_B} \delta_D(\mathbf{\Gamma}_2 - \mathbf{\Gamma}_4) \frac{1}{\Omega} f_B(z_2) p(\varepsilon_{0,2}; z_2) W_{12}^\alpha W_{32}^\beta \langle (1 + \delta_2^g) \hat{\gamma}_{+12}^{\text{LOS}} \hat{\gamma}_{+32}^{\text{LOS}} \rangle, \end{aligned} \quad (\text{A.12})$$

where $\delta_a^g \equiv b(z_a) \delta(z_a, \hat{\mathbf{u}}_a)$ for short.

If we assume that the gravitational potential, and hence all the other quantities that derive from it, is a *Gaussian random field*, then the three-point function $\langle \delta_2^{\text{g}} \hat{\gamma}_{+12}^{\text{LOS}} \hat{\gamma}_{+34}^{\text{LOS}} \rangle$ vanishes, and the above becomes

$$\begin{aligned} & \langle \tilde{p}_{BD}(\mathbf{\Gamma}_2, \mathbf{\Gamma}_4) S_{1234}^{\alpha\beta} \rangle \\ &= \frac{1}{\Omega^2} f_B(z_2) f_D(z_4) p(\varepsilon_{0,2}; z_2) p(\varepsilon_{0,4}; z_4) W_{12}^\alpha W_{34}^\beta \left[\langle \hat{\gamma}_{+12}^{\text{LOS}} \hat{\gamma}_{+34}^{\text{LOS}} \rangle + \langle \hat{\gamma}_{+12}^{\text{LOS}} \delta_2^{\text{g}} \hat{\gamma}_{+34}^{\text{LOS}} \delta_4^{\text{g}} \rangle \right] \\ & \quad + \frac{\delta_{BD}}{G_B} \delta_D(\mathbf{\Gamma}_2 - \mathbf{\Gamma}_4) \frac{1}{\Omega} f_B(z_2) p(\varepsilon_{0,2}; z_2) W_{12}^\alpha W_{32}^\beta \langle \hat{\gamma}_{+12}^{\text{LOS}} \hat{\gamma}_{+32}^{\text{LOS}} \rangle \end{aligned} \quad (\text{A.13})$$

$$\begin{aligned} &= \langle p_B(\mathbf{\Gamma}_2) \rangle \langle p_D(\mathbf{\Gamma}_4) \rangle W_{12}^\alpha W_{32}^\beta \left[\langle \hat{\gamma}_{+12}^{\text{LOS}} \hat{\gamma}_{+34}^{\text{LOS}} \rangle + \langle \hat{\gamma}_{+12}^{\text{LOS}} \delta_2^{\text{g}} \hat{\gamma}_{+34}^{\text{LOS}} \delta_4^{\text{g}} \rangle \right] \\ & \quad + \frac{\delta_{BD}}{G_B} \delta_D(\mathbf{\Gamma}_2 - \mathbf{\Gamma}_4) \langle p_B(\mathbf{\Gamma}_2) \rangle W_{12}^\alpha W_{32}^\beta \langle \hat{\gamma}_{+12}^{\text{LOS}} \hat{\gamma}_{+32}^{\text{LOS}} \rangle, \end{aligned} \quad (\text{A.14})$$

with $\langle p_A(\mathbf{\Gamma}) \rangle = \Omega^{-1} f_A(z) p(\varepsilon_0; z)$ the cosmic-averaged PDF of the galaxy parameters, from which δ has disappeared. The term indicated in **red** in the above will vanish after integrating over, e.g., $\mathbf{\Gamma}_2$, because $\hat{\gamma}_{+12}^{\text{LOS}} \hat{\gamma}_{+34}^{\text{LOS}} \propto \cos(2\psi_{12})$, which averages to zero as the galaxy position $\hat{\mathbf{u}}_2$ moves around the lens at $\hat{\mathbf{u}}_1$. Strictly speaking, this is only true if $\mathcal{F} = \mathcal{S}^2$; if not, there is a residual contribution when $\hat{\mathbf{u}}_1$ lies near the boundary of \mathcal{F} , since $\hat{\mathbf{u}}_2$ may have to exit \mathcal{F} to span a complete annulus around $\hat{\mathbf{u}}_1$. We neglect such boundary effects here (*pseudo-full-sky approximation*).

Isserlis's theorem Since we assume that we are dealing with Gaussian random fields, we may apply Isserlis's theorem [48] and decompose four-point functions in terms of two-point functions. Here, this leads to

$$\langle \hat{\gamma}_{+12}^{\text{LOS}} \delta_2^{\text{g}} \hat{\gamma}_{+34}^{\text{LOS}} \delta_4^{\text{g}} \rangle = \langle \hat{\gamma}_{+12}^{\text{LOS}} \delta_2^{\text{g}} \rangle \langle \hat{\gamma}_{+34}^{\text{LOS}} \delta_4^{\text{g}} \rangle + \langle \hat{\gamma}_{+12}^{\text{LOS}} \hat{\gamma}_{+34}^{\text{LOS}} \rangle \langle \delta_2^{\text{g}} \delta_4^{\text{g}} \rangle + \langle \hat{\gamma}_{+12}^{\text{LOS}} \delta_4^{\text{g}} \rangle \langle \delta_2^{\text{g}} \hat{\gamma}_{+34}^{\text{LOS}} \rangle. \quad (\text{A.15})$$

A.4 Putting everything together

Substituting, in eq. (A.11), the expression of $\tilde{p}(\mathbf{\Lambda}_1, \mathbf{\Lambda}_2)$ and $\langle \tilde{p}_{BD}(\mathbf{\Gamma}_2, \mathbf{\Gamma}_4) S_{1234} \rangle$, we get

$$\begin{aligned} & \frac{1}{L^2 G_B G_D} \sum_{i=1}^L \sum_{b \in \mathcal{G}_B} \sum_{k=1}^L \sum_{d \in \mathcal{G}_D} \langle \langle [S_{ibkd}^{\alpha\beta}] \rangle \rangle \\ &= \int d^6 \mathbf{\Lambda}_1 p(\mathbf{\Lambda}_1) \int d^5 \mathbf{\Gamma}_2 \langle p_B(\mathbf{\Gamma}_2) \rangle \int d^6 \mathbf{\Lambda}_3 p(\mathbf{\Lambda}_3) \int d^5 \mathbf{\Gamma}_4 \langle p_D(\mathbf{\Gamma}_4) \rangle W_{12}^\alpha W_{34}^\beta \\ & \quad \times \left(\langle \hat{\gamma}_{+12}^{\text{LOS}} \delta_2^{\text{g}} \rangle \langle \hat{\gamma}_{+34}^{\text{LOS}} \delta_4^{\text{g}} \rangle + \langle \hat{\gamma}_{+12}^{\text{LOS}} \hat{\gamma}_{+34}^{\text{LOS}} \rangle \langle \delta_2^{\text{g}} \delta_4^{\text{g}} \rangle + \langle \hat{\gamma}_{+12}^{\text{LOS}} \delta_4^{\text{g}} \rangle \langle \delta_2^{\text{g}} \hat{\gamma}_{+34}^{\text{LOS}} \rangle \right) \\ & \quad + \frac{1}{L} \int d^6 \mathbf{\Lambda}_1 p(\mathbf{\Lambda}_1) \int d^5 \mathbf{\Gamma}_2 \langle p_B(\mathbf{\Gamma}_2) \rangle \int d^5 \mathbf{\Gamma}_4 \langle p_D(\mathbf{\Gamma}_4) \rangle W_{12}^\alpha W_{14}^\beta \\ & \quad \times \left(\langle \hat{\gamma}_{+12}^{\text{LOS}} \delta_2^{\text{g}} \rangle \langle \hat{\gamma}_{+14}^{\text{LOS}} \delta_4^{\text{g}} \rangle + \langle \hat{\gamma}_{+12}^{\text{LOS}} \hat{\gamma}_{+14}^{\text{LOS}} \rangle \langle \delta_2^{\text{g}} \delta_4^{\text{g}} \rangle + \langle \hat{\gamma}_{+12}^{\text{LOS}} \delta_4^{\text{g}} \rangle \langle \delta_2^{\text{g}} \hat{\gamma}_{+14}^{\text{LOS}} \rangle \right) \\ & \quad + \frac{\delta_{BD}}{G_B} \int d^6 \mathbf{\Lambda}_1 p(\mathbf{\Lambda}_1) \int d^5 \mathbf{\Gamma}_2 \langle p_B(\mathbf{\Gamma}_2) \rangle \int d^6 \mathbf{\Lambda}_3 p(\mathbf{\Lambda}_3) W_{12}^\alpha W_{32}^\beta \langle \hat{\gamma}_{+12}^{\text{LOS}} \hat{\gamma}_{+32}^{\text{LOS}} \rangle \\ & \quad + \frac{\delta_{BD}}{L G_B} \int d^6 \mathbf{\Lambda}_1 p(\mathbf{\Lambda}_1) \int d^5 \mathbf{\Gamma}_2 \langle p_B(\mathbf{\Gamma}_2) \rangle W_{12}^\alpha W_{12}^\beta \langle (\hat{\gamma}_{+12}^{\text{LOS}})^2 \rangle, \end{aligned} \quad (\text{A.16})$$

where we have replaced $\hat{\gamma}_{\text{LOS}}$ with γ_{LOS} in terms where it is evaluated at two different points, since the LOS measurement noise η_{LOS} is assumed to be uncorrelated for different lenses. In the above expression, we recognise in **blue** the product of expectation values $(L^+ P_B)_\alpha (L^+ P_D)_\beta$,

which will be subtracted in the definition (A.1) of the covariance. Besides, we note that the two terms in grey can be neglected, because they are of the same order of magnitude as the preceding line, but suppressed by the $1/L \ll 1$ prefactor.

The full covariance of eq. (A.1) thus takes the form

$$\begin{aligned}
& \text{Cov} \left[(\widehat{\mathbf{L}^+ \mathbf{P}_B})_\alpha, (\widehat{\mathbf{L}^+ \mathbf{P}_D})_\beta \right] \\
&= \int d^6 \mathbf{\Lambda}_1 p(\mathbf{\Lambda}_1) \int d^5 \mathbf{\Gamma}_2 \langle p_B(\mathbf{\Gamma}_2) \rangle \int d^6 \mathbf{\Lambda}_3 p(\mathbf{\Lambda}_3) \int d^5 \mathbf{\Gamma}_4 \langle p_D(\mathbf{\Gamma}_4) \rangle W_{12}^\alpha W_{34}^\beta \\
&\quad \times \left\{ \left[\langle \gamma_{+12}^{\text{LOS}} \gamma_{+34}^{\text{LOS}} \rangle + \frac{1}{L} \langle \hat{\gamma}_{+12}^{\text{LOS}} \hat{\gamma}_{+14}^{\text{LOS}} \rangle \delta_{\text{D}}(\mathbf{\Lambda}_1 - \mathbf{\Lambda}_3) \right] \left[\langle \delta_2^{\text{g}} \delta_4^{\text{g}} \rangle + \frac{\delta_{BD}}{G_B} \delta_{\text{D}}(\mathbf{\Gamma}_2 - \mathbf{\Gamma}_4) \right] \right. \\
&\quad \left. + \langle \gamma_{+12}^{\text{LOS}} \delta_4^{\text{g}} \rangle \langle \gamma_{+34}^{\text{LOS}} \delta_2^{\text{g}} \rangle \right\}. \tag{A.17}
\end{aligned}$$

We recognise, in the third line, similar expressions to the tilded correlations $\widetilde{\mathbf{L}^+ \mathbf{L}^+}$, $\widetilde{\mathbf{P}_B \mathbf{P}_D}$ introduced in subsec. 4.3, which contain the contributions of noise and sparsity.

A.5 Polarisation angles

The last step of the calculation consists in extracting the misaligned polarisation angles from the integrand of eq. (A.17). The $\mathbf{L}^+ \mathbf{L}^+$ correlation function, for example, is indeed defined as $\langle \gamma_{+ij}^{\text{LOS}} \gamma_{+ji}^{\text{LOS}} \rangle$, while eq. (A.17) features terms like $\langle \gamma_{+12}^{\text{LOS}} \gamma_{+34}^{\text{LOS}} \rangle$.

In order to recover our building blocks, the trick is to introduce by hand the angles that cause the expressions to depart from the relevant axis – here the axis 13 between the points where the LOS shear is evaluated. From the definition (3.3) of the $+/\times$ polarisations,

$$\gamma_{+12}^{\text{LOS}} \equiv \text{Re} \left[\gamma_1^{\text{LOS}} e^{-2i\psi_{12}} \right] \tag{A.18}$$

$$= \text{Re} \left[(\gamma_{+13}^{\text{LOS}} + i\gamma_{\times 13}^{\text{LOS}}) e^{2i(\psi_{13} - \psi_{12})} \right] \tag{A.19}$$

$$= \gamma_{+13}^{\text{LOS}} \cos 2(\psi_{13} - \psi_{12}) - \gamma_{\times 13}^{\text{LOS}} \sin 2(\psi_{13} - \psi_{12}), \tag{A.20}$$

and similarly for $\gamma_{+34}^{\text{LOS}}$, so that

$$\begin{aligned}
\langle \gamma_{+12}^{\text{LOS}} \gamma_{+34}^{\text{LOS}} \rangle &= \overbrace{\langle \gamma_{+13}^{\text{LOS}} \gamma_{+31}^{\text{LOS}} \rangle}^{\mathbf{L}^+ \mathbf{L}^+(\vartheta_{13}; \mathbf{Z}_1, \mathbf{Z}_3)} \cos 2(\psi_{13} - \psi_{12}) \cos 2(\psi_{31} - \psi_{34}) \\
&\quad + \underbrace{\langle \gamma_{\times 13}^{\text{LOS}} \gamma_{\times 31}^{\text{LOS}} \rangle}_{\mathbf{L}^\times \mathbf{L}^\times(\vartheta_{13}; \mathbf{Z}_1, \mathbf{Z}_3)} \sin 2(\psi_{13} - \psi_{12}) \sin 2(\psi_{31} - \psi_{34}), \tag{A.21}
\end{aligned}$$

where we used $\langle \gamma_{+13}^{\text{LOS}} \gamma_{\times 31}^{\text{LOS}} \rangle = 0$. The same applies to hatted quantities. As for the LP terms, a similar calculation yields

$$\langle \gamma_{+12}^{\text{LOS}} \delta_4^{\text{g}} \rangle = \langle \gamma_{+14}^{\text{LOS}} \delta_4^{\text{g}} \rangle \cos 2(\psi_{14} - \psi_{12}) = \mathbf{L}^+ \mathbf{P}(\vartheta_{14}; \mathbf{Z}_1, z_4) \cos 2(\psi_{14} - \psi_{12}), \tag{A.22}$$

$$\langle \gamma_{+34}^{\text{LOS}} \delta_2^{\text{g}} \rangle = \mathbf{L}^+ \mathbf{P}(\vartheta_{32}; \mathbf{Z}_3, z_2) \cos 2(\psi_{32} - \psi_{34}). \tag{A.23}$$

The general rules for such conversions are summarised in **Step 2** of subsubsec. 4.3.2.

A.6 Final expression

Substituting the relevant trigonometric terms, as derived above, into eq. (A.17), and introducing the redshift-averaged correlation functions, we conclude that

$$\begin{aligned}
& \text{Cov} \left[(\widehat{\text{L}^+\text{P}_B})_\alpha, (\widehat{\text{L}^+\text{P}_D})_\beta \right] \\
&= \int_{\mathcal{F}} \frac{d^2 \hat{\mathbf{u}}_1}{\Omega} \int_{\mathcal{F}} \frac{d^2 \hat{\mathbf{u}}_2}{\Omega} W_{12}^\alpha \int_{\mathcal{F}} \frac{d^2 \hat{\mathbf{u}}_3}{\Omega} \int_{\mathcal{F}} \frac{d^2 \hat{\mathbf{u}}_4}{\Omega} W_{34}^\beta \\
&\quad \times \left\{ \left[\widetilde{\text{L}^+\text{L}^+}(\vartheta_{13}) \cos 2(\psi_{13} - \psi_{12}) \cos 2(\psi_{31} - \psi_{34}) \right. \right. \\
&\quad \quad \left. \left. + \widetilde{\text{L}^\times\text{L}^\times}(\vartheta_{13}) \sin 2(\psi_{13} - \psi_{12}) \sin 2(\psi_{31} - \psi_{34}) \right] \widetilde{\text{P}_B\text{P}_D}(\vartheta_{24}) \right. \\
&\quad \left. + \widetilde{\text{L}^+\text{P}_D}(\vartheta_{14}) \cos 2(\psi_{14} - \psi_{12}) \widetilde{\text{L}^+\text{P}_B}(\vartheta_{32}) \cos 2(\psi_{32} - \psi_{34}) \right\}, \quad (\text{A.24})
\end{aligned}$$

in agreement with the general formula (4.7) proposed in subsec. 4.3.

The calculation discussed here illustrates in particular how the summands with coincident indices in the definition (A.1) of the covariance translate into effective PDFs for the lens and galaxy parameters, and can be eventually absorbed in effective (tilded) correlation functions.

B Angular binning procedure

Let $\text{O}_1\text{O}_2(\vartheta)$ be one of the correlation functions considered in this work. The SNR of that correlation function in the angular bin $[\vartheta_\alpha, \vartheta_{\alpha+1})$ is defined as

$$\text{SNR}(\text{O}_1\text{O}_2; \vartheta_\alpha, \vartheta_{\alpha+1}) \equiv \frac{2\pi \int_{\vartheta_\alpha}^{\vartheta_{\alpha+1}} d\vartheta \vartheta \text{O}_1\text{O}_2(\vartheta)}{\sqrt{\text{Var}[(\widehat{\text{O}_1\text{O}_2})_\alpha]}}, \quad (\text{B.1})$$

with $\Omega_\alpha = \pi(\vartheta_{\alpha+1}^2 - \vartheta_\alpha^2)$. Since the full expression of $\text{Var}[(\widehat{\text{O}_1\text{O}_2})_\alpha]$ is computationally expensive to evaluate, we choose to crudely approximate it by its strictly diagonal element (see *Encyclopedia Covariancis*),

$$\text{Var}[(\widehat{\text{LL}})_\alpha^\pm] \approx \frac{\sigma_{\text{LOS}}^4}{L^2} \frac{\Omega}{\Omega_\alpha}, \quad (\text{B.2})$$

$$\text{Var}[(\widehat{\text{LE}_B})_\alpha^\pm] \approx \frac{1}{2} \frac{\sigma_{\text{LOS}}^2}{L} \frac{\sigma_B^2}{G_B} \frac{\Omega}{\Omega_\alpha}, \quad (\text{B.3})$$

$$\text{Var}[(\widehat{\text{L}^+\text{P}_B})_\alpha] \approx \frac{1}{2} \frac{\sigma_{\text{LOS}}^2}{L} \frac{1}{G_B} \frac{\Omega}{\Omega_\alpha}. \quad (\text{B.4})$$

This approximation allows for a quick evaluation of the SNR function, because it does not require us to evaluate any integral. In practice, the approximation is acceptable in the case of LL, but it is poor for LE and LP, especially for large values of ϑ . *Hence, eqs. (B.2) to (B.4) should not be used if one really cares about the uncertainty on LE and LP.* It should be considered to be a first step towards more refined binning procedures in the future.

B.1 Binning algorithm given a target SNR

Suppose that we want all the angular bins of O_1O_2 to have the same SNR, R . Starting from $\vartheta_1 = 0$, we may proceed iteratively and determine $\vartheta_{\alpha+1}$ from ϑ_α as follows:

1. Evaluate $M_\alpha \equiv \max_{\vartheta > \vartheta_\alpha} \text{SNR}(O_1O_2; \vartheta_\alpha, \vartheta)$.
2. If $M_\alpha \geq R$, then numerically solve $\text{SNR}(O_1O_2; \vartheta_\alpha, \vartheta_{\alpha+1}) = R$ for $\vartheta_{\alpha+1}$. The limits of the α^{th} bin are then fixed and we may consider the next one.

Repeat steps 1 and 2 as long as $M_\alpha \geq R$. If $M_\alpha < R$, then no bin starting from ϑ_α would have enough signal to fulfil the target requirement. We may then either stop the procedure here, or add a last bin $[\vartheta_\alpha, \vartheta_{\max}]$ with $\text{SNR}(O_1O_2; \vartheta_\alpha, \vartheta_{\max}) = M_\alpha$, if $M_\alpha \geq M_{\min} = 2.5$.

B.2 Determining the target SNR

Our baseline choice is $R = R_{\min} = 8$. However, for high-SNR observables such as LE and LP in the optimistic scenario (subsec. 5.1), this choice results in a very large number of angular bins. We choose to avoid this by imposing a maximum number of bins, $N_{\max} = 20$, and increasing the target SNR accordingly.

In practice, we found that for all the observables considered here (LL, LE, LP), the number of angular bins, N , and the SNR in each bin, R , roughly follow the empirical relationship

$$N(R) \approx 2 \left(\frac{M_1}{R} \right)^2, \quad (\text{B.5})$$

where $M_1 = \max_{\vartheta > 0} \text{SNR}(O_1O_2; 0, \vartheta)$ as defined above. In order to ensure both conditions $R \geq R_{\min}$ and $N \lesssim N_{\max}$, we thus fix the target SNR as

$$R = \max \left[R_{\min}, M_1 (0.5 N_{\max})^{-1/2} \right]. \quad (\text{B.6})$$

Since this whole procedure relies on the approximations of eqs. (B.2) to (B.4), the actual SNR in each bin can turn out to be quite far from the target.

C Monte Carlo integration and error analysis

Consider the definite integral

$$I = \int_{\mathcal{D}} d^m \mathbf{x} f(\mathbf{x}), \quad (\text{C.1})$$

of a real-valued function f over m variables $\mathbf{x} = (x_1, x_2, \dots, x_m)$, within the integration domain $\mathcal{D} \subset \mathbb{R}^m$. We denote with $V = \int_{\mathcal{D}} d^m \mathbf{x}$ the volume of \mathcal{D} .

I can be efficiently estimated with a Monte Carlo integral. Drawing a random sample of N points $\mathbf{x}_1, \mathbf{x}_2, \dots, \mathbf{x}_N$ uniformly within the domain \mathcal{D} , we can approximate the mean of the function over this sample as

$$\langle f \rangle_N \equiv \frac{1}{N} \sum_{i=1}^N f(\mathbf{x}_i), \quad (\text{C.2})$$

from which our integral can be approximated as

$$I \approx I_N = V \langle f \rangle_N. \quad (\text{C.3})$$

The error in I_N can be estimated from the sample variance of the N evaluations of the function, $f(\mathbf{x}_1), f(\mathbf{x}_2), \dots, f(\mathbf{x}_N)$, as

$$\text{err}(I_N) = \sqrt{\frac{V^2}{N}} s^2, \quad s^2 = \frac{1}{N-1} \sum_{i=1}^N [f(\mathbf{x}_i) - \langle f \rangle_N]^2. \quad (\text{C.4})$$

Each element in the covariance matrices presented in figs. 9 and 11 takes the form of a sum of a cosmic, sparsity and noise contribution, each of which involving one or more integrals over multiple dimensions. The total numerical uncertainty of each element is therefore propagated from the uncertainty arising from each integral. Because the cosmic variance generally involves integrals over five dimensions, rather than four in the case of sparsity and noise, larger samples are generally needed to achieve a similar fractional uncertainty.

We use samples with 10^6 points for noise/sparsity-covariance integrals, and 10^7 for cosmic-covariance integrals. The slowest single redshift “block” in the matrices in figs. 9 and 11 then takes about one day to compute; parallelising to process each block simultaneously means the full covariance matrix can be evaluated numerically on the same timescale. Further improvements with more sophisticated integrators and parallelisation schemes are possible, but we leave this for a future project.

We plot the errors corresponding to fig. 9 in fig. 13, and those corresponding to fig. 11 in fig. 14. From these figures, we see that, while there are elements for which the numerical uncertainty may be comparable to or even larger than the covariance in that block, it is always orders of magnitude smaller than the corresponding variance, and so these errors are not expected to have a perceivable impact on the relative strength of these elements, or in applications such as Fisher forecasting.

References

- [1] M. Bartelmann and P. Schneider, *Weak gravitational lensing*, *Phys. Rep.* **340** (Jan., 2001) 291–472, [[astro-ph/9912508](#)].
- [2] B. Jain and U. Seljak, *Cosmological Model Predictions for Weak Lensing: Linear and Nonlinear Regimes*, *ApJ* **484** (July, 1997) 560–573, [[astro-ph/9611077](#)].
- [3] A. Hall, *Cosmology from weak lensing alone and implications for the Hubble tension*, *MNRAS* **505** (Aug., 2021) 4935–4955, [[arXiv:2104.12880](#)].
- [4] **DES** Collaboration, T. M. C. Abbott et al., *Dark Energy Survey Year 6 Results: Cosmological Constraints from Galaxy Clustering and Weak Lensing*, [arXiv:2601.14559](#).
- [5] S. Sugiyama et al., *Hyper Suprime-Cam Year 3 results: Cosmology from galaxy clustering and weak lensing with HSC and SDSS using the minimal bias model*, *Phys. Rev. D* **108** (2023), no. 12 123521, [[arXiv:2304.00705](#)].
- [6] H. Miyatake et al., *Hyper Suprime-Cam Year 3 results: Cosmology from galaxy clustering and weak lensing with HSC and SDSS using the emulator based halo model*, *Phys. Rev. D* **108** (2023), no. 12 123517, [[arXiv:2304.00704](#)].
- [7] A. H. Wright et al., *KiDS-Legacy: Cosmological constraints from cosmic shear with the complete Kilo-Degree Survey*, *Astron. Astrophys.* **703** (2025) A158, [[arXiv:2503.19441](#)].
- [8] **Euclid** Collaboration, Y. Mellier et al., *Euclid. I. Overview of the Euclid mission*, *Astron. Astrophys.* **697** (2025) A1, [[arXiv:2405.13491](#)].
- [9] **LSST** Collaboration, Ž. Ivezić et al., *LSST: from Science Drivers to Reference Design and Anticipated Data Products*, *Astrophys. J.* **873** (2019), no. 2 111, [[arXiv:0805.2366](#)].

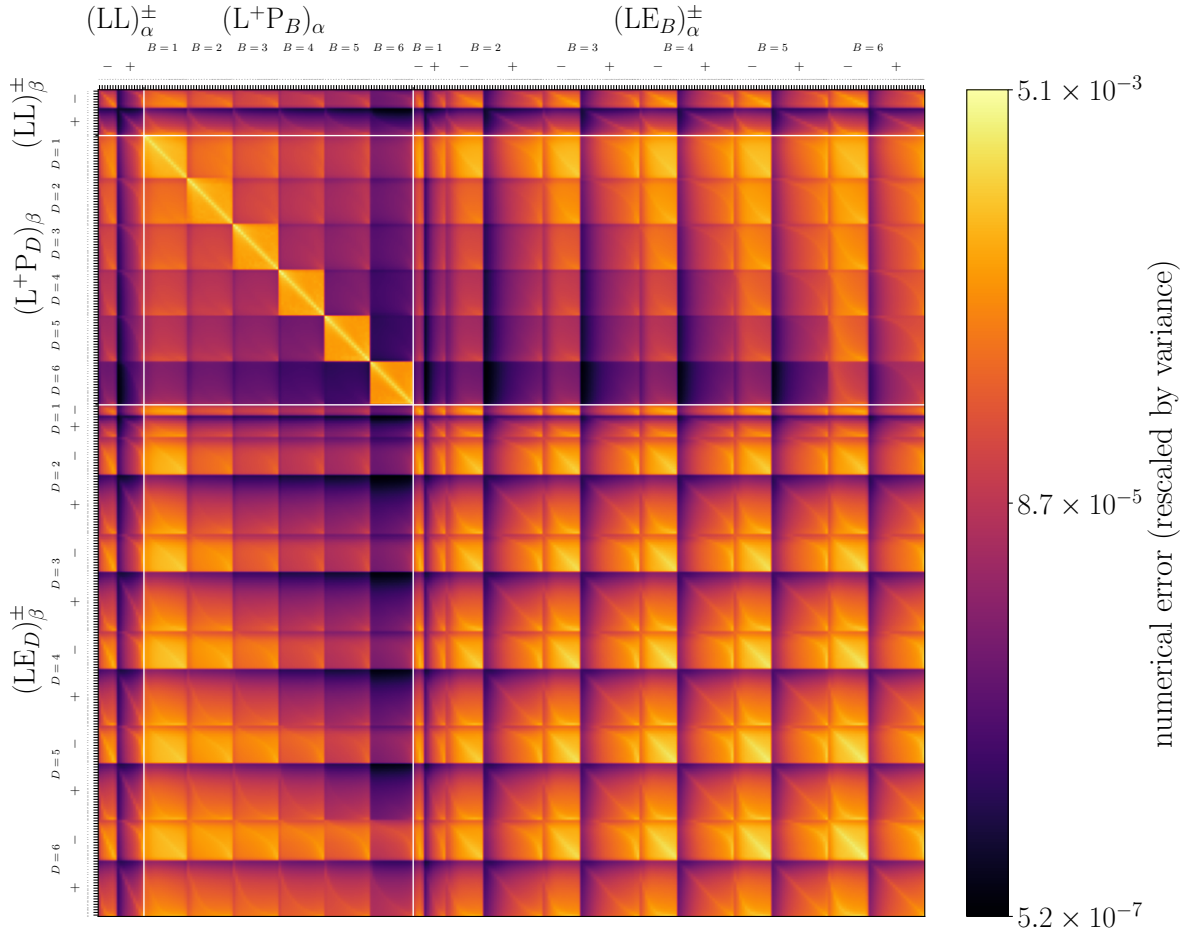


Figure 13. Numerical uncertainty, arising from the Monte Carlo integration, on the covariance matrix of LL, LP and LE in the *optimistic scenario*, normalised by variance according to $\text{err}\{\text{Cov}[(\widehat{O_1O_2})_\alpha, (\widehat{O_3O_4})_\beta]\}/[\text{Var}(\widehat{O_1O_2})_\alpha \text{Var}(\widehat{O_3O_4})_\beta]^{1/2}$.

- [10] **Euclid** Collaboration, A. Blanchard et al., *Euclid preparation. VII. Forecast validation for Euclid cosmological probes*, *Astron. Astrophys.* **642** (2020) A191, [[arXiv:1910.09273](#)].
- [11] T. E. Collett, *The Population of Galaxy-Galaxy Strong Lenses in Forthcoming Optical Imaging Surveys*, *ApJ* **811** (Sept., 2015) 20, [[arXiv:1507.02657](#)].
- [12] I. Kovner, *The Thick Gravitational Lens: A Lens Composed of Many Elements at Different Distances*, *ApJ* **316** (May, 1987) 52.
- [13] P. Schneider, *The Cosmological lens equation and the equivalent single plane gravitational lens*, *Mon. Not. Roy. Astron. Soc.* **292** (1997) 673, [[astro-ph/9706185](#)].
- [14] R. Bar-Kana, *Effect of Large-Scale Structure on Multiply Imaged Sources*, *ApJ* **468** (Sept., 1996) 17, [[astro-ph/9511056](#)].
- [15] C. McCully, C. R. Keeton, K. C. Wong, and A. I. Zabludoff, *A New Hybrid Framework to Efficiently Model Lines of Sight to Gravitational Lenses*, *Mon. Not. Roy. Astron. Soc.* **443** (2014), no. 4 3631–3642, [[arXiv:1401.0197](#)].
- [16] P. Fleury, J. Larena, and J.-P. Uzan, *Gravitational lenses in arbitrary space-times*, *Class. Quant. Grav.* **38** (2021), no. 8 085002, [[arXiv:2011.04440](#)].

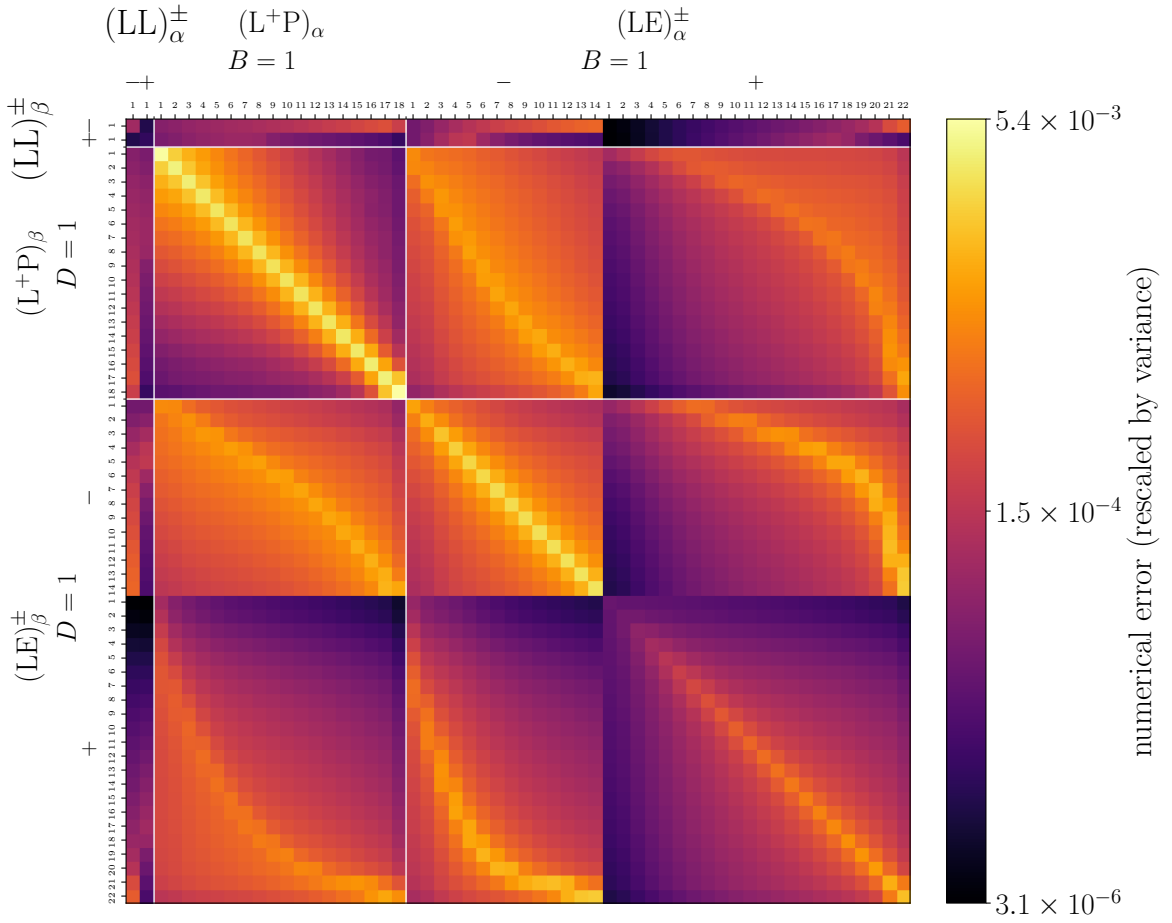


Figure 14. The same as in fig. 13, but for the *conservative scenario*.

- [17] P. Fleury, J. Larena, and J.-P. Uzan, *Line-of-sight effects in strong gravitational lensing*, *JCAP* **2021** (Aug., 2021) 024, [[arXiv:2104.08883](#)].
- [18] S. Birrer, C. Welschen, A. Amara, and A. Refregier, *Line-of-sight effects in strong lensing: Putting theory into practice*, *JCAP* **1704** (2017), no. 04 049, [[arXiv:1610.01599](#)].
- [19] S. Birrer, A. Refregier, and A. Amara, *Cosmic Shear with Einstein Rings*, *Astrophys. J.* **852** (2018), no. 1 L14, [[arXiv:1710.01303](#)].
- [20] N. B. Hogg, P. Fleury, J. Larena, and M. Martinelli, *Measuring line-of-sight shear with Einstein rings: a proof of concept*, *Mon. Not. Roy. Astron. Soc.* **520** (2023), no. 4 5982–6000, [[arXiv:2210.07210](#)].
- [21] N. B. Hogg, D. Johnson, A. J. Shajib, , and J. Larena, *Line-of-sight shear in SLACS strong lenses I: shear and mass model parametrisations*, [arXiv:2501.16292](#).
- [22] N. B. Hogg, D. Johnson, A. J. Shajib, and J. Larena, *Line-of-sight shear in SLACS strong lenses II: validation tests with an extended sample*, [arXiv:2512.05050](#).
- [23] A. S. Bolton, S. Burles, L. V. E. Koopmans, T. Treu, and L. A. Moustakas, *The Sloan Lens ACS Survey. I. A Large Spectroscopically Selected Sample of Massive Early-Type Lens Galaxies*, *ApJ* **638** (Feb., 2006) 703–724, [[astro-ph/0511453](#)].
- [24] P. Schneider, J. Ehlers, and E. E. Falco, *Gravitational Lenses*. Springer, 1992.

- [25] T. Duboscq, N. B. Hogg, P. Fleury, and J. Larena, *Weak lensing of strong lensing: beyond the tidal regime*, *JCAP* **08** (2024) 021, [[arXiv:2405.12091](#)].
- [26] D. M. Goldberg and D. J. Bacon, *Galaxy-Galaxy Flexion: Weak Lensing to Second Order*, *ApJ* **619** (Feb., 2005) 741–748, [[astro-ph/0406376](#)].
- [27] P. Fleury, *Light propagation in inhomogeneous and anisotropic cosmologies*. PhD thesis, Paris U., VI, IAP, 2015. [[arXiv:1511.03702](#)].
- [28] P. Schneider and D. Sluse, *Source-position transformation: an approximate invariance in strong gravitational lensing*, *A&A* **564** (Apr., 2014) A103, [[arXiv:1306.4675](#)].
- [29] D. Johnson, P. Fleury, J. Larena, and L. Marchetti, *Foreground biases in strong gravitational lensing*, *JCAP* **2024** (Oct., 2024) 055, [[arXiv:2405.04194](#)].
- [30] S. Birrer, *Gravitational Lensing Formalism in a Curved Arc Basis: A Continuous Description of Observables and Degeneracies from the Weak to the Strong Lensing Regime*, *Astrophys. J.* **919** (2021), no. 1 38, [[arXiv:2104.09522](#)].
- [31] L. Van de Vyvere, M. R. Gomer, D. Sluse, D. Xu, S. Birrer, A. Galan, and G. Varnardos, *TDCOSMO. VII. Boxyness/discyness in lensing galaxies: Detectability and impact on H_0* , *A&A* **659** (Mar., 2022) A127, [[arXiv:2112.03932](#)].
- [32] A. Etherington et al., *Strong gravitational lensing’s ‘external shear’ is not shear*, *Mon. Not. Roy. Astron. Soc.* **531** (2024), no. 3 3684–3697, [[arXiv:2301.05244](#)].
- [33] L. Van de Vyvere, D. Sluse, M. R. Gomer, and S. Mukherjee, *Consequences of the lack of azimuthal freedom in the modeling of lensing galaxies*, *Astron. Astrophys.* **663** (2022) A179, [[arXiv:2206.00022](#)].
- [34] J. N. Goldberg, A. J. Macfarlane, E. T. Newman, F. Rohrlich, and E. C. G. Sudarshan, *Spin-s Spherical Harmonics and δ* , *Journal of Mathematical Physics* **8** (Nov., 1967) 2155–2161.
- [35] P. G. Castro, A. F. Heavens, and T. D. Kitching, *Weak lensing analysis in three dimensions*, *Phys. Rev. D* **72** (July, 2005) 023516, [[astro-ph/0503479](#)].
- [36] P. Holloway, A. Verma, P. J. Marshall, A. More, and M. Tecza, *On the detectability of strong lensing in near-infrared surveys*, *MNRAS* **525** (Oct., 2023) 2341–2354, [[arXiv:2308.00851](#)].
- [37] G. Ferrami and J. S. B. Wyithe, *A model for galaxy–galaxy strong lensing statistics in surveys*, *Mon. Not. Roy. Astron. Soc.* **532** (2024), no. 2 1832–1848, [[arXiv:2404.03143](#)].
- [38] F. A. Kuhn, S. Birrer, C. Bruderer, A. Amara, and A. Refregier, *Combining strong and weak lensing estimates in the Cosmos field*, *JCAP* **04** (2021) 010, [[arXiv:2010.08680](#)].
- [39] C. Faure, J.-P. Kneib, G. Covone, L. Tasca, A. Leauthaud, P. Capak, K. Jahnke, V. Smolcic, S. de la Torre, R. Ellis, A. Finoguenov, A. Koekemoer, O. Le Fevre, R. Massey, Y. Mellier, A. Refregier, J. Rhodes, N. Scoville, E. Schinnerer, J. Taylor, L. Van Waerbeke, and J. Walcher, *First Catalog of Strong Lens Candidates in the COSMOS Field*, *ApJS* **176** (May, 2008) 19–38, [[arXiv:0802.2174](#)].
- [40] J. W. Nightingale et al., *The COSMOS-Web Lens Survey (COWLS) I: discovery of >100 high redshift strong lenses in contiguous JWST imaging*, *Mon. Not. Roy. Astron. Soc.* **543** (2025), no. 1 203–222, [[arXiv:2503.08777](#)].
- [41] G. Mahler et al., *The COSMOS-Web Lens Survey (COWLS) II: depth, resolution, and NIR coverage from JWST reveal 17 spectacular lenses*, *Mon. Not. Roy. Astron. Soc. L* **8** (2025) L14, [[arXiv:2503.08782](#)].
- [42] N. B. Hogg et al., *The COSMOS-Web Lens Survey (COWLS) III: forecasts versus data*, *Mon. Not. Roy. Astron. Soc.* **544** (2025), no. 1 782–798, [[arXiv:2503.08785](#)].
- [43] P. Schneider, L. van Waerbeke, M. Kilbinger, and Y. Mellier, *Analysis of two-point statistics of cosmic shear. I. Estimators and covariances*, *A&A* **396** (Dec., 2002) 1–19, [[astro-ph/0206182](#)].

- [44] D. A. Varshalovich, A. N. Moskalev, and V. K. Khersonskii, *Quantum Theory of Angular Momentum*. 1988.
- [45] S. E. Hoffmann, *Uniform analytic approximation of Wigner rotation matrices*, *Journal of Mathematical Physics* **59** (Feb., 2018) 022102, [[arXiv:1710.11282](#)].
- [46] M. Kilbinger, C. Heymans, M. Asgari, S. Joudaki, P. Schneider, P. Simon, L. Van Waerbeke, J. Harnois-Déraps, H. Hildebrandt, F. Köhlinger, K. Kuijken, and M. Viola, *Precision calculations of the cosmic shear power spectrum projection*, *MNRAS* **472** (Dec., 2017) 2126–2141, [[arXiv:1702.05301](#)].
- [47] P. Fleury, *Sparsity covariance: a source of uncertainty when estimating correlation functions with a discrete sample of observations in the sky*, *The Open Journal of Astrophysics* **8** (May, 2025) 57, [[arXiv:2502.18327](#)].
- [48] L. Isserlis, *On a formula for the product-moment coefficient of any order of a normal frequency distribution in any number of variables*, *Biometrika* **12** (Nov., 1918) 134–139.
- [49] A. Lewis, A. Challinor, and A. Lasenby, *Efficient computation of cosmic microwave background anisotropies in closed friedmann-robertson-walker models*, *The Astrophysical Journal* **538** (Aug., 2000) 473–476.
- [50] C. Howlett, A. Lewis, A. Hall, and A. Challinor, *Cmb power spectrum parameter degeneracies in the era of precision cosmology*, *Journal of Cosmology and Astroparticle Physics* **2012** (Apr., 2012) 027–027.
- [51] S. G. Murray and F. J. Poulin, *hankel: A python library for performing simple and accurate hankel transformations*, *Journal of Open Source Software* **4** (2019), no. 37 1397.
- [52] C. R. Harris, K. J. Millman, S. J. van der Walt, R. Gommers, P. Virtanen, D. Cournapeau, E. Wieser, J. Taylor, S. Berg, N. J. Smith, R. Kern, M. Picus, S. Hoyer, M. H. van Kerkwijk, M. Brett, A. Haldane, J. F. del Río, M. Wiebe, P. Peterson, P. Gérard-Marchant, K. Sheppard, T. Reddy, W. Weckesser, H. Abbasi, C. Gohlke, and T. E. Oliphant, *Array programming with NumPy*, *Nature* **585** (Sept., 2020) 357–362.
- [53] P. Virtanen, R. Gommers, T. E. Oliphant, M. Haberland, T. Reddy, D. Cournapeau, E. Burovski, P. Peterson, W. Weckesser, J. Bright, S. J. van der Walt, M. Brett, J. Wilson, K. J. Millman, N. Mayorov, A. R. J. Nelson, E. Jones, R. Kern, E. Larson, C. J. Carey, Í. Polat, Y. Feng, E. W. Moore, J. VanderPlas, D. Laxalde, J. Perktold, R. Cimrman, I. Henriksen, E. A. Quintero, C. R. Harris, A. M. Archibald, A. H. Ribeiro, F. Pedregosa, P. van Mulbregt, and SciPy 1.0 Contributors, *SciPy 1.0: Fundamental Algorithms for Scientific Computing in Python*, *Nature Methods* **17** (2020) 261–272.
- [54] J. D. Hunter, *Matplotlib: A 2d graphics environment*, *Computing in Science & Engineering* **9** (2007), no. 3 90–95.
- [55] N. Martinet, J. Harnois-Déraps, E. Jullo, and P. Schneider, *Probing dark energy with tomographic weak-lensing aperture mass statistics*, *A&A* **646** (Feb., 2021) A62, [[arXiv:2010.07376](#)].
- [56] **Euclid** Collaboration, A. Pocino et al., *Euclid preparation. XII. Optimizing the photometric sample of the Euclid survey for galaxy clustering and galaxy-galaxy lensing analyses*, *Astron. Astrophys.* **655** (2021) A44, [[arXiv:2104.05698](#)].